Rational Design of Nanostructured Electrode Materials for High-performance Supercapacitors

by

Xingye Fan

A thesis
presented to the University of Waterloo
in fulfillment of the
thesis requirement for the degree of
Master of Applied Science
in
Chemical Engineering

Waterloo, Ontario, Canada, 2015

AUTHOR'S DECLARATION

I hereby declare that I am the sole author of this thesis. This is a true copy of the thesis, including any required final revisions, as accepted by my examiners.

I understand that my thesis may be made electronically available to the public.

Abstract

Supercapacitors, which are also known as electrical double-layer capacitors or electrochemical capacitors are promising energy storage devices due to their evident advantages such as high power density, long cycle and shelf life. Although the lithium-ion battery is a dominate energy storage device for both electrical vehicles and portable electronics at the current stage, it is still not perfect in terms of performance. One of the main issues that the lithium-ion battery is usually blamed for is its safety problem. Besides, power density is playing a significant role in more and more electronic products. However, the lithium-ion battery can barely satisfy the requirements of such high power density. In situations like this, supercapacitors have attracted growing attention owing to their high power density and safety performance. In addition, the lithium-ion battery stores energy by intercalation and deintercalation of lithium ions in two electrodes, between which lithium ions move from one electrode to the other during charging and discharging. Thus, compared to the rate of ions inserting into and extracting from electrodes, supercapacitors are able to charge and discharge much faster by absorbing and desorbing charges on the surface of electrodes. The above advantages of supercapacitors have made them promising candidates to serve as the next generation energy storage technology.

As is well known, the update of various electronic products is getting faster and faster to meet the requirements of electronic market. In this proposed circumstance, supercapacitors with high performance including energy density, power density, cycling stability, long shelf duration and short charging time, are highly demanded. Moreover, as a sustainable development strategy requested, it is also necessary to consider the environmental benignity, low cost and natural benignity when designing supercapacitor electrode materials. In this thesis, a novel electrode material of supercapacitors is designed and investigated to solve the problems that are commonly encountered among current energy storage technologies.

Partially graphitized hierarchical porous carbon was combined with manganese dioxide to use as supercapacitor electrode material, providing both high power density and energy density. Manganese dioxide has been studied and proven to be a suitable potential electrode material for supercapacitors due to high theoretical specific capacitance, low cost, non-toxicity and a large reservation in nature. Combining the carbon framework with transition metal oxide is an effective method of increasing the total conductivity of electrodes. Thus, special carbon substrate was synthesized with the aerosol assisted spray drier method using sucrose as the carbon precursor, TEOs and colloidal silica as dual templates.

A hierarchical nanostructured porous carbon was achieved, in which were two types of pores with different diameters. On one hand, the large pores in this material mainly aim to establish rapid ion transfer channels, which is beneficial for the rate capability. On another, the small pores are fabricated to increase the total specific surface area, which is significant to the capacity of supercapacitors. Owing to the unique design, a specific capacitance of 412 F/g has been achieved with a good rate capability and cycling stability. A cycling test which was conducted at the current density of 1 A/g showed that 88% of initial capacitance was retained after over 4000 cycles.

Acknowledgements

The work reported herein was financially supported by the Nature Sciences and Engineering Research Council of Canada and University of Waterloo.

The author would like to thank the tremendous guidance and assistance of my supervisors Dr. Zhongwei Chen and Dr. Aiping Yu in my master's study.

Special thanks go to my colleagues including, Xiaolei Wang, Ge Li, Ji Yan, Wook Ahn, Jingde Li, Xiaogang Fu, Xinglong Ma, Hao Liu, Drew Higgins, Fathy Hassan, Hadis Zarrin, Qianqian Hu, Moon Gyu Park, Ja-Yeon Choi, Ariful Hoque, Yun-seok Jun, Jared Lenos, Dongun Lee, Gaopeng Jiang, Rasim Batmaz, Raihan Ahmed, Abdul Rahman Ghannoum, Abel Sy, Gregory Lui, Guihua Liu, Min Ho Seo, Pouyan Zamani, Salah Abureden and Zhiyu Mao for their assistance and support.

Moreover, I would like to acknowledge the support from my reviewers, including Professor Zhongwei Chen, Professor Bo Cui, and Professor Zhongchao Tan

Table of Contents

List of Figures

List of Abbreviations, Symbols and Nomenclature

3D	three dimensional
ε	electrolyte dielectric constant
ε_r	dieletric constant
ε_0	dieletric constant of vacuum
A	surface area of electrode
AC	activited carbon
C_c	compact layer capacitance
C_d	diffuse layer capacitance
CNT	carbon nanotube
d	thinkness of electric double layer
DMC	dimethyl carbonate
E	energy density
EC	ethylene carbonate
EDLC	electrode double layer capacitor
ESR	equivelant series resistance
F	Faraday
g	gram
GCD	Galvanostatic charge discharge
LIBs	lithium ion batteries
NMP	*N*-methylpyrrolidinone
PANI	polyaniline

PPy	polypyrrole
PTh	polythiophene
SCE	Saturated calomel electrode
SCs	supercapacitors
SEM	scanning electron microscope
SHE	standard hydrogen electrode
SSA	specific surface area
SWNT	single-walled carbon nanotube
TEM	transmission electron microscope
TGA	Thermogravimetic analysis
TMO	transition metal oxide
V	potential window
WMNT	multi-walled carbon nanotube
XRD	X-ray diffraction
XPS	X-ray photoelectron spectroscopy

Chapter 1
Introduction

1.1 Introduction of Thesis Project

The ever-growing concerns about fossil fuel crisis and ecological deterioration have attracted attention to the utilization of renewable energies such as tidal, solar and wind. However, these energies are produced intermittently, therefore energy storage, especially electrical energy storage, has become one of the essential issues which lead to better utilization of sustainable energies in the future. Among various energy storage technologies, lithium-ion batteries (LIBs) and supercapacitors hold great promise in broad applications such as portable electronics, smart grids and electrical vehicles. LIBs, as a kind of secondary batteries, have been prevalently used in people's daily lives since they were first commercialized by Sony Company in 1991. LIBs have high energy density, around 150 ~ 200 Wh/kg, which enables it to store electrical energy in lightweight devices. Therefore, LIBs are widely used not only in portable electronics, but also in aircrafts and automotive vehicles, which are commonly powered by fossil fuel. Besides, compared to conventional secondary batteries, which suffer from memory effect, LIBs can be charged at any time even after being only partially discharged. However, there are still some technical challenges posed by LIBs. First, the electrolyte containing flammable organic solvents such as ethylene carbonate (EC), dimethyl carbonate (DMC) and diethyl carbonate are highly hazardous in the case of short circuit. The explosion of LIBs is usually able to cause extremely serious safety issues even death. The second concerns are related to the battery life. Based on manufacturers' information, the capacity of LIBs drops linearly to 80% after 500 cycles indicating batteries of phones that are used daily can barely last for more than three years. In addition, for rechargeable batteries, a short recharge time is significant, especially for electric cars. For example, a Tesla electric car can charge at the rate of 92 km of range per hour with a wall connector and dual chargers, which is less convenient for long distance travelling than traditional cars; however when a single charger and mobile connector are utilized the charge rate is even lower. Therefore, the widespread adoption of environmental friendly electrical vehicles is still hampered by the long charge time of LIBs. At last, LIBs are extremely hard to compare with fossil fuels in terms of power density, which are at least two magnitudes lower than that of fossil fuel. As a result, to replace fuels with LIBs, a large quantity of LIBs is needed, thus leading to a sharp increase in the mass of products. Thus, SCs seem to be a promising technology for the next-generation energy storage devices due to their safety, long cycling life, short charge duration and high power.

In this report, a basic background of SCs and the ongoing development of novel SCs electrode materials will be presented. Based on the energy storage mechanism of SCs, the electrode materials will be divided into carbonaceous materials and transition metal oxides, both of which will be explicitly discussed in the introduction part in the thesis. Subsequently, morphologic and structural characterization methods involved in my master's studies are summarized. The rest parts of the thesis will be the contents associated with the author's investigation and studies towards novel SCs electrode materials. To specific, a type of porous carbon material with a special rational designed structure was synthesized and studied. Moreover, the special porous carbon was combined with MnO_2, which is considered as a rising-star for SCs electrode material, to test the electrochemical performance. In summary, the thesis contains the following contents:

i. A brief introduction about the mechanism, electrode materials and current challenges to supercapacitors.
ii. Structural and morphologic characterization methods of electrode materials. This chapter will focus on the manipulation and basic mechanism of these methods.
iii. Hierarchical porous carbon with engineered structure was synthesized by the aerosol assisted spray method. This chapter will focus on the advantages of hierarchical porous carbon and the mechanism of the synthesis method.
iv. Composites of MnO_2 and hierarchical porous carbon were served as supercapacitors electrode materials. In this chapter, the structural and electrochemical characterization of this material will be discussed.

1.2 Introduction of Supercapacitors

The growing crisis of fossil fuels and the severe environmental pollution resulting from exhaust gas of internal combustion engine have made researchers focus on developing new energy storage devices to replace conventional engines. Great effort has already been made towards developing hybrid powers, fuel cells, and chemical cells. However, due to their short service life, high cost and low temperature performance, it is hard to solve all the problems at the same time. The emergence of supercapacitors which have outstanding features such as long cycling life, high temperature performance and environmental benignity, has opened a way to solve almost all the problems that are faced by current energy storage technologies. Because of the advantages of supercapacitors, they can replace conventional batteries or even novel energy storage devices utilized in electrical vehicles. Moreover,

supercapacitors have more widespread applications than traditional batteries. Therefore, many researchers are sparing no efforts to study the electrode materials of supercapacitors.

The discovery of electrolytic capacitors was a coincidence when researchers were conducting experiments for fuel cells and secondary batteries using porous carbon as the electrode in early 1950s. Researchers found that porous activated carbon (AC) with high specific surface area could be used for energy storage. Although the mechanism of electric double layer had not been thoroughly studied, the first "Low voltage electrolytic capacitor with porous carbon electrode" was still reported in 1957 by H.I. Becker. [1]

Electrolytic capacitors are energy storage devices with a special metal and electrolyte as anode and cathode materials, respectively. The metal which is used in the electrolytic capacitor is easy to form a layer of metal oxide as the dielectric of the capacitors. Three family members of electrolytic capacitors are aluminum electrolytic capacitors, tantalum electrolytic capacitors and niobium electrolytic capacitors.[2-4] Since the first report of electrolytic capacitors, hundreds of patents and articles related to various aspects of this field were subsequently written by developers. However, electrolytic capacitors only have limited capacitance.[5, 6] Researchers were not able to achieve a breakthrough until the emergence of electrochemical capacitors.

In the early stage, electrodes of electrochemical capacitors were usually made of activated carbon coating on aluminum foil and the electrodes were soaked in liquid or solid electrolyte with a porous separator between them. This mechanical design established the prototype of electrochemical capacitors, which greatly increased the capacitance to the order of 1 farad. In 1971, this invention was successfully commercialized as "supercapacitors" by the Japanese company, NEC Corporation. At that time, SCs only had limited applications and were mainly used as back-up power supplies for volatile clock chips or computer memories.[7] The capacitance of first generation SCs was mainly hampered by large internal equivalent series resistance (ESR), owing to the low conductivity of electrodes and electrolytes used during that time. These problems were basically solved with improved electrode materials and electrolyte by the 1980s; when large amount of SCs were marketed, most of them were applied in the military due to their high cost. From 1975 to 1980, Brain Evan Conway, a researcher form the University of Ottawa, conducted a large number of experiments using ruthenium oxide as SCs electrode material.[8] This special material not only can store electrostatic charges by electrical double layer, but also generate a kind of "pseudocapacitance" resulting from faradaic reaction or underpotential

depositon on the surface of electrode. Based on his research, the concept of SCs has been extended, and B.E. Conway explained the difference between batteries and supercapacitors in his report in 1991.[9]

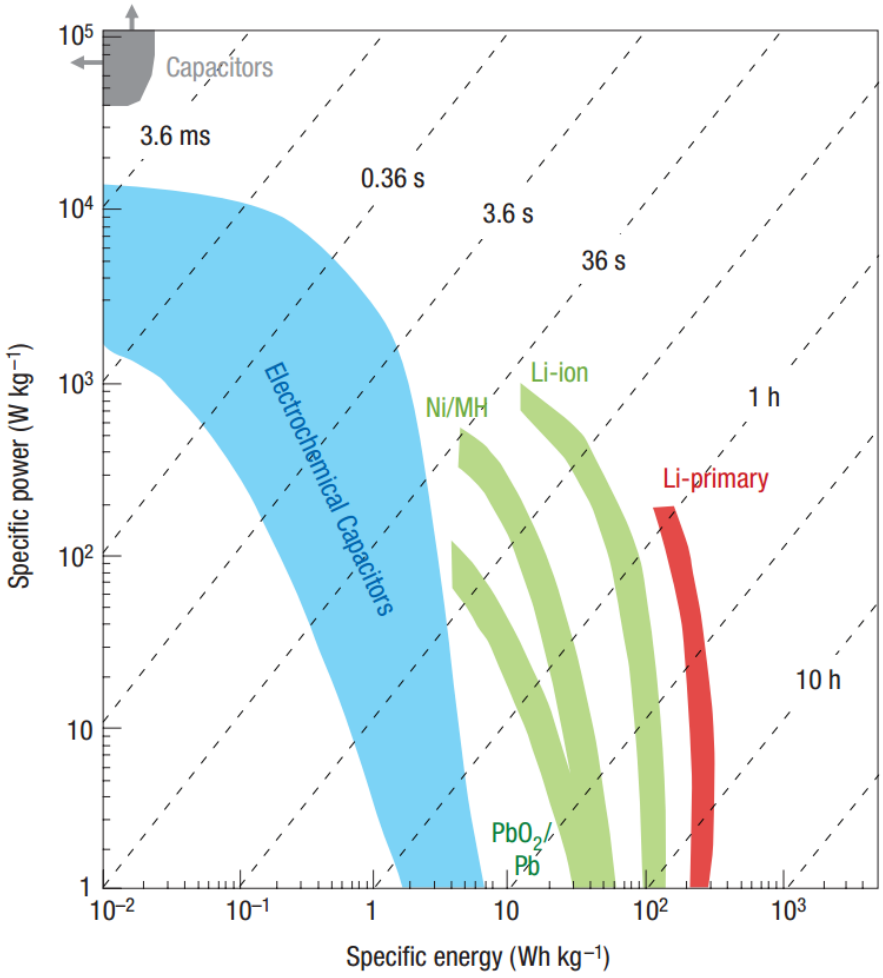

Figure 1: A diagram of gravimetric energy density and specific power density of different energy storage technologies such as electrochemical capacitors, PbO_2/Pb batteries, Ni/MH batteries, Lithium-ion Batteries and Li-primary batteries

Recently, in order to combine the high power density of SCs and the high energy density of LIBs, hybrid capacitors have been popular in the reseach which are also known as lithium-ion capacitors.[10-12] This techonology was first reported by FDK company who used carbon and pre-doped lithium-ion as the electrode materials in 2007. The pre-intercalation of lithium ions is capable of lowering the potential of anode electrodes leading to higher a potential widow and a higher energy density of

capacitors. For example, the initial potential of canbonaceous electrodes are approximately -0.1 V versus Standard Hydrogen Electrode (SHE). After doping of lithium ions, the electrode potential can be reduced to -2.8V. As can be seen in **Figure 1**, lithium-ion capacitors have at least one magnitude higher energy density than electrode double layer capacitors (EDLC). However, the power density of lithium-ion capacitors are comparable with EDLCs. But, the organic solvent containing in the lithium-ion capacitor electrolyte has potential risk of explosion when a short circuit occurs. In order to avoid the safty issue that exists in lithium-ion capacitors, many other scenatios of improving energy density of supercapacitors are being studied. Compared with dangerous onganic electrolytes, aquous supercapacitors hold more promise. But at the same time, novel electrode materials are highly demanded for aqueous supercapacitors to increase the capacitance.

1.3 Physical Model of Supercapacitors

A typical structure of a supercapacitor involves two polarized electrodes connected with current collectors. Power source is able to be applied on the current collectors to polarize the electrodes to charge the device. A separator which is located between two electrodes is ion-permeable but can prevent electrons from passing through. Both electrodes and the separator is immersed into electrolyte, which contains positive and negative ions. When a voltage is applied, the ions with opposite polarity to the electrode will be absorbed onto the corresponding electrode, forming an electric double layer on the interface between the electrode and the electrolyte. The electric double layer model was firstly proposed by Helmholtz in 1853.[13] Helmholtz model can be simply described as a capacitor since he supposed that only a single layer of ions is absorbed on the surface. The electric double layer capacitance calculated by this model is indicated as:

$$C = \frac{\varepsilon}{d} \tag{1}$$

where ε is the electrolyte dielectric constant, which is also known as permittivity of the electrolyte, and d is the thickness of electric double layer. However, the Helmholtz model is not accurate enough to

show the relation between capacitance and voltage, because Helmholtz failed to consider the resistance in the electrolyte which can lead to a different distribution of charges.

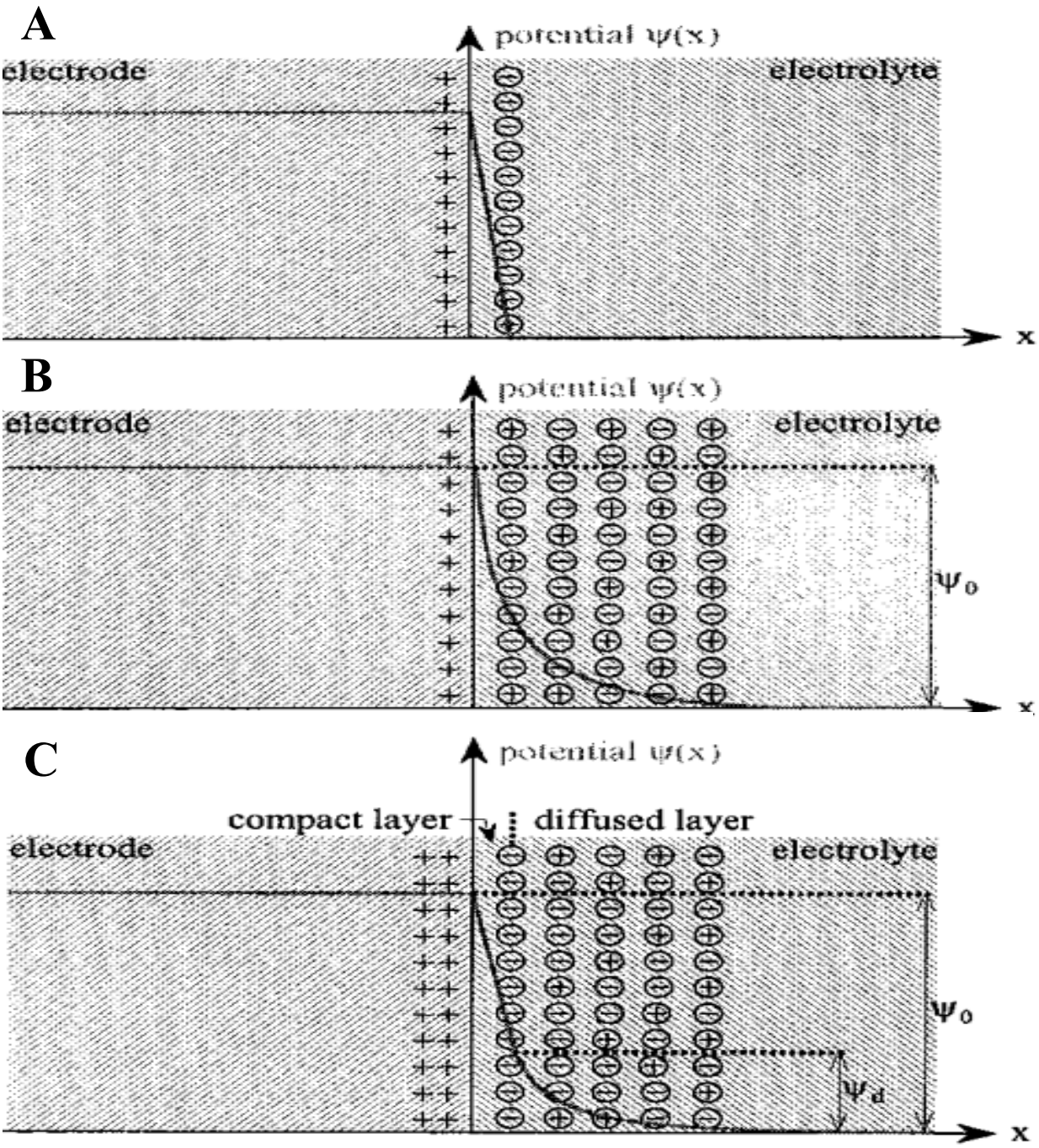

Figure 2: The relation of potential with distance away from interfacial layer between electrode and electrolyte in three models: Helmholtz's model (A), Gouy and Chapman's model (B), and Stern's model. Reproduced with permission from [13]

The Helmholtz model was later modified by Gouy and Chapman who proposed the existence of a diffuse layer of ions which leads to an exponentially decrease of the electric potential from the electrode surface to the bulk of electrolyte. As Gouy and Chapman did not involve the dimension of ions and molecules in their model, the relationship between surface capacitance versus surface potential cannot be described correctly especially at high surface potential. To solve this problem, Sterrn established a new model by combining theories of Helmholtz and Gouy and Chapman, which separates the space of charges into two parts: the compact, formed by absorption of electrolyte ions and diffused layer, explained by Gouy and Chapman.[14, 15] Thus, the total specific capacitance *C* depends on the surface capacitance of the compact layer C_c and the diffused layer C_d:

$$\frac{1}{C} = \frac{1}{C_c} + \frac{1}{C_d} \tag{2}$$

For a conventional capacitors or parallel electrode capacitors, their capacitance can be determined by the following equation:

$$C = \frac{\varepsilon_r \varepsilon_0 A}{d} \tag{3}$$

where ε_r is the dielectric constant, ε_0 is the dielectric constant of vacuum, d is the distance between separated charges, and A is the surface area of the electrode.[16] According to electric double layer theory, if larger surface area of an electrode can contact with the electrolyte and if more charges can be absorbed onto the electrode, a supercapacitor can have higher capacitance. Therefore, porous materials (e.g. activated carbon), which have large specific surface area (SSA) and are highly conductive, are ideal supercapacitors electrode materials. It is possible to imagine that each pore in the porous electrode works as a conventional parallel electrode capacitor. Thus, as shown in **Figure 3**, a supercapacitor is composed of billions of small electric double layer capacitors. When a supercapacitor is converted to a circuit model, it is necessary to involve the resistance of each pore, the external resistance and the membrane resistance.[17]

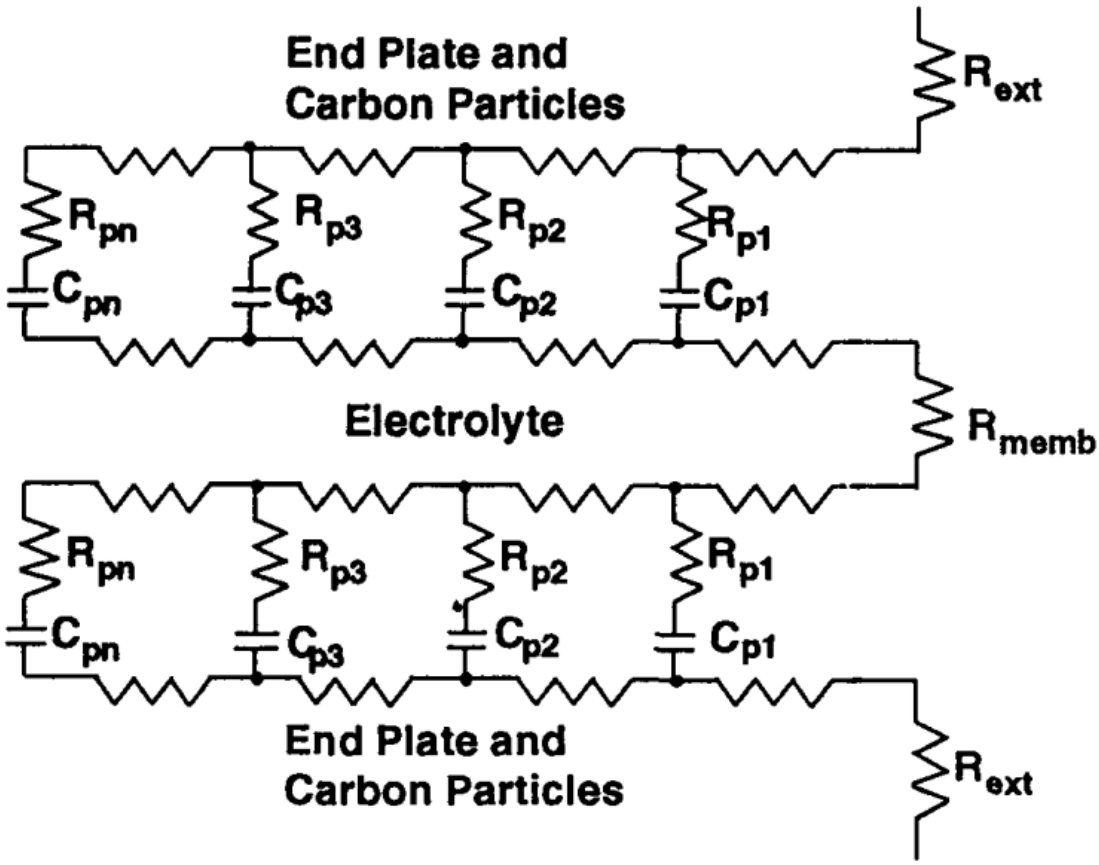

Figure 3: The circuit model of a supercapacitor which includes capacitance and resistance in each small pores as well as the external and membrane resistance. Reproduced with permission from [13]

1.4 Operation Principle of Supercapacitors

Unlike traditional capacitors whose energy is stored on the two metal electrodes separated by a dielectric media, Supercapacitors can store energy by forming electric double layers between the electrode and the electrolyte. Depending on whether a faradaic reaction occurs in an energy storage process, the capacitance of supercapacitor is classified into electric double layer capacitance and pseudocapacitance. The capacitor which has electric double layer capacitance is called electric double layer capacitor because it stores energy in an electrostatic way by separating electrons and electrolytic ions in the electric double layer. The capacitor which has pesudocapacitance is called electrochemical

capacitor since it stores energy in an electrochemical way by having fast faradaic redox reaction on the surface of electrodes.

1.4.1 Mechanism of Electric Double Layer Capacitors

In an electric double layer capacitor, there is no faradaic reaction involved in the energy storage process leading to the major difference from batteries whose electrodes have redox reaction during charging and discharging. On the electrodes of electric double layer capacitor, there are only absorption and desorption of ions when external voltage is applied. Thus, the electrode polarization of electric double layer capacitor is much faster than batteries due to the absence of limitation of chemical reaction kinetics. The fast charge and discharge features of supercapacitors can lead to better power performance than that of batteries. From the Ragone Plot shown in **Figure 4**, double layer capacitors have one magnitude higher power density than LIBs, solar batteries and fuel cells. In addition, faradaic reactions that occur in active materials on the electrodes may result in the swell or dissolve of active materials during charge and discharge. For example, the dendritic Li growth on the electrode during charge and discharge may penetrate the separator between two electrodes and causes a short circuit or even explosion.[18-21] Similar phenomena also present in silicon based anode of LIBs. Insertion and extraction of lithium ions can cause large volume and morphology change of silicon based electrode. This drawback is the main reason for degradation of electrode materials and inferior cycling stability of silicon based LIBs.[22-25] Lithium sulfur batteries also suffer from the loss of active electrode materials because sulfur can convert to dissolvable products during charge and discharge, which is well known as the “shuttle effect”.[26-30] However, electric double layer capacitors take the advantage of absence of faradaic reaction, so generally, double layer capacitors can maintain over 100,000 cycles. Compared with SCs, batteries can only survive thousands of cycles. Besides, double layer capacitors have more choices in terms of the electrolyte. Unlike batteries, the reactions of electrodes and electrolytes are fixed, double layer capacitors can adopt various electrolyte to satisfy different functions.

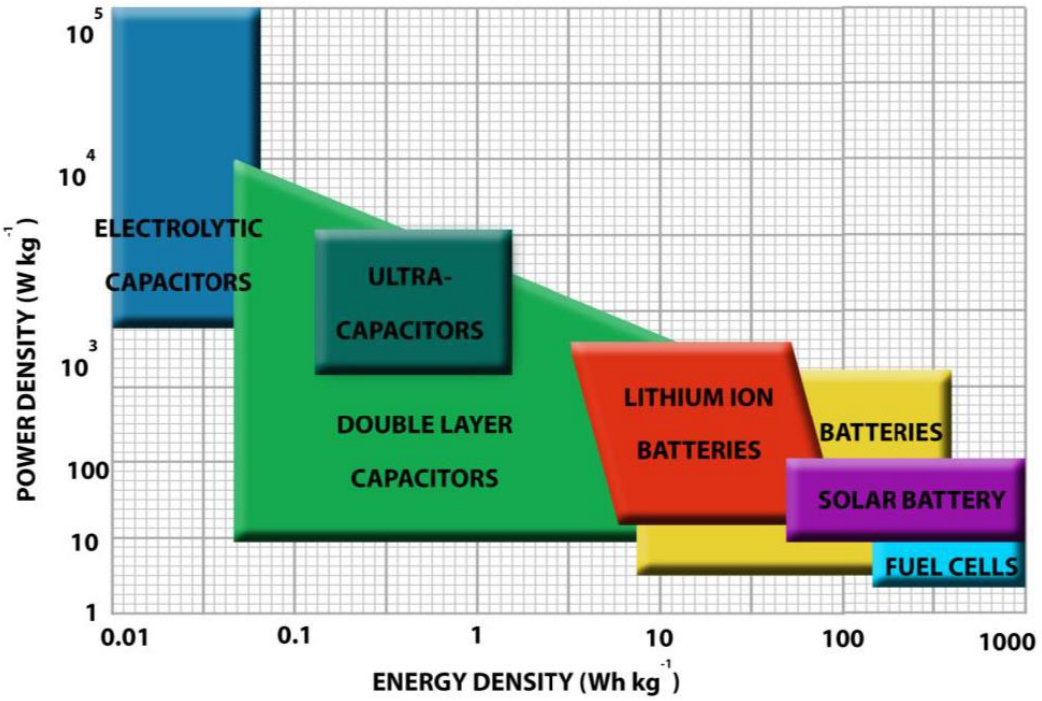

Figure 4: Ragone Plot showing energy density versus power density of common electrical energy storage devices. Reproduced with permission from [31]

1.4.2 Mechanism of Electrochemical Capacitors

Electrochemical capacitors are designed by using the active materials which can have fast and reversible reaction on the surface of electrodes. Due to the presence of faradaic reactions, electrochemical capacitors are similar to batteries. Thus, electrochemical capacitors are also called pseudo-capacitors, and the capacitance of electrochemical capacitors is defined as pseudocapacitance. When a voltage is applied on the two electrodes of electrochemical capacitors, faradaic redox reaction occurs on the surface of the electrode to transfer charges between electrodes and the electrolyte, generating circuit in the electrochemical capacitors system. Transition metal oxides such as MnO_2, [32-35] RuO_2, [36, 37] NiO, [38-41] Co_3O_4, [42-44] and V_2O_5 [45]are common active materials of electrochemical capacitors. In addition to conventional transition metal oxides, materials that possess pseudocapacitance also include: ternary metal oxides and metal hydroxides such as $NiCo_2O_4$, [46]$ZnCo_2O_4$,[47-49] $Ni(OH)_2$,[50-53] and $Co(OH)_2$;[54, 55] metal sulfides; and conductive polymers such as polypyrrole, polyaniline, and polythiophene.[56-60]

Generally, pseudocapacitance is higher than electric double layer capacitance because electrochemical capacitors not only store electrical energy on electrode surface but also store energy in the bulk of the electrode near the surface. The average specific capacitance of AC is only 150 F/g whereas specific capacitance of some pseudo-capacitors can reach over 1000 F/g [61-63]. Therefore, electrochemical capacitors are able to provide higher energy density than electric double layer capacitance according to the Equation (4).

$$E = \frac{1}{2} C V^2 \tag{4}$$

where *E* refers to energy, *C* is the capacitance, and *V* is the potential window of the capacitor. Some electrochemical processes can even increase the working potential window to further enhance the energy density. However, the rate of electrochemical processes is limited by chemical kinetics, resulting in the sacrifice of the power density. Moreover, electrochemical capacitors also suffer from poor cycle life due to the presence of reversible redox reaction, which can lead to loss of active materials.

1.5 SCs Capacitance, Energy Density and Power Density

In the structure of a supercapacitor, the two electrodes are able to be treated as two capacitors in series. Thus, the total capacitance of a supercapacitor can be described using the following equation:

$$\frac{1}{C_T} = \frac{1}{C_1} + \frac{1}{C_2} \tag{5}$$

or

$$C_T = \frac{C_1 C_2}{C_1 + C_2} \tag{6}$$

Herein, C_T is the total capacitance and C_1, C_2 are individual capacitance of each electrode. When the materials of two electrodes are same, C_1 is equal to C_2. According to equation (6), the total capacitance is half of individual capacitance of one electrode. This type of SCs is called symmetric supercapacitors. On the other hand, if C_1 is not equal to C_2, which illustrates the materials of two electrodes are different, the corresponding supercapacitors are named asymmetric supercapacitors. Based on Equation (6), the total capacitance of asymmetric supercapacitors is mainly determined by the electrode which has lower capacitance. Depending on the total capacitance and the operational voltage of the supercapacitor, it is possible to evaluate the total energy that can be stored in this device by Equation (4). In addition, the power of a supercapacitor is given by the following equation:

$$P = \frac{V^2}{4R_S} \tag{7}$$

where R_s represents the equivalent series resistance (ESR) of a supercapacitor. ESR generally derives from the intrinsic resistance of electrode materials and electrolyte, transfer resistance of the diffusion of ions from electrolyte to the surface of the electrode as well as the resistance between electrodes and current collectors due to poor contact.

Hence, in order to achieve a high power, it is necessary to reduce the inner resistance of a supercapacitor. On the other hand, since the value of power is proportional to the square of voltage, extending the potential window of a supercapacitor is a more effective way to increase the power. Basically, the potential window is associated with the intrinsic property, structure of the electrode materials and the stability of the electrolyte. With regard to energy density, it can be determined by Equation (4). In addition to increasing the potential window, enhancing the specific capacitance of a supercapacitor is also beneficial for its energy density. The specific capacitance is defined as the amount of capacitance possessed by unit mass of a material. The relationship of specific capacitance and mass is indicated by the following equation:

$$C_s = \frac{C_T}{W} \tag{8}$$

where C_s is the specific capacitance whose unit is F/g, C_T is the total capacitance of an electrode whose unit is Faraday (F), and W is the weight of the electrode whose unit is gram (g). However, although some materials have extremely high theoretical specific capacitance, they may be unable to exert their capacitance completely in practical operation because of the low utility ratio of electrodes. On one hand, the utility ratio is hampered by the bad diffusion of electrolyte ions, which makes the ions fail to arrive at the whole surface of the electrode. On the other hand, poor conductivity of the electrode materials can also reduce the utility ratio of an electrode by impeding the formation of an electric double layer or by retarding the reversible redox reactions. Thus, to boost the utility ratio of an electrode, it is essential to build a rational electrode structure with effective electrons and ions transition channels.

1.6 Carbon Materials for EDLC

Carbon materials are found to be suitable materials for supercapacitors electrodes in early stage due to their large reservation in nature, low cost, environmental benignity, facile processing procedure, controllable pore size, high specific surface area, high electrical conductivity, good chemical stability

and stable performance in wide range of temperature. Carbon materials are basically utilized in electric double layer capacitors. Due to the stability of carbon materials in electrolyte, it can hardly be used as electrochemical capacitors electrodes which store electrical energy by fast reversible reaction. As shown in **Figure 5**, the cyclic voltammetry of carbon materials are approximately rectangular without any redox peaks. With regard to the galvanostatic charge-discharge curves, the charge curves and corresponding discharge curves are basically symmetrical, indicating the high coulombic utility ratio of electrostatic energy storage method.

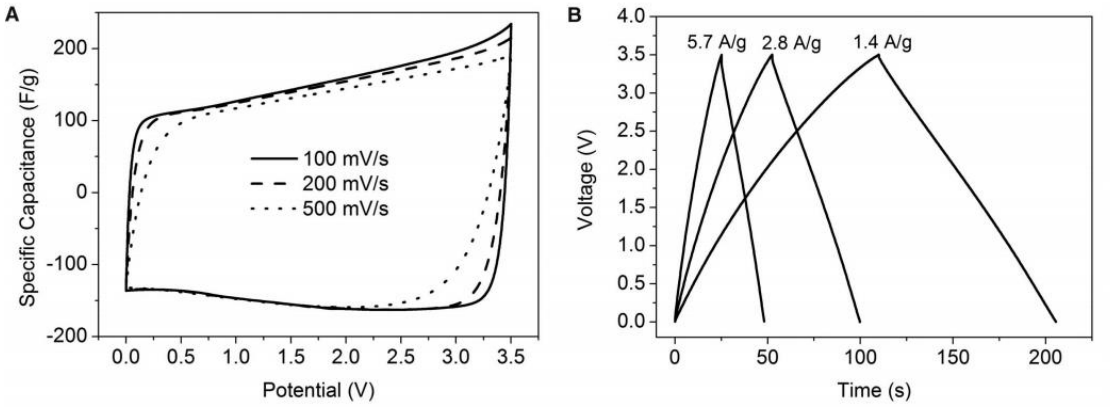

Figure 5: (A) Cyclic voltammetry curves of microwave exfoliation/reduction of GO electrode at different scan rate of 100 mV/s, 200 mV/s and 500 mV/s. (B) Galvanostatic charge-discharge curves of microwave exfoliation/reduction of GO electrode under different current density. Reproduced with permission from[64].

Since carbon materials are only able to store electrical energy on the surface of the electrode, the capacitance of carbon materials is mainly associated with the characteristics of electrode surface such as specific surface area, pore volume, pore shape, pore size distribution, and conductivity. As reported by Jiujun Zhang, [65] among all the factors mentioned above, the performance of carbon materials are dominantly influenced by specific surface area and pore size distribution. Currently many carbon materials with high surface area have been reported such as AC [66-70], templated porous carbon[71-73], carbon aerogels[74], carbon nanotubes (CNTs), [75-77] and graphene[78-80].

High specific surface area plays an essential role in supercapacitor electrode materials. Since carbonaceous materials only store energy on the interface between electrode and electrolyte by the absorption and desorption of charges, higher specific surface area can allow the electrode to accumulate more charges in unit mass materials. Based on Brunauer–Emmett–Teller (BET) theory, the specific

surface areas (SSA) of different carbonaceous materials are studied. SSA of commercial AC is between 500-1700 m^2/g. [81-83] The SSA of activated carbon fiber varies with the processing techniques. The highest SSA of AC can be more than 3000 m^2/g. [84, 85] SSA of templated porous carbons is mainly associated with the property of templates. Some templated porous carbons can achieve as high as 4000 m^2/g. [86-89]

In addition to specific surface area, pore size also has significantly effect on specific capacitance. But the mechanism of this effect is still not quite clear. A theoretical formula is reported by Huang *et al.*[90] In case of mesoporous carbon whose pore size is larger than 2 nm and smaller than 100 nm, the model showing the relation of pore size and specific capacitance with fixed SSA can be described in the following equation:

$$\frac{C}{A} = \frac{\varepsilon_r \varepsilon_0}{b ln\left(\frac{b}{b-d}\right)} \tag{9}$$

where *b* is the radius of the pores, *d* is the distance between electrolyte ions and carbon surface. Recent study shows that when the pore size is below 1 nm, the capacitance increases sharply and reaches the maximum value when the pore size is the same as that of ions, indicating the highest capacitance is achieved when a single ion is in one pore. Further research was carried out to demonstrate that it is necessary for ions to remove the solvation shells when they enter into pores.

1.6.1 Activated Carbon

Activated carbon materials not only have the general characteristics of carbonaceous materials such as benign conductivity, chemical stability, and application in a wide temperature range, but also have high SSA, making it preferred materials for supercapacitors. AC is enormously popular due to the low cost and facile processing techniques. Many carbonaceous materials, such as coke wood, and charcoal, can be used as precursors of AC. Materials with low degree of porosity are able to be processed to AC by suitable activation including chemical activation, physical activation, and hybrid activation. [91] Carbonization is usually applied to synthesize AC, since most of other elements such as hydrogen, oxygen, and nitrogen are removed by the heat treatment in the inert atmosphere. After calcination, the carbonized materials only generate a little porosity. In order to largely increase the SSA of carbonized product, further activation is necessary.

Basically two scenarios: chemical activation and physical activation, are able to be adopted. In chemical activation procedures, some activation agents such as $ZnCl_2$, H_3PO_4, KOH, K_2S and KCNS are added

and are subsequently removed by washing to obtain pores. Physical activation is also known as partial gasification which uses steam, carbon dioxide, and air as the activation agents. Following reactions may happen during the physical activation such as endothermic reaction of carbon with steam:

$$C + H_2O \rightarrow CO + H_2 \quad (10)$$

reaction of carbon with carbon dioxide:

$$C + CO_2 \rightarrow 2CO \quad (11)$$

reaction of vapor with carbon oxide:

$$CO + H_2O \leftrightarrow CO_2 + H_2 \quad (12)$$

The performance of supercapacitors using activated carbon electrodes is not only related to the surface area but also to the pore size distribution. It is reported that an activated carbon based supercapacitor with up to 3000 m^2/g specific surface area only has the specific capacitance less than 10 $\mu F/cm^2$, which is smaller than theoretical capacitance. Thus, the utility ratio of high specific surface area is also essential to the behavior of supercapacitors. [92] To increase the efficiency of surface area, it is necessary to adjust the pore shape, pore size distribution, and the pore structure. Generally, the capacitance of AC in aqueous electrolyte is from 100 F/g to 300 F/g.[93-96] However, in organic electrolyte, the capacitance is relative smaller (approximately 150 F/g). This is mainly because the ions in organic electrolyte are larger than the ions in aqueous solvent, making some small pores in the AC unable to store charges any more.

1.6.2 Carbon Nanotubes

Carbon nanotubes are advanced carbon materials due to their superior properties such as high conductivity, good mechanical property, benign chemical and thermal stability, as well as the unique porosity. Based on directions of rolling a graphene sheet, carbon nanotubes are categorized as Zig-zag

CNTs, chiral CNTs, and armchair CNTs. The atomic structures of various CNTs are shown in the following figures:

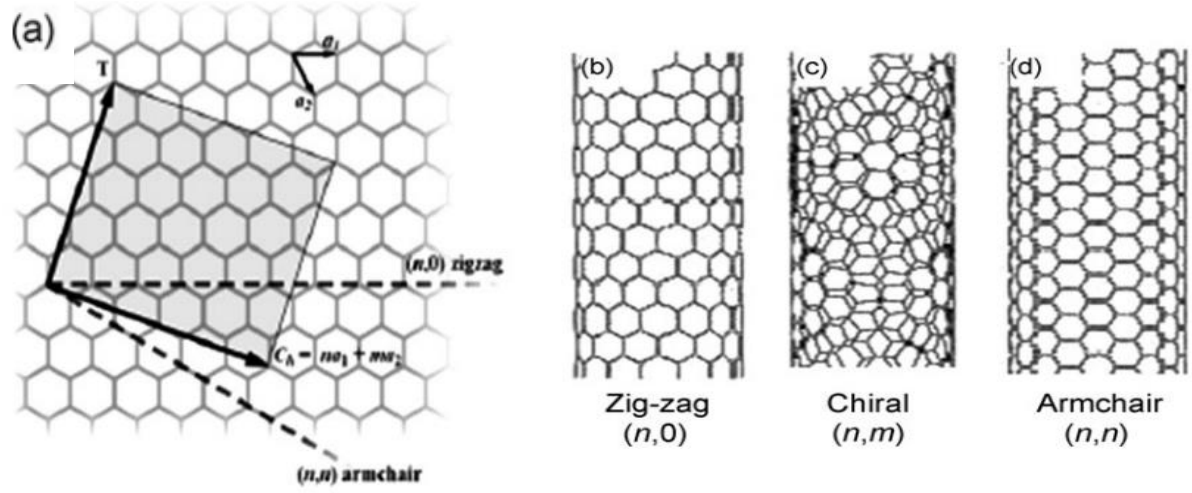

Figure 6: (a) Different atomic structures corresponding to the directions of rolling a graphene sheet. Atomic structure of Zig-zag CNTs (b), atomic structure of Chiral CNTs (c), and atomic structure of Armchair CNTs (d). Reproduced with permission from [97].

CNTs are preferred electrode materials for high power density devices owing to their low resistance. As mentioned above that the power is determined by Equation (7) which shows that a low resistance value can lead to high power density. Besides, the small resistance in CNTs is also able to show good rate capability. In addition to the good conductivity, the unique structure and mechanical stability has made CNTs good substrates for other active materials. Combination of CNTs and faradaic materials such as TiO_2, [98] MnO_2, [99-103] and V_2O_5[62], are widely studied. The composites take advantage of the high power density of CNTs and high energy density of faradaic materials.

1.6.3 Templated Porous Carbon

Owing to overwhelming advantages of porous carbon in the area of supercapacitors, active carbon cannot meet the requirements of high-performance supercapacitors. The templating methods are very effective to synthesize carbon materials with high specific surface area, interconnected pore structure, and proper pore size, which are essential factors for advanced supercapacitor electrodes.[104] Basically, the process of templating techniques includes the preparation of carbon precursors, introduce of the carbon precursors into the template, and removal of the template.

To synthesize porous carbon materials with different pore shape, pore order, and pore size, various templates have been used to fabricate specific porous carbon. Silica spheres are one of very common templates. Since the presence of silica spheres with different sizes, it is possible to produce high ordered porous carbon with micropores, mesopores, and macropores. A mesoporous carbon spheres with silica spheres as the templates have been studied and achieved 159 F/g at 0.5 A/g.[105] Other types of hard templates are also studied such as SBA-15 ordered mesoporous silica[106], MCM-41 mesostructured silica[107], and zeolites[108]. In addition to hard templates, soft templates (surfactant templates) such as Pluronic P-123 and F-127 are also common templates for synthesizing porous carbon. [109, 110] A three-dimensional ordered mesoporous carbon sphere electrode was synthesized by using Pluronic P-123 as the template. The mesoporous carbon sphere electrode can achieve a specific capacitance of 14 $\mu F/cm^2$ with specific surface area of 601 m^2/g and pore volume of 1.70 cm^3/g.

1.6.4 Graphene

Graphene is a two-dimensional carbon sheet forming by sp^2-hybridized. This specific honeycomb structure is possible to be built into many other allotropes of carbon such as CNTs, graphite, and fullerenes. Graphene was discovered during the study of graphite when people tried to utilize fewer layers. Finally, a single layer of graphite was exfoliated in Manchester University in 2004 by Geim and his colleagues.[111]

Basically, a single layer graphene is composed of hexagonal sp^2 carbon atoms. The specific structure exhibits high mechanical stability, thermal stability, and great electrical property. In addition, graphene also has extraordinary high specific surface area (2675 m^2/g) which especially benefits for the performance of electric double layer capacitors. If the large specific surface area can be fully utilized, the specific capacitance of an EDLC is able to reach 550 F/g, proving that graphene is a promising materials for supercapaictor electrodes.

Many graphene-based electrode materials of supercapacitors have been studied both in aqueous and organic electrolytes. Among the synthesis of these electrode materials, different methods have been adopted such as chemical modification, microwave irradiation, thermal treatment of graphene oxide at high temperature, and at low temperature but in vacuum circumstance. Normally, the capacitance of aqueous supercapacitors with graphene electrodes is between 130 F/g and 200 F/g, [112] and the capacitors tested in organic electrolyte show lower capacitance from 100 F/g to 150 F/g. The reason that the specific capacitance of practical graphene-based supercapacitors cannot reach theoretical

specific capacitance of 550 F/g is mainly because that graphene sheet has high possibility of restacking during the preparation, leading to the lack of sufficient utilization of surface area in graphene.

Due to the high conductivity and mechanical stability, graphene is also suitable for using as the substrate for active materials like faradaic materials with pseudocapacitance. A 3D macroporous graphene frameworks combined with thin layer of MnO_2 have been reported for supercapacitor electrodes. The porous graphene frameworks successfully offer high surface area, interconnected channels for electrolyte ions, and conductive channels for electrons. A thin layer of MnO_2 is essential for the high specific capacitance of 389 F/g at a current density of 1 A/g owing to its high pseudocapacitance.[113] The contribution of faradaic materials strongly depends on their effective surface being used and their uniform coating on the carbon substrates. Although pure carbon materials are hard to achieve high energy density and power density for supercapacitors, they still play an important role in obtaining high-performance supercapacitors owing to their high surface area and superior conductivity. Currently, one strategy of developing supercapacitors with high power density and energy density is to uniformly coat a thin layer of faradaic materials on carbon materials. With the help of high-surface-area and conductive carbon materials, active materials are able to exert high pseudocapacitance and greatly contribute to the energy density.

1.7 Faradaic Materials

Unlike carbon materials, which store charges in the Helmholtz Double layer, faradaic materials store charges with fast redox reactions on the surface or in the bulk of the electrode near the surface. Basically, the specific capacitance of carbon-based materials is from 10 $\mu F/cm^2$ to 50 $\mu F/cm^2$. However, the specific pseudocapacitance is approximately 10-100 times higher than carbon materials, which is very attractive. Therefore, pseudocapacitive materials are widely studied in recent years in order to develop advanced electrode materials for the next generation of supercapacitors. Typically, the pseudocapacitive materials are able to be divided into two categories: conductive polymers and transition metal oxides.

1.7.1 Conductive Polymers

Conductive polymers are generally low-cost, environmental friendly, and their source is extensive. Besides conductive polymers have high conductivity, wide potential widow, and high porosity, making them promising candidates for supercapacitor electrode materials. During charging and discharging process, redox reactions occur not only on the surface of the conductive materials but also in the bulk.

When oxidation reaction occurs, ions are attracted from the electrolyte to the polymers, and released to the electrolyte during reduction. The redox reactions are highly reversible, since there is no phase transition, making conductive polymers competent for long cycle life. The conductive behavior of conductive polymers is mainly because conductive polymers are positively or negatively charged by oxidation or reduction processes. These specific oxidation and reduction processes are generally named as doping. Conductive polymers only have conductive property at a doped state.

There are three types of conductive polymers commonly used as electrode materials for supercapacitors: polyaniline (PANI), polypyrrole (PPy), polythiophene (PTh), and their derivative materials. Since conductive polymers are active and can work well only under certain conditions, it is important to use them in the right electrolyte and right potential ranges. For example, the negative doping potentials of PANI and PPy are usually lower than the reduction potential of electrolyte, therefore they can only be positively doped and better to be used as the cathode electrode materials. In addition, PANI performs better in acidic electrolyte, where contains the necessary protons for PANI during its charging and discharging.[114] The working potential window is also essential for conductive polymers. Under an improper potential, conductive polymers may be degraded or lose the conductivity. Thus, the potential range plays a key role in the performance of conductive polymer based supercapacitors.

1.7.2 Transition Metal Oxides

Transition metal oxides (TMOs) are widely studied as the electrode materials for supercapacitors because of their high pseudocapacitance and better cycle stability compared to conductive polymers. As faradaic materials, TMOs have two or more oxidation states in the same phases. When charging and discharging take place, TMO_S are able to convert between different oxidation states and protons can insert into and extract from the oxide lattice during reduction and oxidation. The redox reactions are fast and reversible, since no phase changing occurs in the process. Several TMOs such as RuO_2, [115] MnO_2, [116] V_2O_5, [117] NiO, [118] and Co_3O_4 [119], have been found to have the above properties and been tested as supercapacitor electrode materials.

RuO_2 is one of extensively studied TMOs for the electrode of supercapacitors, which exhibits high conductivity, long cycle life, high capacitance, and high rate capability. In addition, RuO_2 can have high potential window, thus facilitating the energy density of RuO_2-based electrodes. Three oxidation states are accessible for RuO_2 at the voltage of 1.2 V to attract and release ions during charging and

discharging. Electric double layer mechanism also presents in RuO_2 electrodes; however, up to 90 % of the total capacitance is contributed by pseudocapacitance. The pseucapacitance of RuO_2 is widely studied in both acidic and alkaline electrolyte, and it is reported that RuO_2 can exhibit different faradaic behaviors with distinct reversible redox reaction mechanisms. [120] In an acidic solvent, the rapid redox reaction can be described as the following chemical equation:

$$RuO_2 + xH^- + xe^- \leftrightarrow RuO_{2-X}(OH)_X \quad (13)$$

where protons are absorbed to the surface of RuO_2 and the RuO_2 can convert from oxidation states Ru(II) to Ru (IV). However, the conversion of oxidation state is different in alkaline environment. When discharge occurs, RuO_2 will be oxidized to higher valence state compounds in alkaline electrolyte. Generally, RuO_2 based electrode materials can achieve high capacitance and moderate rate capability. A RuO_2/CNT nanocomposite has been reported with a specific capacitance up to 953 F/g, which is approximately 10 times higher than the specific capacitance of normal carbon materials. [121] Although RuO_2 is very attractive due to the high pseudocapacitance, it is still hindered by the high cost and limited reservation in nature for extensively application.

Therefore, transition metal oxides with low cost, extensive source in nature and high theoretical specific capacitance are highly demanded for the next generation supercapacitors. Many transition metal oxides have been explored as supercapacitors electrode materials such as the oxides of nickel, cobalt, iron, and vanadium. However, among all the transition metal oxides, manganese dioxide holds the brightest promise in pseudocapacitive supercapacitor electrode materials and has been most widely investigated because of the low cost, large natural reservation, high theoretical capacitance (1370 F/g), and nontoxicity. [122] The pseudocapacitive behavior of MnO_2 is typically considered as the surface adsorption of Cations such as K^+ and Na^+ or Protons (H^+). The mechanism can be generally described as the following chemical equation:

$$MnO_2 + xNa^+(K^+) + yH^+ + (x+y)e^- \leftrightarrow MnOOC_xH_y \quad (14)$$

The redox reaction of MnO_2 in electrolyte is fast, reversible, and continuous, thus leading to a cyclic voltammetry similar to that of carbon materials. MnO_2 electrodes are usually tested in aqueous neutral electrolyte with a specific capacitance of more than 200 F/g. Compared to the theoretical specific capacitance of MnO_2, the practical specific capacitance of MnO_2 is much lower, which is ascribed to the low usage of MnO_2 materials due to their interior conductivity and agglomeration. Therefore, many methods have been considered to increase the utility ratio of MnO_2. The most common method that

researchers thought out is to combine MnO_2 with carbon based materials, which have better conductivity and can be used as a stable framework to hinder the agglomeration of MnO_2. To date, many nanocomposites involving MnO_2 have been reported such as MnO_2/graphene, MnO_2/CNT, MnO_2/porous carbon, and MnO_2/carbon fiber etc. [32, 123-126]

1.8 Summary

In order to apply advanced energy storage devices in commerce with high energy density and high power density, supercapacitors still need to overcome some challenges. The largest obstacle for supercapacitors to compete batteries is their low energy density. Typically, pseudocapacitive materials are adopted to mitigate this problem. However, pseudocapacitive materials always suffer from low utility ratio. Thus, it is essential to design a rational structure to increase the contribution of pseudocapacitive materials, and meanwhile, provide effective electron and ion channels to achieve high power density.

In this project, MnO_2, as a promising supercapacitor electrode material, is used to combine with porous carbon with rational design structure for advanced supercapacitor electrode. The high conductive porous carbon is able to use as effective electron transmission channels to make MnO_2 be utilized more efficient. On the other hand, porous carbon is also an extremely stable framework for MnO_2 to prevent active from agglomeration during charging and discharging. In addition, the hierarchical pores in the porous carbon are capable of increasing the specific surface area and of enhancing the efficiency of ion transportation in the active materials.

Chapter 2

Structural and Electrochemical Characterization Techniques

Structural and electrochemical characterization techniques play crucial roles in the design of nanostructured electrode materials. Structural characterization techniques are essential for researchers to recognize if they have achieved the expected materials and structures, and meanwhile, they are also helpful to obtain a basic understanding of the mechanism within their experiments. By using scanning electron microscope (SEM) and transmission electron microscope (TEM), it is possible to obtain the morphological information of the samples. X-ray diffraction (XRD) is an effective instrument to provide samples' composition and crystalline structure. Thermogravimetric analysis (TGA) can help to determine the proper ratio of various materials in a composite. Besides, Raman spectroscopy, micrometric analyzer, and Energy-dispersive X-Ray (EDX) spectroscopy, etc. are also necessary characterization techniques for nano-scale materials, which can help to characterize materials and to modify the experiment to achieve expected results. In addition, electrochemical analysis is also indispensable for this project to evaluate the electrochemical performance of the as-synthesized materials. Several electrochemical analysis such as cyclic voltammetry (CV), galvanostatic charge-discharge (GCD), electrochemical impedance spectroscopy (EIS), are involved in this project.

2.1 Scanning Electron Microscopy

Scanning electron microscopy is an electron microscope which can obtain sample's information by using electron beams to scan the surface of samples and obtain 3D high-resolution images. It is an effective instrument to detect the topology and composition of samples, which allows researchers to unveil the morphology and the structure of microscale and nanoscale materials. A typical SEM image is shown in the following figure:

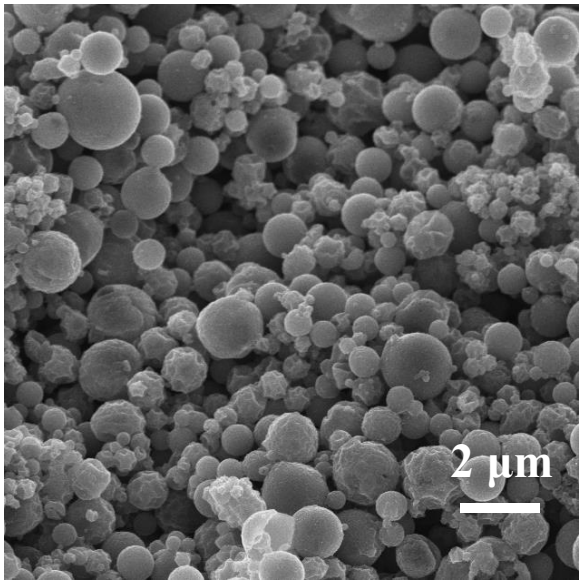

Figure 7: A SEM image of a MnO_2/porous carbon nanocomposite sample.

As shown in the **Figure 7**, it is possible to observe the spherical morphology of porous carbon spheres whose diameters range from 500 nm to 2 µm. In some specific particles, it is also able to detect the mesopores on the surface of carbon spheres; however, to confirm the presence of micropores, higher resolution images should be used.

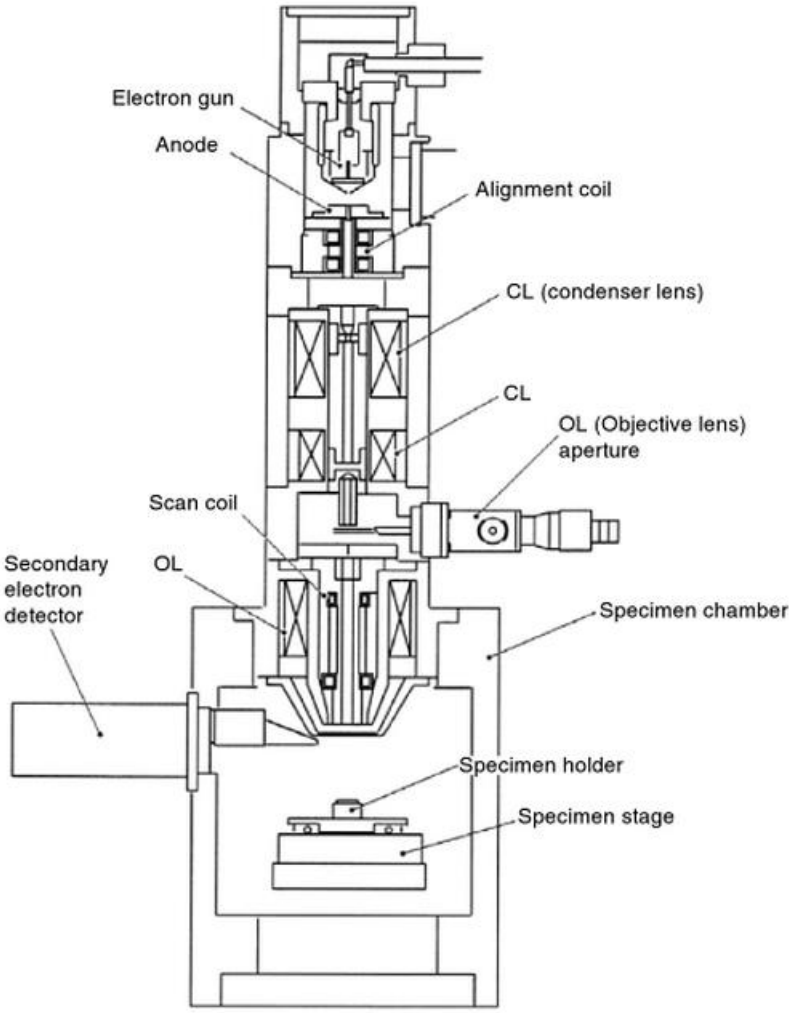

Figure 8: A schematic view of a SEM (JSM-5410, courtesy of JEOL, USA). Reproduced with permission from[127].

The **Figure 8** has shown the general configuration of a SEM. Basically the SEM has a column shape. On the top of the columns is the electron gun which can produce electrons with the energy of 0.1-30 keV. Below the electron gun is the condenser lens, apertures, and objective lens, which can help to reduce the diameter of electron beam and focus the electron beam on the specimen. To prevent the electrons from being scattered by air, a high-vacuum atmosphere with less than 10^{-5} mbar is created.

When is SEM is working, electrons are produced by the electron gun and accelerated by electric field to reach a high energy level. Subsequently, the beam is condensed by condenser lens and apertures to

nanoscale and reaches the specimen holder to scan samples. After electrons interact with samples, the properties of samples will be reflected, collected, amplified and produced as high-resolution images.

2.2 Transmission Electron Microscopy

Transmission electron microscopy is another microscopy technique, which is similar to SEM. However, in a TEM, an ultra-thin specimen which is less than 200 nm is used so that a beam of electrons can transmitted through the specimen. The beam of electrons with high energy will interact with the sample and form a high-resolution image. Basically, TEM is able to get images with higher resolution than SEM, because an electron has extremely short de Broglie wavelength which can allow researchers to explore the details such as a single atom and the arrangement of crystal lattices.

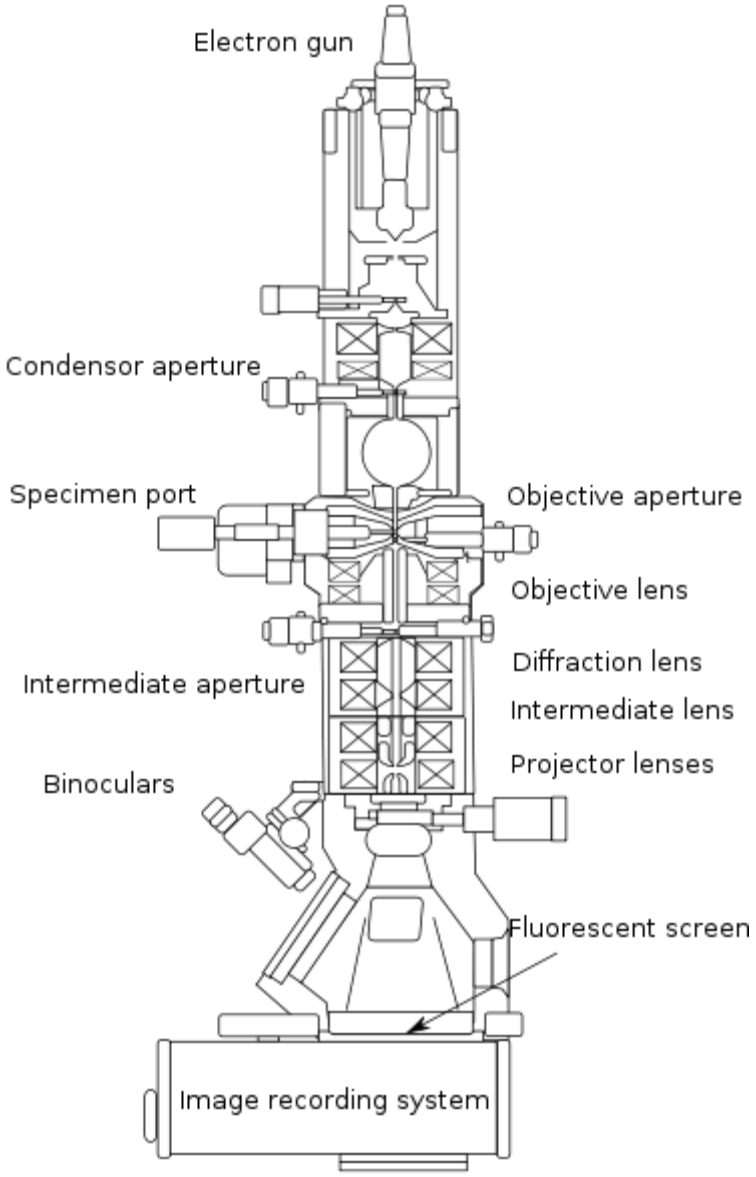

Figure 9: A schematic view of a TEM.

The configuration of a TEM is similar to a SEM. A TEM system generally consists of an electron gun, electron lens, apertures, a specimen stage, and a vacuum system. The electron gun is on the top of the whole system and is the electron source. After electrons are emitted from the electron gun, they will be accelerated. Different from SEM, the energy of electrons is 100 keV-400 keV which is much higher than the energy in SEM. As shown in **Figure 9**, apertures and electron lens are below the electron gun which can condense the electron beam. Electron lens is mainly operated by electrostatic or

electromagnetic methods to focalize parallel electron rays. Subsequently, the electrons will interact with the sample to form transmitted images which are projected onto the florescent screen.

2.3 Nitrogen Adsorption/ Desorption Isotherm Technique

Nitrogen adsorption/desorption isotherm technique is a powerful tool to identify the surface area and pore volume of porous materials. The adsorption/desorption is carried out at very low temperature, around the boiling temperature of liquid nitrogen. Generally, the adsorption of gas molecules on solid surface is reversible because of the weak physical bond with Van der Waals force. Dependence on the pore structure of different materials, the adsorption/desorption isotherm (an analysis method) can be classified into various types. Six basic types of Nitrogen adsorption/desorption isotherm are shown in the following figures. Herein, Type I isotherm generally occurs in materials with micropores. Type II isotherm indicates non-porous materials. Type III isotherm shows a typical plot of vapour adsorption. Type IV and V isotherms with hysteresis loop indicates the presence of capillary condensation in mesoporous materials. Type VI isotherm usually occurs in special carbon.

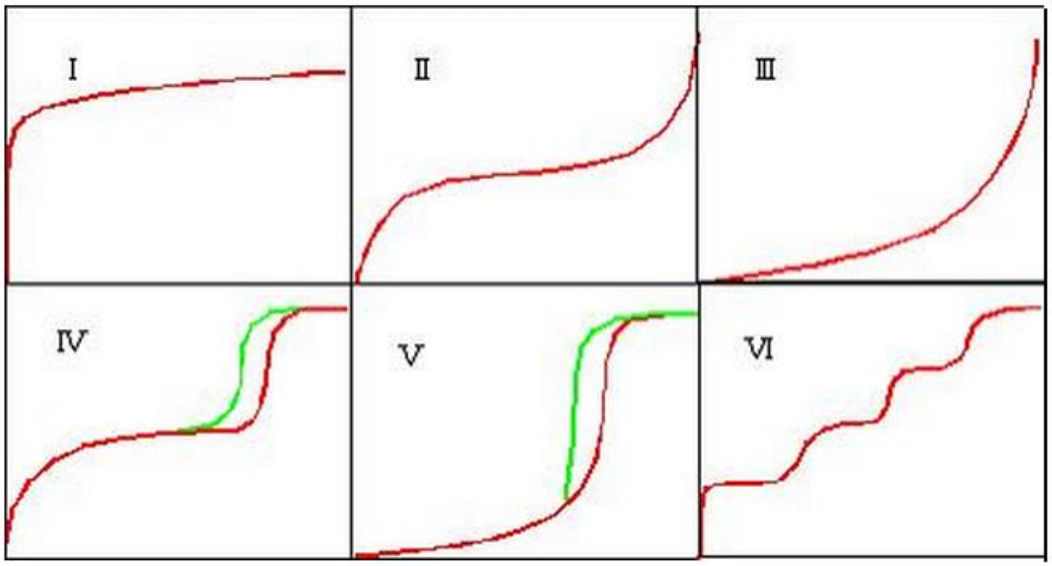

Figure 10: A schematic view of different types of Nitrogen adsorption/ desorption isotherms.

The sample which is going to be tested is kept at liquid nitrogen temperature. Adsorbate is introduced consecutively to the sample. Due to the injection of adsorbate gas, the pressure decreases and becomes stable at the equilibrium pressure. The equilibrium pressure is measured with the increase of the amount

of gas that is adsorbed. Finally, the amount of gas which is adsorbed can be calculated from the equilibrium pressure.

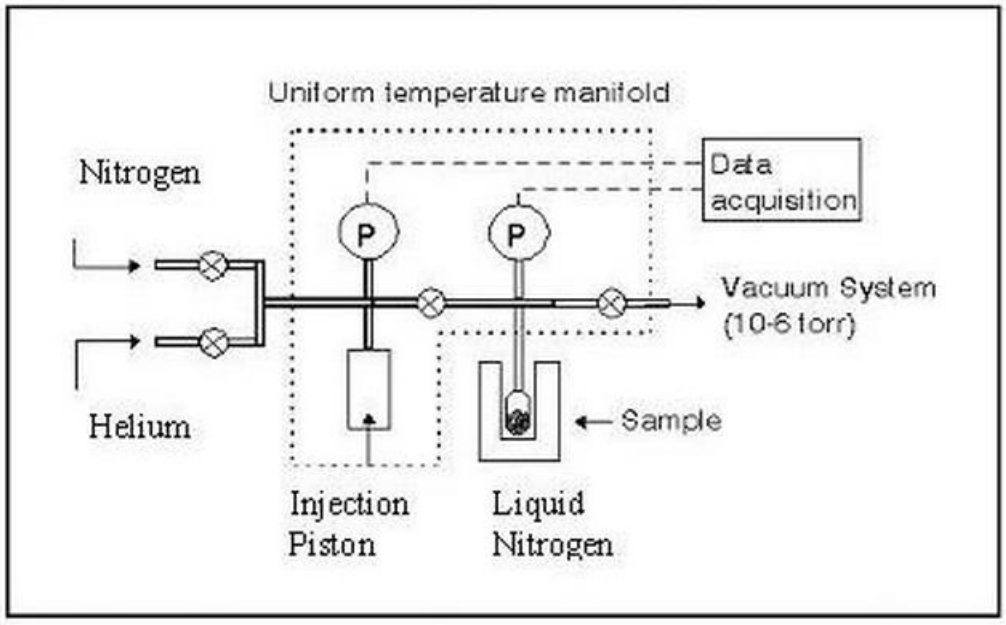

Figure 11: A schematic view of the configuration of Nitrogen adsorption/ desorption instrument.

Based on the BET theory, which is established and named by Stephen Brunauer, Paul Hugh Emmett, and Edward Teller; the specific surface area can be obtained by Nitrogen adsorption/desorption method. The BET theory is an extension of Langmuir theory upon some proper hypotheses. The principle of BET theory is specifically shown in the following equations:

$$\frac{1}{v[\left(\frac{p_0}{p}\right)-1]}=\frac{c-1}{v_m c}\left(\frac{p}{p_0}\right)+\frac{1}{v_m c} \tag{14}$$

where v is the volume of absorbed gas, p is equilibrium pressure, p_0 is saturation pressure, v_m is the volume of monolayer absorbed gas, and c is the BET constant. The BET constant can be determined by the following equation:

$$c=\exp\left(\frac{E_1-E_L}{RT}\right) \tag{15}$$

where E_1 and E_L are the first layer heat of adsorption and other layers heat of adsorption. Suppose if $\varphi = p/p_0$, the Equation (14) can be written as a function of $\frac{1}{v}\cdot\frac{\varphi}{1-\varphi}$ with φ as the variable. The function

can be plotted as a straight line when φ is in the range of $0.05 < \varphi < 0.35$ (**Figure 12**). Suppose if the slope of the straight line is *A* and the y-intercept is *I*, it is possible to obtain the following equations:

$$v_m = \frac{1}{A + I} \tag{16}$$

$$c = 1 + \frac{A}{I} \tag{17}$$

Finally, the specific surface area (BET surface area) can be determined by the following equation:

$$S_{BET} = \frac{(v_m N s)}{V a} \tag{18}$$

Where v_m is molar volume of the monolayer adsorbate gas, *N* is the Avogadro's number, *s* is the cross section of the adsorbing species, *V* is the molar volume of absorbate gas, and *a* is the mass of adsorbent.

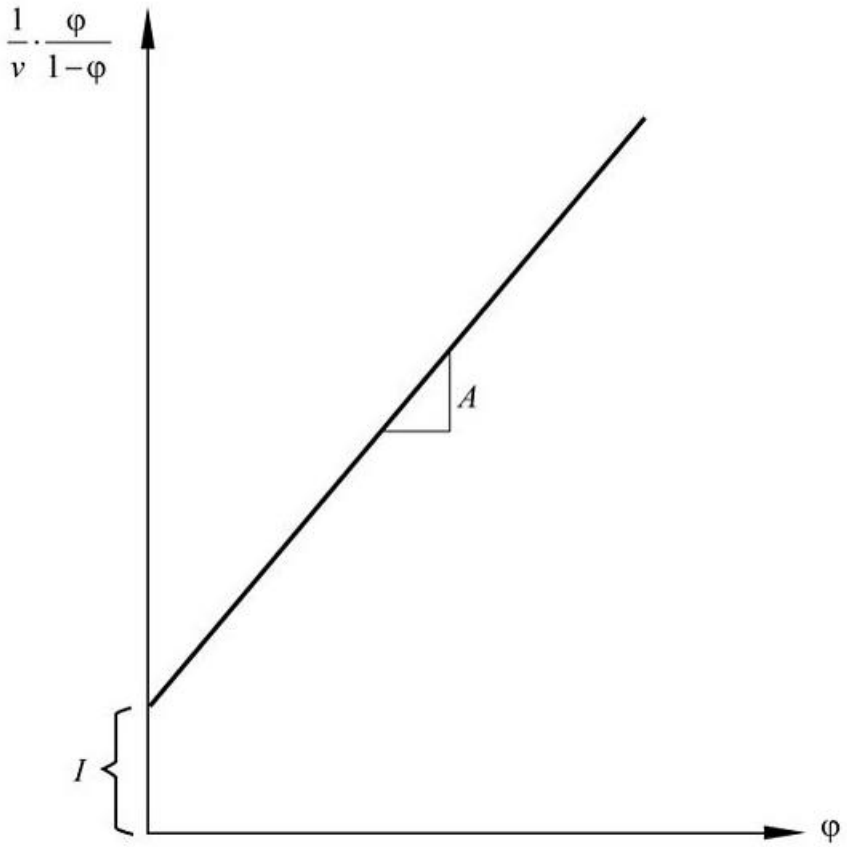

Figure 12: A schematic illustration of BET plot.

2.4 Raman Spectroscopy

Raman spectroscopy is a powerful technique to detect the vibration, rotation, and other low-frequency modes of a system, which is a helpful technique to identify a molecule in chemistry. When a molecule is irradiated by electromagnetic radiation, the radiation will interact with the bonds or electron cloud of the molecule. Then, the Raman Effect occurs in a form of inelastic scattering. When the electromagnetic radiation impinges the molecule, the molecule is excited from the vibrational energy state to virtual energy state. After relaxation for a short period of time, there is a form of inelastic scattering with a lower (Strokes) or higher energy (anti-Strokes). The molecule will come back to vibration energy state from virtual energy state. However, this vibration energy state is different from the original vibration energy state, before electromagnetic radiation has interacted with the molecule. This mainly because that although elastic scattering (Rayleigh scattering) has very strong signal strength, inelastic scattering still exists, causing the energy of electromagnetic radiation shift up or down.

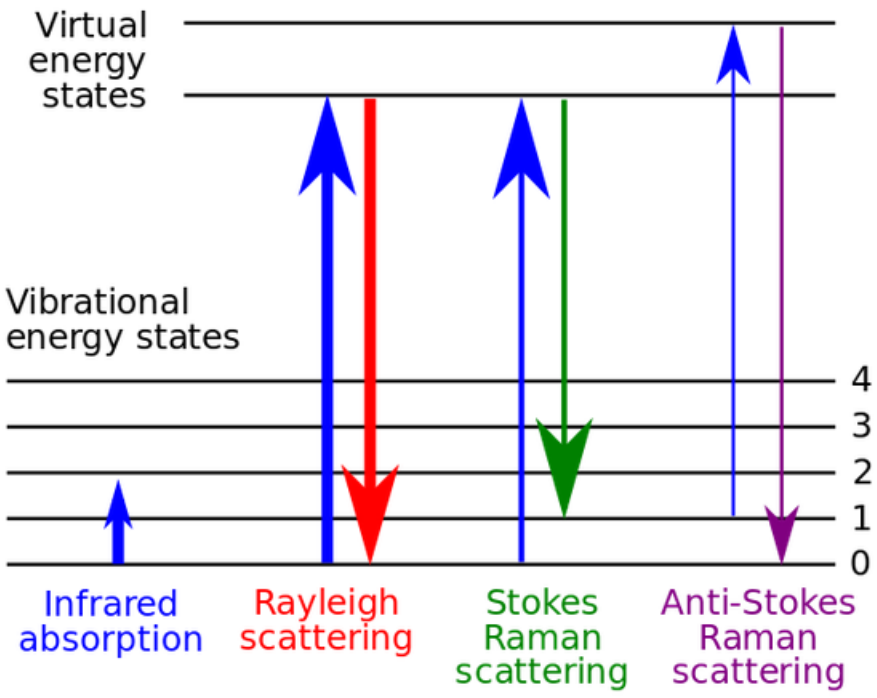

Figure 13: A schematic view of the energy level involved in Raman signal and the types of scattering taking place in Raman spectroscopy. The thickness of the line can roughly indicate the strength of signal from different transitions.

The electromagnetic radiation is usually in a form of laser light. The laser light can be in the visible range, near infrared range, and near ultraviolet range. Generally, the type of laser light used in Raman spectroscopy depends on the property of the samples. The samples in Raman can exist in many states. No matter solid, liquid, or even gaseous samples are all able to be characterized by Raman spectroscopy. In the area of supercapacitors, Raman spectroscopy is commonly used to analyze the structural disorder and degree of defects present in carbon materials. Typically, two types of peaks are often observed with carbon materials, referred to as D band and G band. The G band is mainly ascribed to the sp^2 bonded carbon species and D band is related to the Raman scattering resulting from the structural disorder such as vacancies, impurities, and other defects. The intensity of the D band to G band, which can also be expressed as I_D/I_G, can provide effective information about the presence of heterogeneous atomic doping which is a common method to enhance the performance of supercapacitor electrode materials.

2.5 X-ray Photoelectron Spectroscopy

X-ray photoelectron spectroscopy (XPS) technique focuses on the surface chemical characterization from the top 0 to 10 nm of a sample to measure the elemental composition of the surface, empirical formula of pure materials, elements that contaminate a surface, chemical or electronic state of each element, and uniformity of elemental composition. To analyze the bulk of a material, some treatment is necessary such as fracturing, cutting, and scraping to remove the contamination on the surface and expose the deep layer for further characterization.

The samples of XPS are usually solid, since XPS requires high vacuum atmosphere, approximately 10^{-8} millibar; or ultra-high vacuum, less than 10^{-9} millibar. When a sample material is irradiated by the X-ray beam, the electrons on the surface of the material will escape, and it is able to measure the number and kinetic energies of the electrons. Then, the binding energy can be determined by the following equation:

$$E_{binding} = E_{photon} - E_{kinetic} - \emptyset \quad (16)$$

Where $E_{kinetic}$ is the kinetic energy of the escaped electrons, E_{photon} is the energy of incident X-ray photon, and $\emptyset$ is the work function which depends on both spectrometer and the material. E_{photon} is a known energy which can be calculated by the Equation (17).

$$E_{photon} = hv \quad (17)$$

where *h* is the Plank constant and *v* is the frequency of X-ray beam.

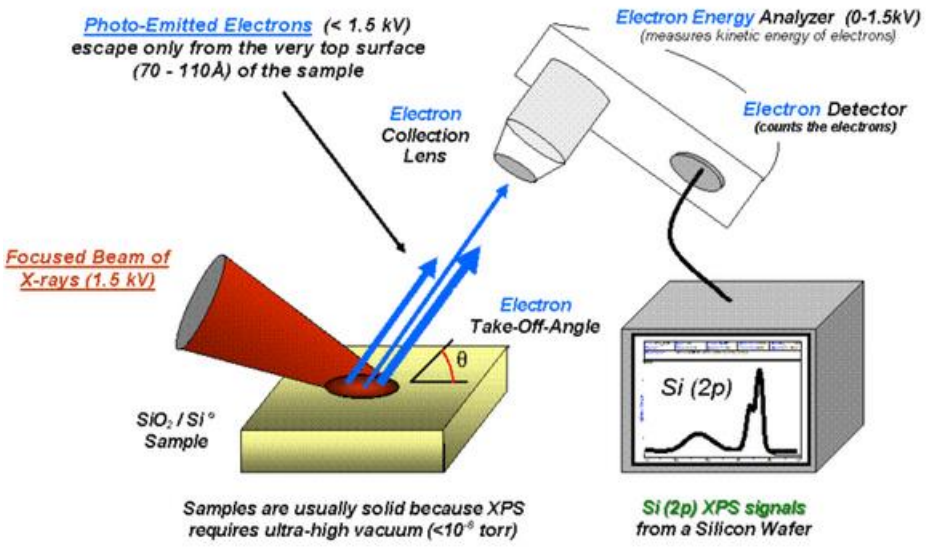

Figure 14: A schematic view of the configuration of the XPS.

As shown in **Figure 14**, the emitted electrons, resulting from the irradiation of X-ray, are received by the electron collection lens. The kinetic energy of the emitted electrons will be analyzed by the electron energy analyzer and be converted to XPS signals.

2.6 Thermogravimetric Analysis

Thermogravimetric analysis (TGA) is a useful characterization technique to measure the thermal property of a sample, such as the melting point, boiling point, dehydration temperature and so on. In addition, TGA can also characterize the composition of a material by measuring the weight of a material under continuously changing temperature. For example, in this project, the sample is heated in the TGA burning chamber at atmosphere to determine the composition of MnO_2 and porous carbon. A ramp rate of 10 ℃/min is used to increase the temperature from room temperature to 800 ℃. With the increase of the temperature, moisture and porous carbon will be completely converted to water vapor and CO_2 respectively; however, MnO_2 cannot combust in air. Thus, according to the weight recorded by the precise balance in the TGA chamber at different temperature, the composition of MnO_2 is able to be calculated.

2.7 Supercapacitor Electrochemical Characterization Techniques

Electrochemical characterization techniques are very crucial for the evaluation of the electrochemical performance of electrode materials. Typically, a high-performance supercapacitor electrode material has many necessary properties such as good rate capability, high capacitance, high columbic efficiency, and low electrical resistance. Basic electrochemical characterization techniques involved in supercapacitor evaluation are galvanostatic charge discharge (GCD), cyclic voltammetry (CV), and electrochemical impedance spectroscopy (EIS).

In order to characterize the electrode material, an active electrode can be tested in a three electrode system, which is common for testing half cells. In a three electrode system, there are three components, working electrode, counter electrode, and reference electrode, where the active electrode is used as the working electrode. To record the potential of this working electrode, a reference electrode whose potential is almost a constant in a narrow potential range is used. In addition, a counter electrode which is usually a platinum wire, is also necessary to carry the current coming across from the working electrode, which can prevent the reference electrode from carrying current, leading to potential change of the reference electrode.

Full cell test, which usually takes place in a two electrode system, can show more practical performance of active materials than half cell, because full cell test works similar to a practical supercapacitor which has a positive electrode and a negative electrode. In a full cell system, both electrodes are assembled with active materials. According to if the active materials in the two electrodes are same or not, the supercapacitor can be divided into symmetric and asymmetric supercapacitor respectively. Depending on Equation (5), the maximum total capacitance is achieved when two electrodes have the same capacitance. Thus, it is significant to control the loading of each electrode to obtain a high total capacitance.

In this project, the working electrode is assembled by drop casting the electrode slurry directly onto a current collector made from nickel foam. In addition to active electrode materials, 10 wt% of conductive carbon black and 10 wt% of polyvinylidene fluoride (PVDF) are utilized as conductive additive and binder material respectively. The electrode slurry should be well dispersed onto the current collector to enhance the utilization efficiency of the active material. Wet electrodes need to be dried in a vacuum oven and pressed at 2.0 MPa to enhance the contact between active materials and current collectors. After these procedures, electrodes are able to be characterized by different techniques in a three

electrode system or in a full cell. The details of various electrochemical analysis techniques will be discussed in the following sections.

2.7.1 Cyclic Voltammetry

Cyclic voltammetry is a common electrochemical characterization technique to study the electrochemical property of a material. A potential on the working electrode ramps linearly with time from the open circuit potential to a set potential. Then the potential returns to the other set potential in the same way. Both the scan rate and cycles can be controlled. Basically, the redox potential of the active material should be contained within the potential window of CV to analyze the electrochemical property of the material. A typical cyclic voltammogram is shown in **Figure 15**. The corresponding current is a function of the scanning potential. From a cyclic voltammogram, researchers can obtain a large amount of qualitative information with regards to the active material such as the capacitance, conductivity, polarization, reversibility and the position of reduction and oxidation peaks.

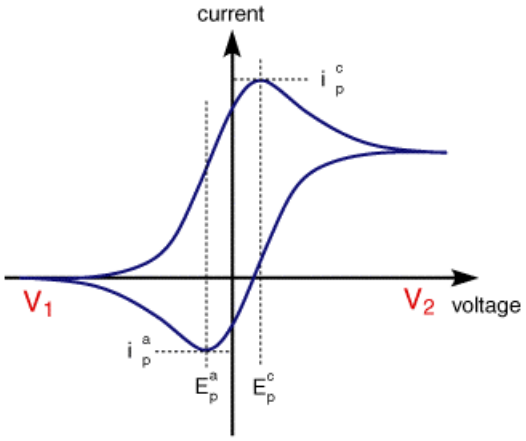

Figure 15: a schematic view of cyclic voltammogram.

From the area of a CV curve, the specific capacitance of the active material can be calculated with the following equation:

$$C = \frac{1}{2}\left(\frac{\int idv}{mvU}\right) \tag{18}$$

where C is the specific capacitance, m is the mass of active material, U is the potential window, v is the scan rate, and $\int idv$ is the area of the CV curve. Since a cycle contains both charging and discharging processes, the entire area should be divided by two to obtain the specific capacitance.

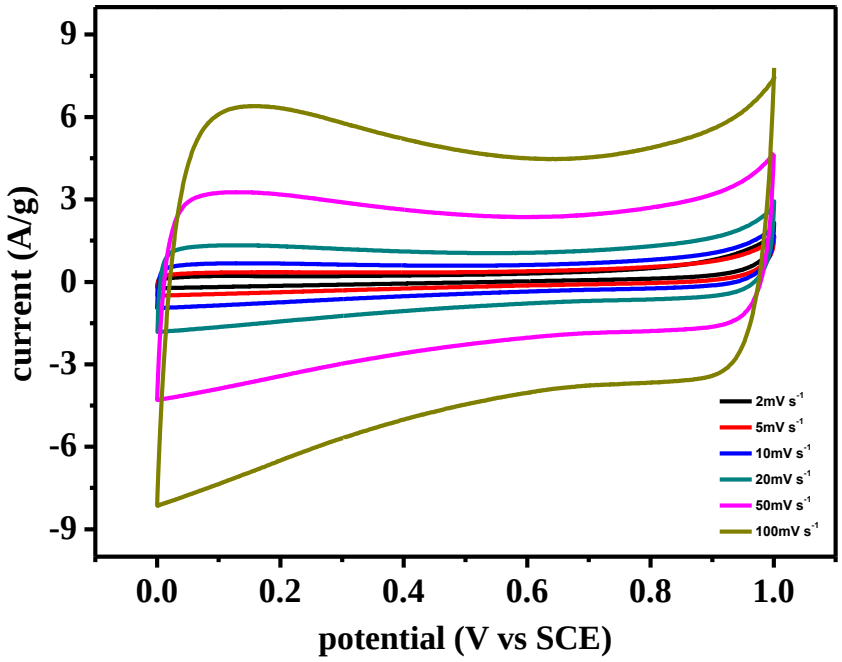

Figure 16: Cyclic voltammogram of as synthesized partially graphitized hierarchical porous carbon spheres at various scan rates, which are tested in 1 mol/L sodium sulphate solution with three electrode system.

An example is shown in **Figure 16**; the CV curve of carbon materials with electric double layer capacitance is similar to rectangular with no redox peaks. With the increase of scan rate, the area of CV curves becomes larger and larger. However, due to the growing resistance at high scan rate, the specific capacitance will slightly decrease. Thus, it is significant to reduce the resistance at high scan rate by developing a rational structure for supercapacitor electrode materials.

2.7.2 Galvanostatic Charge and Discharge

Galvanostatic charge and discharge is a more accurate technique to evaluate the specific capacitance of active materials than CV method. Positive and negative constant currents come across the working electrode to charge and discharge the electrode in a set voltage range with recording the time. A typical GCD curve is shown in **Figure 17**, in which the voltage is drawn as a function of the time. Then, the specific capacitance can be determined by the potential window, current density and discharge time with the following equation:

$$C = \frac{\mathrm{I}\Delta t}{mU} \tag{19}$$

where I is the current, Δt is the discharge time, m is the mass of electrode material, and U is the potential window.

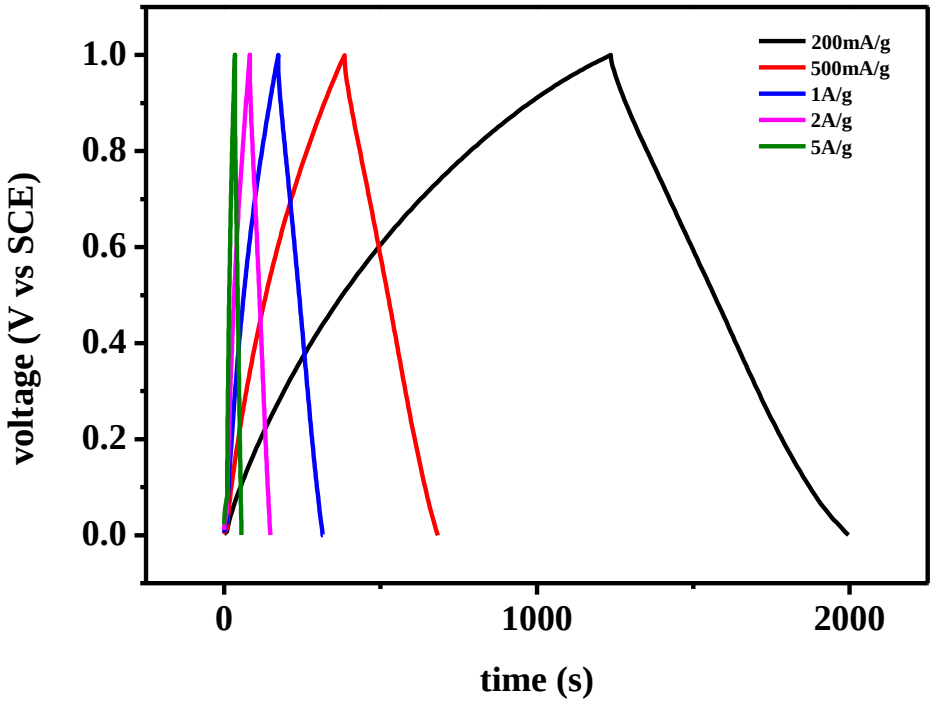

Figure 17: Galvanostatic charge-discharge profile of MnO_2 and porous carbon nanocomposite with the voltage range from 0.0 V to 1.0 V vs. saturated calomel electrode (SCE) at different current densities

2.7.3 Electrochemical Impedance Spectroscopy

Electrochemical impedance spectroscopy is a powerful tool to analyze the impedance of an electrochemical system, wherein an alternating potential with changing frequency is applied onto an electrochemical system to test the ratio of alternating potential to the corresponding current signal as a function of sinusoidal wave frequency. The Impedance resulting from the quotient of potential divided by current is a complex number. To use the real part as X axis and the imaginary part as Y axis, it is able to obtain a Nyquist plot, which is important in the analysis of electrochemical impedance. Generally a Nyquist plot consists of a semicircle followed by a 45° straight line. In practice, at high frequency region, the intercept on X axis represents the series resistance of the electrode. The semicircle region mainly reflects charge transfer resistance which is related to reactive kinetics. At low frequency

region, the 45° straight line which is known as Warburg diffusion regime, is attribute to the diffusion transmission resistance in the electrode. However, for some complex EIS curves, the electrochemical system should be studied by representing the system with an equivalent circuit which consists of resistance, capacitance, and inductance etc. basic electrical elements, and analyzed by circuit modelling software.

Chapter 3
Partially Graphitized Hierarchical Porous Carbon Spheres

3.1 Introduction and Motivation

Carbon materials with high SSA are highly demanded for supercapacitor electrode materials due to their chemical stability, thermal stability, good conductivity, and high electric double layer capacitance. However, most commonly used porous carbon materials (activated carbon) cannot meet the requirement for high-performance supercapacitors. An ideal carbon based supercapacior electrode material should not only have high SSA, which can facilitate the energy density determined by Equation (4); but also need high conductivity and rational structure for the fast diffusion of electrolyte to exhibit high power density. Thus, to meet the above demands, many templated carbons with unique structures are developed to utilize as supercapacitor electrode materials [71, 128, 129].

Herein, partially graphitized hierarchical porous carbon spheres are developed with a template technique. Two types of silica based templates are utilized to fabricate hierarchical pores in the carbon materials. The hierarchical porous carbon is synthesized through an aerosol-assisted spray direr. The configuration of an aerosol assisted spray drier is shown in the **Figure 18**. The flask is used to contain precursor solution, and it is connected with an atomizer to spray the precursor solution into the mist. The drying zone and heating zone can contribute to the evaporation of aqueous solution, leading to the self-assembly of template and carbon precursor. The formed nanocomposites of template and carbon precursor come through the heat zone and finally arrive at a filter, where the product can be collected. After the removal of template and calcination, it is able to obtain the hierarchical porous carbon.

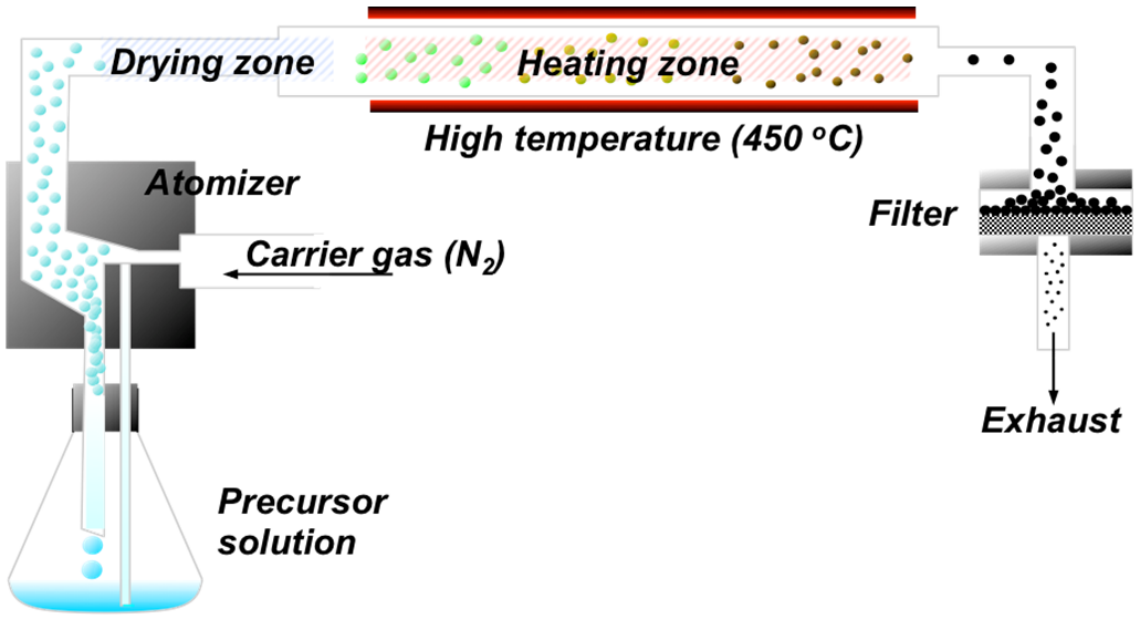

Figure 18: A schematic view of the configuration of aerosol assisted spray drier which is used to synthesize hierarchical porous carbon spheres [130, 131].

Herein, the two templates utilized to synthesize hierarchical porous carbon are colloidal silica and tetraethyl orthosilicate (TEOs) respectively. The colloidal silica is a suspension of spherical silica particles whose diameter is approximately 20 nm. Colloidal silica is used as the template for bigger pores in the hierarchical porous carbon which is benefit for the transportation of electrolyte ions. The smaller pores are attributed to the presence of TEOs which has the crosslinking structure. Generally, the diameter of small interconnected pores is around 2 nm, which greatly contribute to the SSA of this hierarchical porous carbon. TEOs are very easy to hydrolyze and convert to silicon dioxide with the following reaction:

$$Si(OC_2H_5)_4 + 2H_2O \rightarrow SiO_2 + 4C_2H_5OH \quad (20)$$

Therefore, it is very important to adjust the PH in the precursor solution to inhibit the hydrolysis process.

3.2 Experimental Procedure

The hierarchically porous graphitized carbon was synthesized using an aerosol-assisted spray drier technique. To specific, 6.0 g sucrose, 5.0 g nickel nitrate, 0.1 M, 10 g HCl solution, 40 mL distilled de-

ionized water (DDI water), 8.0 g tetraethyloxylic silicate (TEO_S) and 10 g colloidal silica solution (LUDOX AS-40) was mixed by stirring on a stir station with a stir rate of 350 rmp. After the solution was homogenized by stirring, it was sent through an atomizer using nitrogen as the carrier gas. The solution was sprayed into aerosol droplets by the atomizer, which were then carried to drying zone (450 ℃) by nitrogen. Solvent evaporation occurred continuously on interface between the air and liquid of the aerosol droplets in the drying zone. Finally products were collected on a membrane filter.

The collected spherical particles were carbonized at 900 ℃ under Ar flow with a slow ramping rate. During this process, sucrose which is used as the carbon precursor was converted to amorphous carbon. Under such high temperature (900 ℃), the nickel catalyzed graphitization reaction on the surface of spherical carbon particles. Finally, the excess of Nickel and the silica template was removed by HCl and NaOH solution, respectively.

3.3 Physical Characterization

Scanning electron microscope (SEM) was used to characterize the morphology of the materials, and was conducted on a LEO FESEM 1530. Transmission electron microscopy (TEM) was also used for high resolution imaging, and was performed at the Canadian Center for Electron Microscopy (CCEM, McMaster University), using a JEOL 2010F TEM/STEM field emission microscope. The Nitrogen sorption isotherms were collected from a Micromeritics ASAP 2020 analyzer.

3.4 Results and Discussion

Morphology of as-synthesized porous carbon materials can be revealed by the representative SEM images (**Figure 19**). As can be seen, the porous carbon is spherical with the particle size between several hundred nanometers and a few microns, resulting from the size of aerosol droplets. Compared to activated carbon particles whose particle size ranges from 5 to 20 μm, as-synthesized porous carbon spheres are much smaller. Small particle size can usually reduce the resistance of electrolyte diffusion in the electrode, which is benefit for achieving supercapacitor electrodes with high power density. However, on the other hand, nano-scale materials have higher surface energy, which may lead to side reactions during charge and discharge.

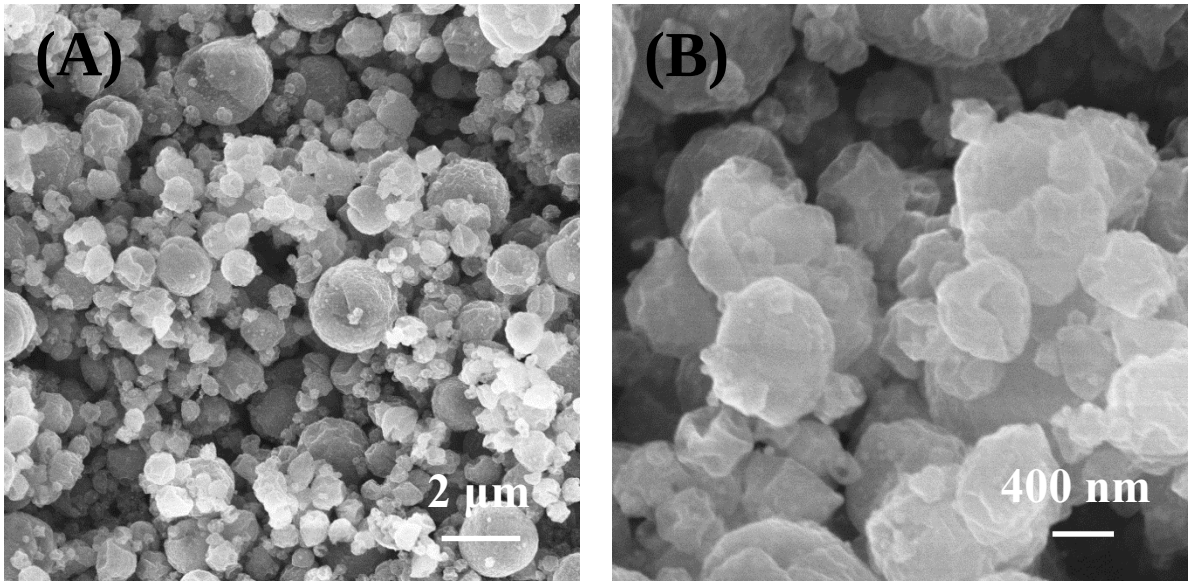

Figure 19: SEM images of as-synthesized hierarchical porous carbon spheres

The highly porous structure can be clearly observed in the representative TEM images of the carbon spheres (**Figure 20**). As can be seen, interconnected meso- and micro-pores co-exist in this type of carbon. The average mesopore diameter was around 20 nm, which aligned very well with the size of the colloidal silica template particle (~20 nm). However, it is hard to observe the interconnected channels contributed by TEOs, which is mainly because that the template particles of TEOs only have a diameter of 2 nm. Therefore, to further reveal the unique pore structure of the hierarchically porous carbon spheres, high-resolution TEM was performed.

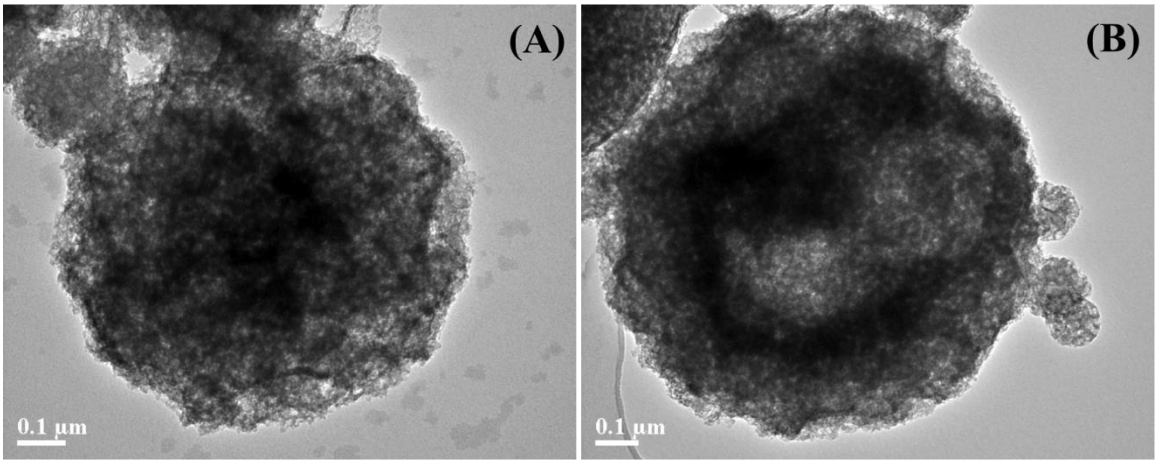

Figure 20: Representative TEM images of hierarchical porous carbon spheres. The mesopores can be clearly observed, with the pore size of around 20 nm, which is ascribed of the size of colloidal silica.

As shown in **Figure 21**, the pore walls of graphitic carbon can be found, which suggests that the carbon material is graphitized partially. Compared to amorphous carbon, graphitized carbon has higher conductivity, because electrons are free to migrate in the plane of graphite. By using graphitized carbon to replace amorphous carbon materials; supercapacitors can achieve higher energy density.

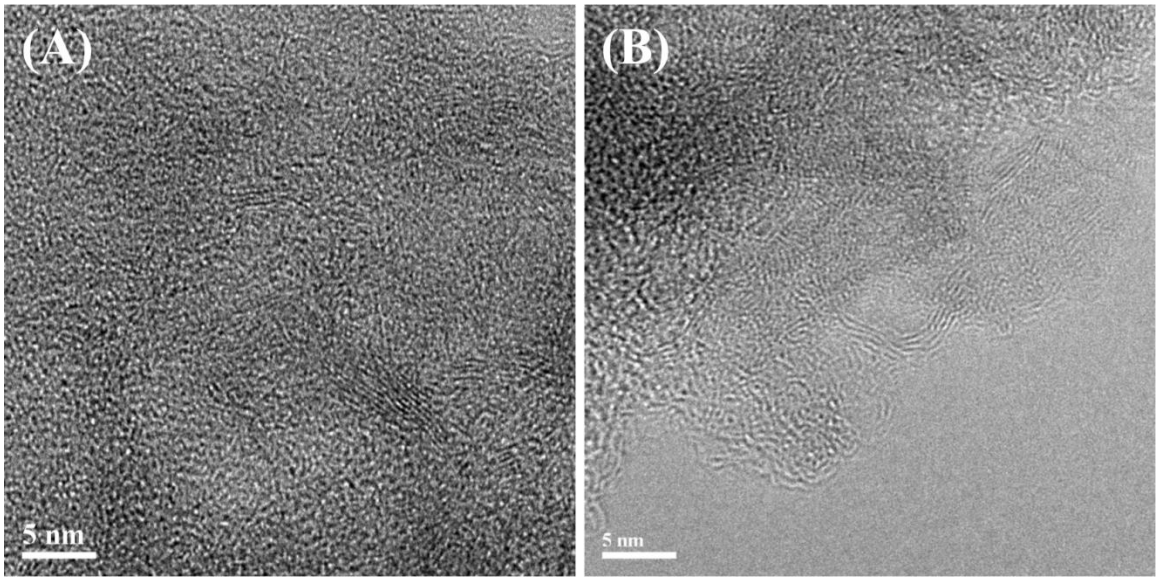

Figure 21: High-resolution TEM images of partially graphitized carbon spheres. The graphitic carbon exists not only on the surface of the carbon spheres, but also within the whole spheres as the pore walls.

The pore structure of hierarchical porous carbon was analyzed by nitrogen adsorption/desorption technique and calculated based on the BET theory. A type-IV nitrogen adsorption/desorption isotherm is achieved with nitrogen absorbed at relative pressure below 0.2 and between 0.6 and 0.9, respectively, which suggest the presence of both micropores and mesopores.

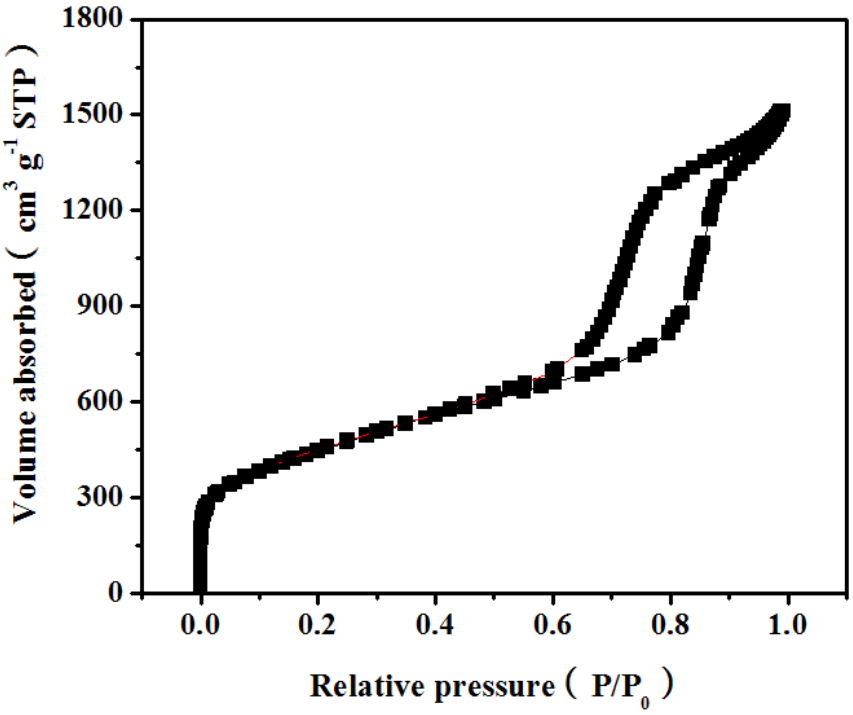

Figure 22: A type IV Nitrogen adsorption/desorption isotherms suggesting the hierarchical structure of the as-synthesized porous carbon spheres.

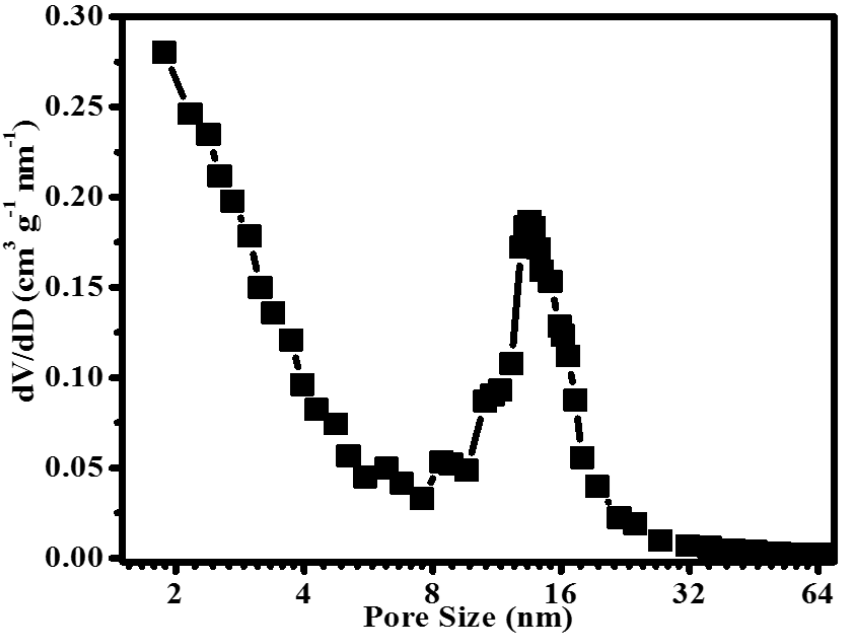

Figure 23: Pore size distribution of as-synthesized hierarchical porous carbon.

The pore size distribution derived from nitrogen adsorption/desorption technique is shown in **Figure 23**. As shown in **Figure 23**, there are two peaks in the pore size distribution which locate at ~14 nm and below 2 nm, respectively. The pore size distribution can suggest that there are two types of pores exist in the carbon materials, suggesting the hierarchically porous structure. The mesopores are approximately 14 nm which is a little smaller than the size of colloidal silica. This is mainly because of the graphitization process which is induced by Ni catalyst. During the graphitization process, amorphous carbon was partially converted to graphitized carbon. Due to the transformation of carbon structure, some pores are collapsed which lead to the shrinkage of the pore size. Based on BET theory, the SSA and pore volume are calculated. The hierarchical porous carbon spheres possess a high BET surface area of 1173 $m^2 g^{-1}$ with a high pore volume of 2.46 $cm^3 g^{-1}$.

3.5 Summary

Partially graphitized porous carbon spheres have been successfully synthesized by aerosol assisted spray drier method with colloidal silica and TEOs as the template. SEM confirms that the as-synthesized porous carbon particles have spherical morphology. In addition, TEM can suggest that there are mesopores and interconnected micropores in the carbon spheres. With the help of high-resolution TEM, it is able to observe partially graphitized carbon on the pore walls, which is benefit for the enhancement of electrical conductivity. The pore structure is analyzed by nitrogen adsorption/desorption technique. The nitrogen adsorption/desorption isotherms shows type IV shape which further confirm the mesopores and micropores coexist. Besides, the hierarchical structure can also be proved by pore size distribution, which shows the diameters of mesopores and micropores are ~14 nm and 2 nm, respectively. Based on BET theory, the SSA and pore volume are calculated.

Chapter 4

Partially Graphitized Hierarchical Porous Carbon Spheres/ MnO_2 Nanocrystal Composites for Supercapacitors

4.1 Introduction and Motivation

Owing to the crisis for unrenewable fuel resources, development of high-performance energy storage devices has become a crucial topic. Among various energy storage technologies, lithium-ion batteries and supercapacitors are promising in broad applications such as portable electronics, smart grids, and electrical vehicles.[132] Compared to LIBs which have been commercially available for longer time and have higher energy density, SCs show much higher power, long cycling life and rapid charge rate, making them a ideal energy storage devices in applications where safety and high power are highly demanded.[133-135] However, SCs are usually hampered by poor energy density, which is determined by the equation $E = ½ CV^2$, where E is the energy density, C is the total capacitance, and V is the device potential window.[136] To date, high surface area carbonaceous materials are most common electrode materials in SCs, but can only achieve a specific capacitance of ~150 F g^{-1} with the mechanism of electric double layer capacitors.[137] Thus, carbon-based SCs usually suffer from low energy density (<10 Wh kg^{-1}). By comparison, pseudocapacitors assembled by inorganic non-carbon based materials (e.g., RuO_2) have much higher capacitance (>1000 F g^{-1}) through reversible faradaic reactions.[9, 138, 139].

MnO_2 has been considered as a highly promising material for SCs among various transition metal oxides. MnO_2 generally takes the advantages of its large reserves in nature, environmental benignity, and a large theoretical capacitance of 1370 F g^{-1}.[133, 140-144] In practical applications, however, the performance of manganese oxide is hampered by agglomeration, low electrical conductivity and slow redox rate which is similar to most of metal oxides, and a low capacitance and a poor rate capability is often observed.[145] To address the above issues, a general strategy is to combine MnO_2 with conductive components[146-148] such as carbon nanotubes (CNTs),[124, 149, 150] graphene,[66, 151] and conductive polymers.[152, 153] For example, the conductive polymer wrapped graphene/MnO_2 composite exhibits a high specific capacitance of ~380 F g^{-1} at a current density of 0.1 mA cm^{-2} and ~175 F g^{-1} at 5 mA cm^{-2},[154] while MnO_2/CNT composite delivers a capacitance of 201 F g^{-1} at a current density of 1.0 A g^{-1} and 140 F g^{-1} at 20 A g^{-1}.[99] Beyond this, it is also important to design and build novel architectures with efficient ion- and electron-transport pathways as well as robustness

to further improve the electrode kinetics and integrity, which is highly demanded by high-performance supercapacitors.[155, 156] In this context, it is essential but challenging to design and fabricate MnO_2-based electrode materials with novel architectures for high-performance supercapacitors.

Herein, we report a composite material of MnO_2 nanocrystals/hierarchically porous carbon spheres with partially graphitized surface (MnO_2/C), which exhibits excellent electrochemical performance for asymmetric supercapacitors. Such a composite with unique structure possesses several features favoring high-performance electrodes: (i) the interconnected hierarchically porous structure with micro- and meso-pores not only provides high surface area resulting in high capacitance but also facilitates ion transport leading to high rate capability; (ii) the partially graphitized carbon improves the electron conductivity which further increase high rate capability; (iii) the *in-situ* growth of MnO_2 on carbon spheres ensures an intimate contact between the two components, providing the composites with both high rate and robustness. Moreover, the micrometer-sized composites can be easily fabricated into electrodes by a slurry-coating process compatible with existing battery manufacturing, which makes it a promising material for future practical applications.

4.2 Experimental

4.2.1 Synthesis of Porous and Graphitized Carbon Spheres/ MnO_2 Composites

The carbon/MnO_2 composites were synthesized by directly reacting $KMnO_4$ with carbon spheres. Briefly, the hierarchically porous graphitized carbon spheres (40 mg) were soaked in Na_2SO_4 solution (0.1 M, 25 mL) for 30 min, and then stirred with an aqueous solution (15 mL) containing Na_2SO_4 (0.1 mol L^{-1}) and $KMnO_4$ (0.1 mol L^{-1}) for various reaction times. The rate of stir station is set to be 350 rmp. The product was washed with DDI water for several times and then dried at 80 ℃ at vacuum oven, and denoted to be MnO_2/C-XX based on different reaction time.

4.2.2 Materials Characterization

Scanning electron microscope (SEM) was used to characterize the morphology of the materials, and was conducted on a LEO FESEM 1530. Transmission electron microscopy (TEM) was also used for high resolution imaging, and was performed at the Canadian Center for Electron Microscopy (CCEM, McMaster University), using a JEOL 2010F TEM/STEM field emission microscope. The Nitrogen sorption isotherms were collected from a Micromeritics ASAP 2020 analyzer. The composition was

determined by thermal gravimetric analysis (TGA, TA instrument Q500) with a ramp rate of 10 ℃ min^{-1} from 25 ℃ to 850 ℃ in air.

4.2.3 Electrode Fabrication

The electrodes were fabricated from a convention slurry-coating process. The active material powders, SuperP carbon and poly(vinylidene fluoride) were mixed in *N*-methylpyrrolidinone (NMP) with a mass ratio of 8:1:1, and then homogenized before coated on the nickel current collectors. The coated electrodes were dried overnight at 100 ºC and then pressed at 2.0 MPa. The mass loading of active materials was controlled to be around 2.0 mg cm^{-2}.

To test electrodes, open cells were assembled using a platinum (Pt) wire as the counter electrode, a SCE reference electrode, and 1 M Na_2SO_4 aqueous solution as the electrolyte. Cyclic voltammetric and galvanostatic charge-discharge measurements were carried out on a VMP3 potentiostat/galvanostat (Bio-Logic LLC, Knoxville, TN) using cutoff voltages of 1.0 and 0.00 at various scan rates and current densities. The specific capacitance can be calculated based on the equation $C = I/(dE/dt) \approx I/(\Delta E/\Delta t)$, where E is the cell voltage, I is the constant discharge current density, and dE/dt *(or* $\Delta E/\Delta t$*)* is the slope of the discharge curve. All electrochemical measurements were carried out at room temperature.

4.3 Results and Discussion

Figure 24 shows the representative SEM images of as-synthesized porous and graphitized carbon spheres/ MnO_2 composites. As can be seen from **Figure 24**, the MnO_2/C composites show darker colour than pure porous carbon spheres due to the in-situ reaction with $KMnO_4$ for 240 min. However, the spherical morphology and particle size of the MnO_2/C composites can be retained. Even with SEM images, the pores on the composite spheres can also be observed clearly.

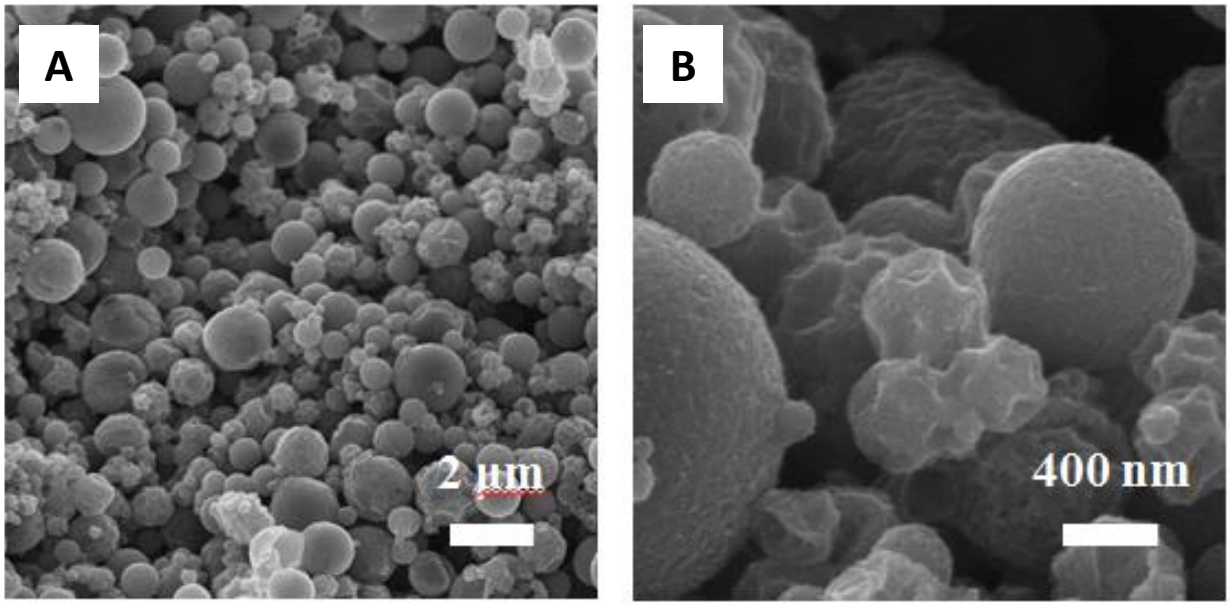

Figure 24: SEM images of porous and graphitized carbon spheres/ MnO_2 composites

TEM images (**Figure 25**) of a single MnO_2/C particle indicates that MnO_2 is uniformly distributed in the carbon substrate, since the TEM image is much darker than the TEM of pure hierarchical porous carbon spheres. Besides, on the edge of the composite sphere, it is also able to observe MnO_2 nanocrystal clearly. Due to the high ratio of MnO_2 in the composite, it is hard to see pores from TEM images. The evidence of pore structure of the composite will be shown in the following sections.

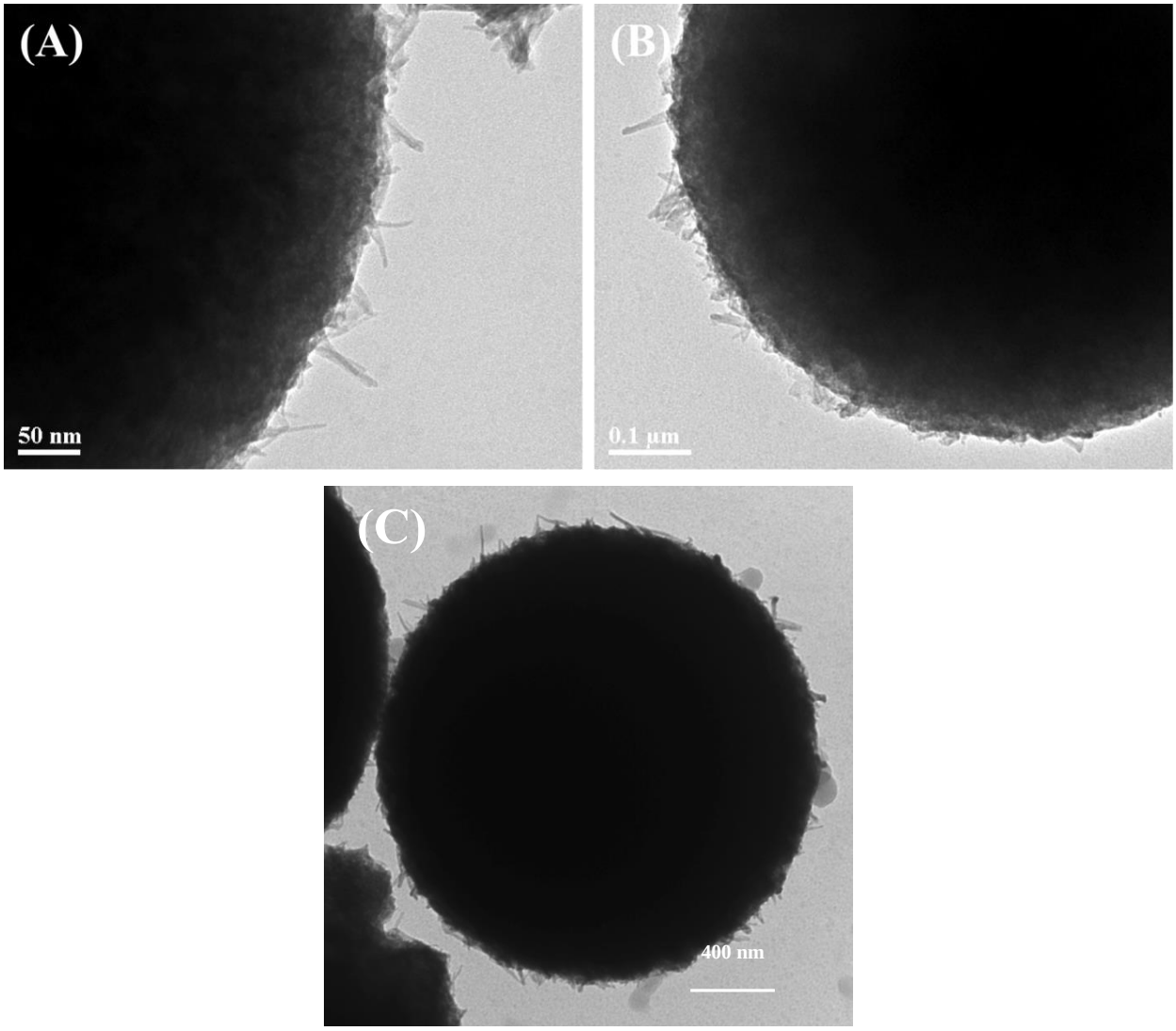

Figure 25: TEM images of a single hierarchical porous and graphitized carbon sphere/MnO_2 composite.

From high-resolution TEM (**Figure 26**), it is able to see MnO_2 nanocrystals with polycrystalline property. In addition, the highly conductive graphitic pore walls still remain, which is revealed by high-resolution TEM. This phenomenon suggests that the $KMnO_4$ preferably reacts with amorphous carbon rather than graphitized carbon, leading to successful survival of fast electron transfer pathways.

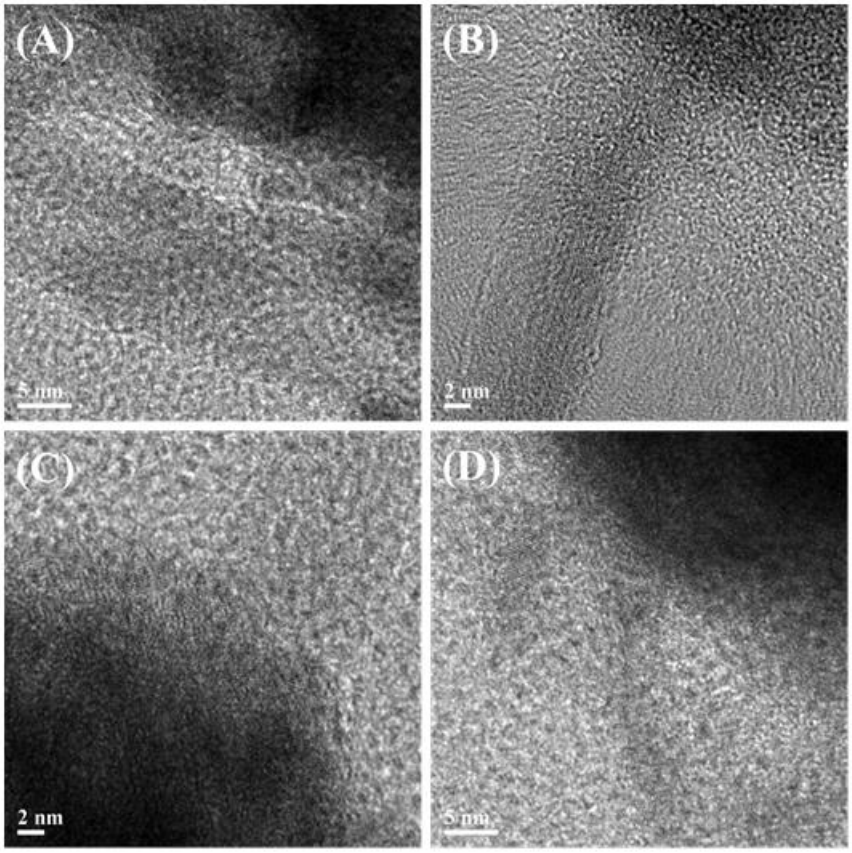

Figure 26: High-resolution TEM images of as-synthesized partially graphitized carbon spheres. The graphitic carbon exists not only on the surface (**A** and **B**) of the carbon spheres, but also within the whole spheres as the pore walls. (**C** and **D**)

The successful *in-situ* growth of MnO_2 was further confirmed by XPS. The obtained XPS survey spectrum (**Figure 27**) presents the signals from Mn, O, and C elements, suggesting the existence of manganese oxide on porous carbon materials. **Figure 28** shows the core-leveled scan of Mn $2p_{3/2}$ and Mn $2p_{1/2}$ with binding energies at 642.5 and 654.1 eV, respectively. Both the binding energies and the spin energy of 11.6 eV are consistent with literatures reported previously, confirming the formation of MnO_2.[157, 158]

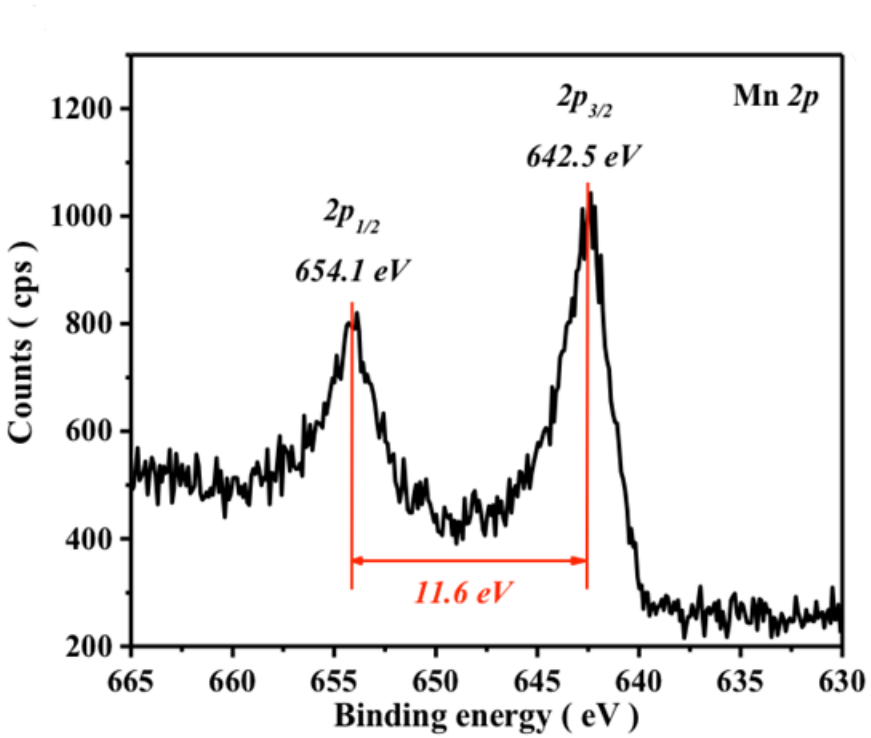

Figure 27: Core-leveled scan Mn $2p_{3/2}$ and Mn $2p_{1/2}$ XPS spectra of MnO_2/C composites.

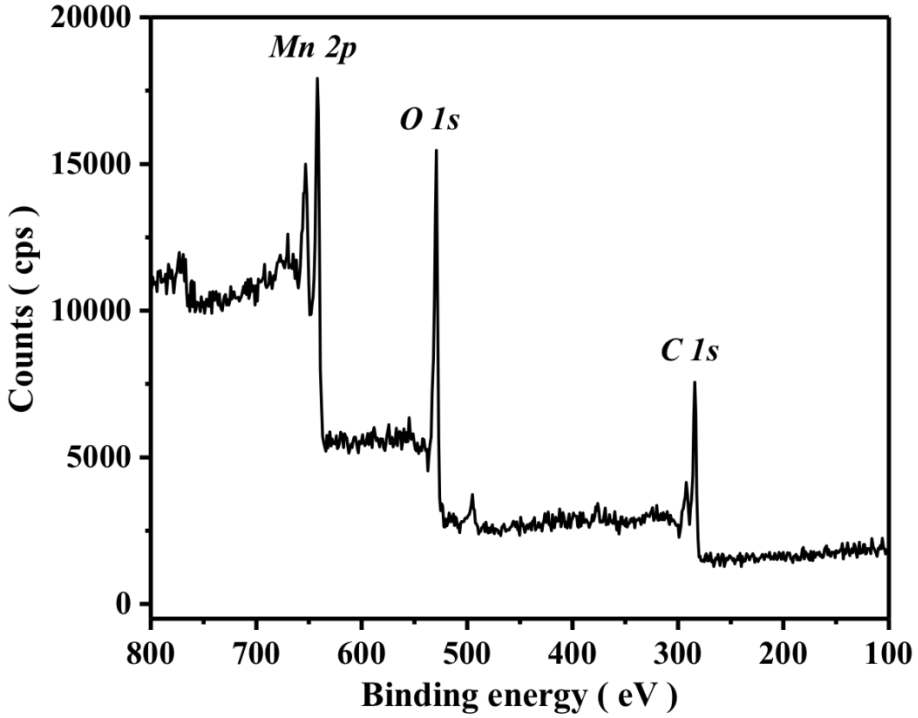

Figure 28: Survey-leveled scan XPS spectrum of MnO_2/C-240 composites.

The amount of MnO_2 grown on porous carbon can be controlled by adjusting the reaction time of $KMnO_4$ with carbon spheres substrates. The longer the carbon substrates contacts with $KMnO_4$ solution, the higher amount of MnO_2 will grow on the porous carbon. In order to determine the mass loading of MnO_2 and pure carbon in the composites, TGA is used to analyze the composites. **Figure 29.** shows the TGA curves of MnO_2/C composites with different reaction times, where three main regions can be observed. Below 200 ^oC, a gradual mass decrease is found, mainly due to the removal of moistures and some of the remaining hydroxyl- or carboxyl- groups on carbon materials. The sharp mass loss below 400 ^oC is ascribed to the consumption of carbon catalyzed by MnO_2 and its derivatives.[159] During this process, MnO_2 is transformed into Mn_3O_4 while oxygen is released, which also contributes to the weight loss. Above 500 ^oC, the carbon materials are consumed completely, while Mn_3O_4 is transformed to Mn_2O_3. The final weight percentage was calculated to be 44, 65, 72, and 76 % for reaction time of 60, 120, 240, and 360 min, corresponding to MnO_2 content of 49, 72, 79, and 84 % in composites (**Figure 30**). Based on the TGA analysis, it is able to find that large content of MnO_2 has been successfully grown on the carbon spheres. However, the reaction of carbon with $KMnO_4$ solution is a self-limited reaction, since the MnO_2 produced previously can cover the carbon substrates and hamper the $KMnO_4$ from further reacting with the carbon. The large amount of MnO_2 in our composite

materials is mainly attributed to the hierarchical structure of the carbon substrates. The mesopores in the composites can be used as effective permanganate ion channels solution pathways to enable $KMnO_4$ to react with interior carbon. Besides, carbon possesses large surface area, which is provided by micropores, to contact with $KMnO_4$ solution.

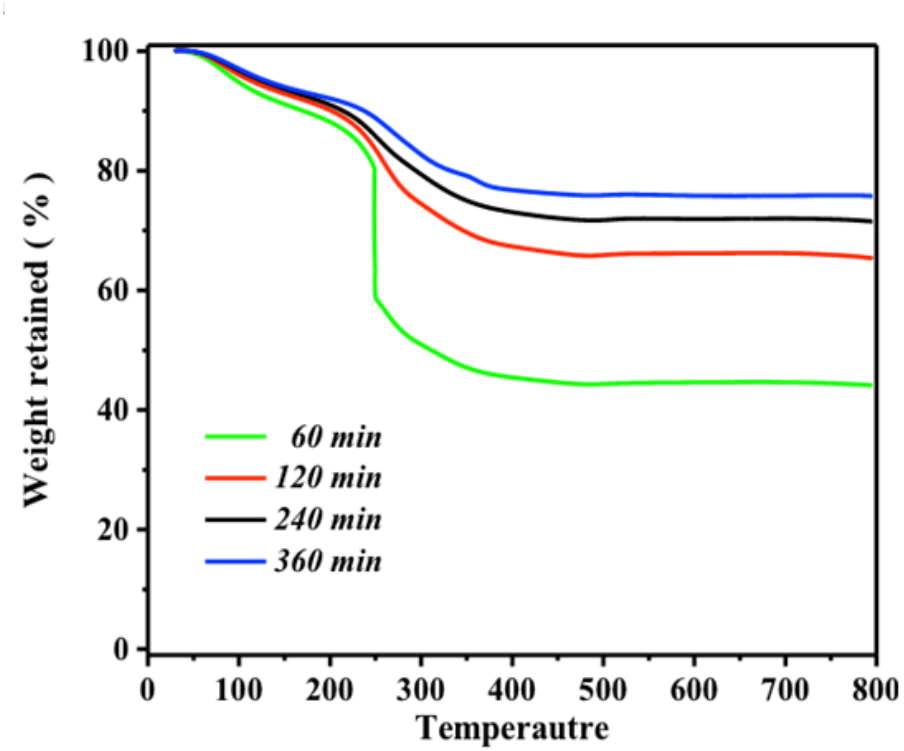

Figure 29: Survey-leveled scan XPS spectrum of MnO_2/C-240 composites.

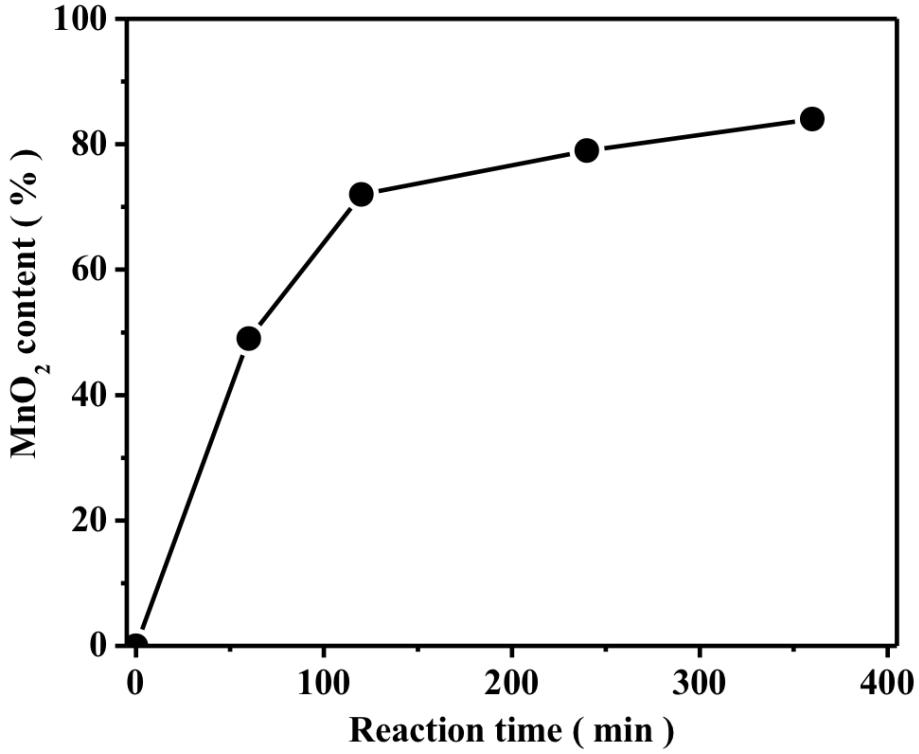

Figure 30: The MnO_2 weight content in MnO_2/C composites materials with various reaction time of $KMnO_4$ with porous carbon spheres.

The pore structure of MnO_2/C composites was analyzed by nitrogen adsorption/desorption technique. The nitrogen adsorption/desorption isotherms of MnO_2/C composites is shown in **Figure 31**. By comparison with the nitrogen adsorption/desorption isotherms, the MnO_2/C-240 also exhibits a type-IV isotherm with nitrogen uptake at relative pressure below 0.2 and between 0.6 and 0.9, respectively. The type IV isotherms can suggest that mesopores and micropores coexist even after reacting with $KMnO_4$ solution. The distribution shown in **Figure 32** is also an evidence to prove the presence of two types of pores in the composites. From the pore size distribution plot, it is able to find a decreased pore size of ~9 nm which is ascribed of the growth of MnO_2. In addition, a lower BET surface area of ~100 $m^2\ g^{-1}$ is calculated by the BET theory, also suggesting the successful and homogeneous growth of MnO_2. However, due to the hierarchically porous structure still exists with interconnected micro- and meso- pores, the MnO_2/C composites can still have fast the ion transportation.

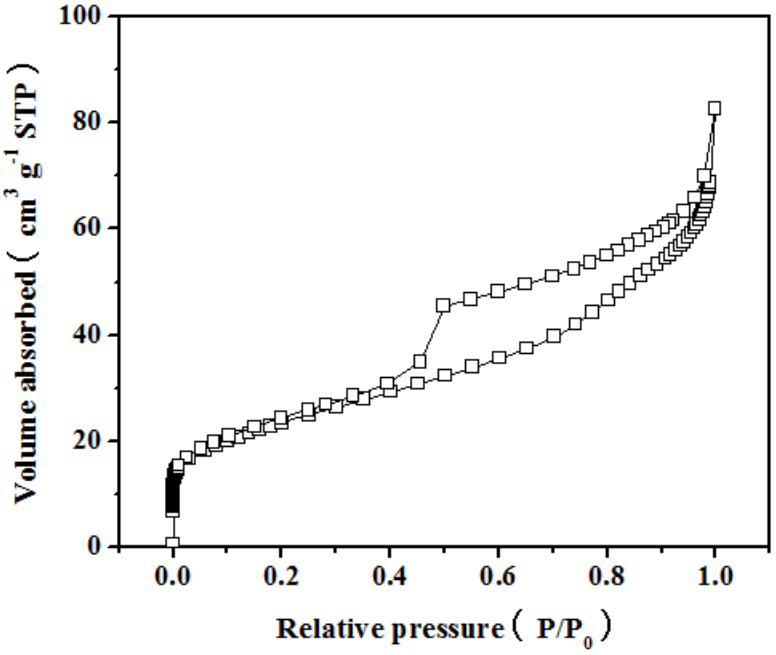

Figure 31: Nitrogen adsorption/ desorption isotherms of as-synthesized MnO_2/C-240 composites.

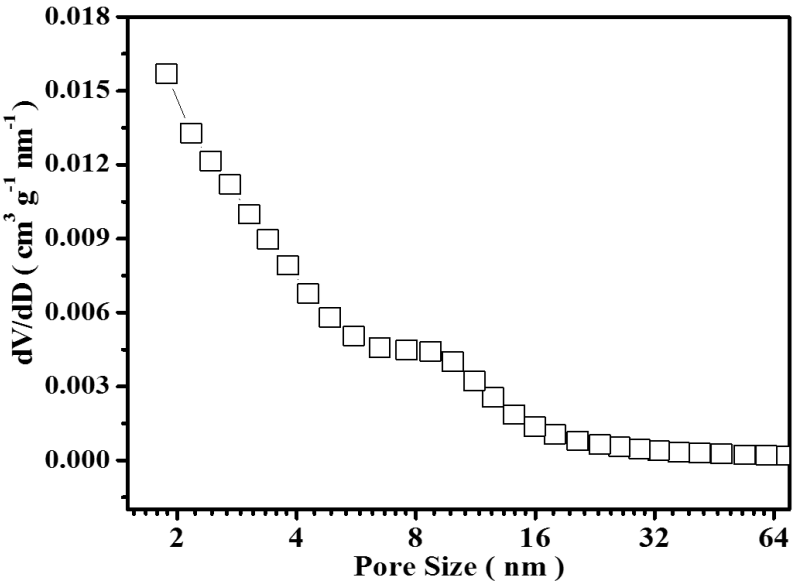

Figure 32: Pore size distribution of MnO_2/C-240 composites.

The electrochemical properties of as-synthesized hierarchically porous carbon and MnO_2/C composites were firstly characterized by cyclic voltammetry (CV) in a three electrode open cell using Na_2SO_4

solution as the electrolyte, a Pt wire as the counter electrode and SCE reference electrode. **Figure 34 (A)** shows the typical CV curves of the as-synthesized hierarchically porous carbon. Nearly symmetrical rectangular shape can be observed from all CV curves at various scan rates, corresponding to the electrical double-layer capacitance where all charge stores on the surface of the materials. The rectangular shape remains as scan rate increases, owing to the connected pores and excellent conductivity stemmed from the partially graphitized carbon. By comparison, MnO_2/C-240 electrode also exhibits symmetric rectangular shaped CV curves, suggesting fast reversible Faradic reactions and ideal capacitive performance. However, an obvious distortion occurs as the scan rate increases, indicating the polarization resulted from the increased transport resistance.

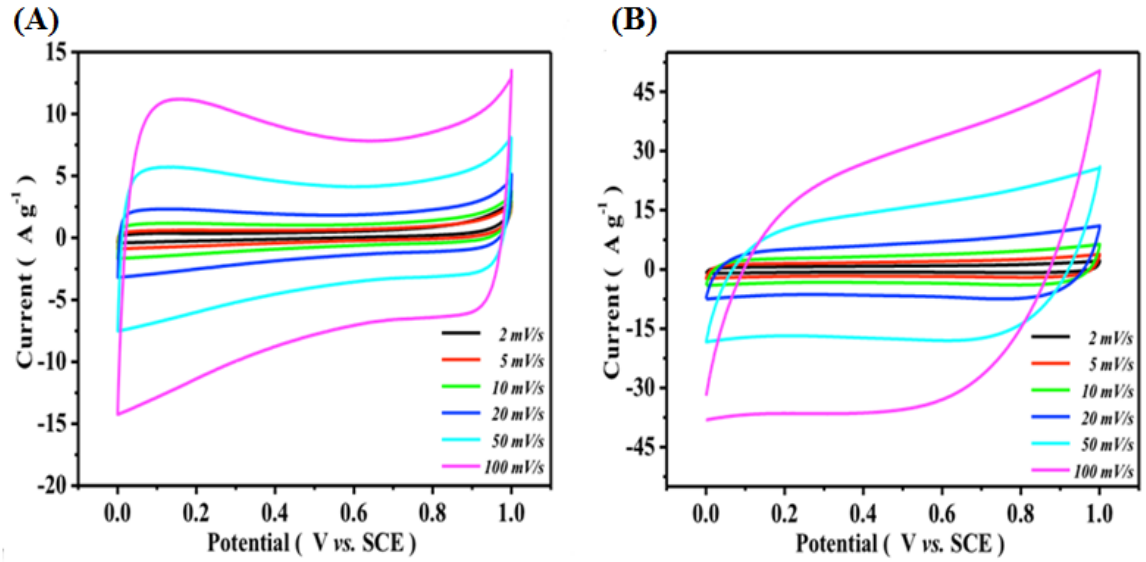

Figure 33: Cyclic voltamogram of (A) as-synthesized hierarchical porous carbon spheres, and (B) MnO_2/C-240 at various scan rates from 2 to 100 mV s^{-1} at a cutting-off voltage of 1.0 and 0.0 V *vs.* SCE.

The specific capacitance can be calculated from CV curve based on the Equation (19). **Figure 34** compares the specific capacitance of as-synthesized hierarchically porous carbon and MnO_2/C-240 calculated from CV curves at different scan rates of 2 to 100 mV s^{-1} (corresponding to the charge/ discharge times from 500 to 10 s). Obviously, the hierarchically porous carbon electrode exhibits a high rate capability with a low capacitance of 91 F g^{-1} from electrical double-layer capacitance. In contrast, the MnO_2/C-240 electrode possesses a much higher capacitance of 412 F g^{-1} at a scan rate of 2 mV s^{-1}. Such a high specific capacitance is mainly ascribed to the high MnO_2 ratio in the composites, which

has seldom been reported previously. Even at high scan rate of 50 and 100 mV s^{-1}, the composite electrode still delivers a high capacitance of 286 and 251 F g^{-1}, respectively, which is 70 % and 61 % of the capacitance at 2 mV s^{-1}. Such an observation indicates a much improved rate performance of pseudocapacitive metal oxides mainly attributed to the unique hierarchically porous structure and the highly conductive graphitic pore walls.

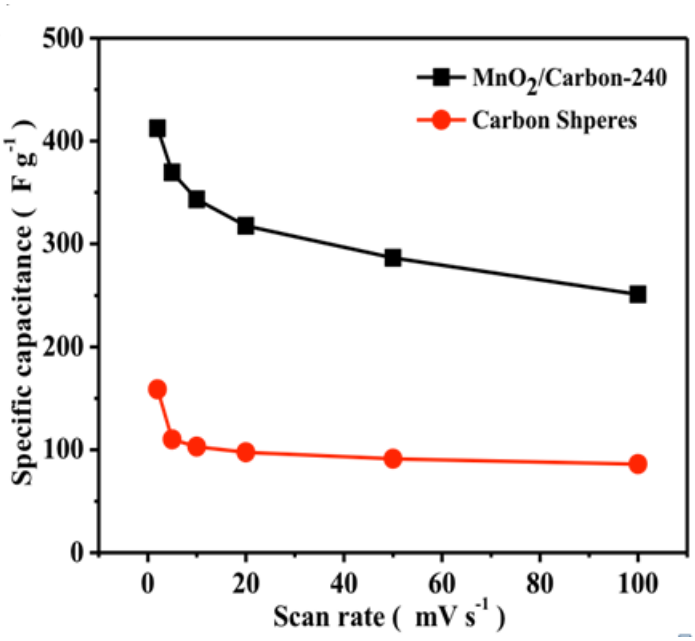

Figure 34: Comparison of specific capacitance dependence on scan rates for both as-synthesized hierarchically porous carbon spheres and MnO_2/C-240.

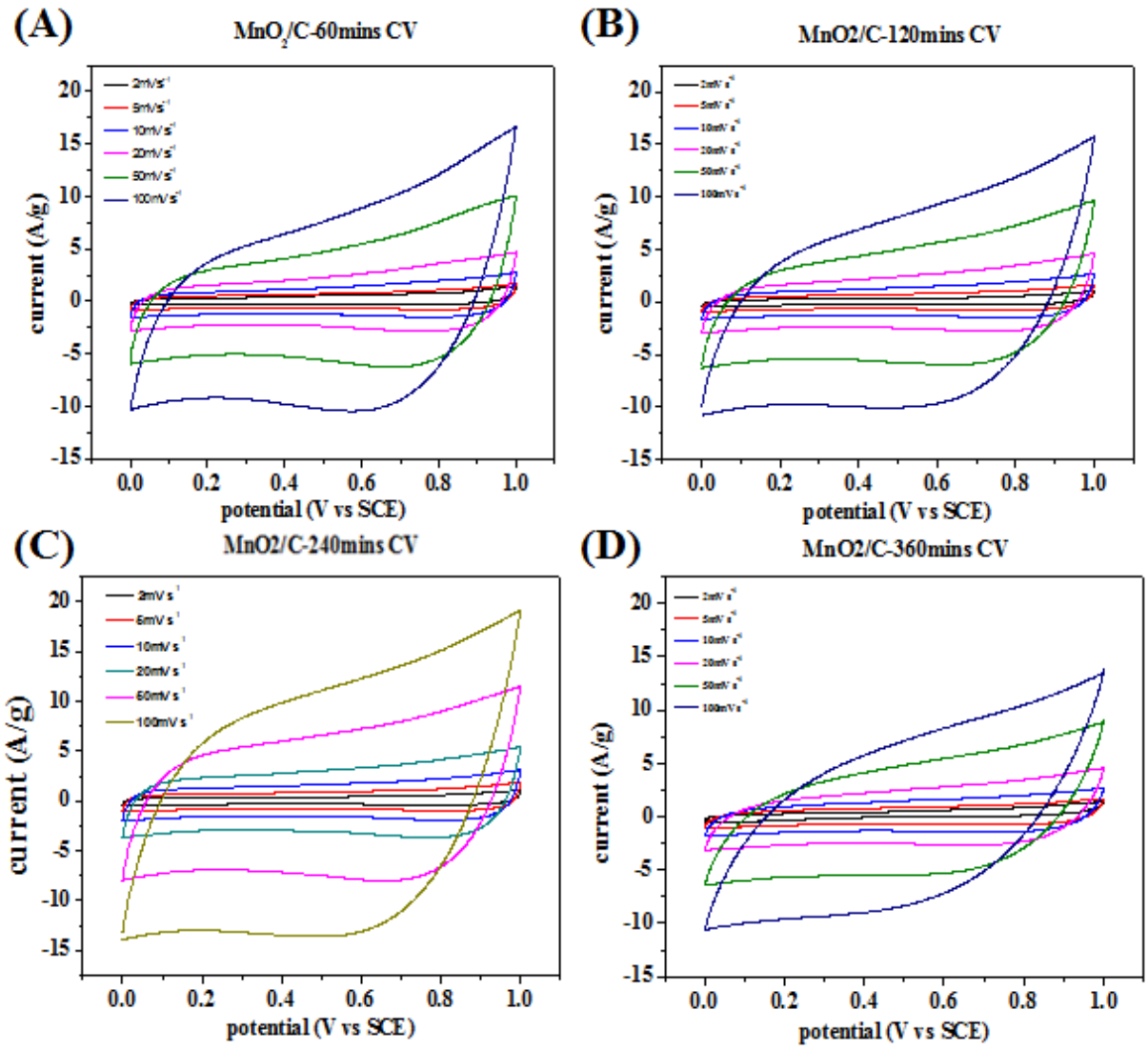

Figure 35: Comparison of cyclic voltamograms of MnO_2/C composites with different MnO_2 contents.

Figure 35 further compares the capacitance and rate capability of MnO_2/C composites with different MnO_2 contents. With the increase of reaction times, the area of CV curves increase gradually and achieve an maximum value at 240 min, but decrease sharply when reaction time reach 360 min. The increase of CV curve area can be ascribed of the rising content of high pseudocapacitive material MnO_2. However, when the ratio of MnO_2 is too high, electrolyte ions are so hard to pass through the thick MnO_2 layer that large amount of MnO_2 fails to be utilized. In addition, superabundant MnO_2 can also deteriorate the electron transportation pathways and occupy most of the pore volume, leading to inferior electrolyte diffusion.

The capacitance and rate capacity is also shown in **Figure 36 (A)**, which shows that the rate performance deteriorates as the MnO_2 increases. For low MnO_2 ratio, the composite electrode gives a good rate capability but a low specific capacitance as shown in **Figure 36 (B)** due to the limited contribution from pseudocapacitance. For high MnO_2 ratio, although the composite electrode delivers a much higher capacitance at low scan rate, the rate capability would be compromised as shown in **Figure 36 (B)**. On one hand, the *in-situ* growth of MnO_2 on porous carbon with long reaction time results in the collapse of hierarchical pores and the interconnected channels, and the loss of highly conductive graphitic carbon part, which significantly affects the ion- and electron- transportation. On the other hand, the formation of MnO_2 leads to less specific surface area and pore volume, which also increases the diffusion resistance. Therefore, an optimal MnO_2 ratio where both high capacitance and rate capability can be obtained is highly needed.

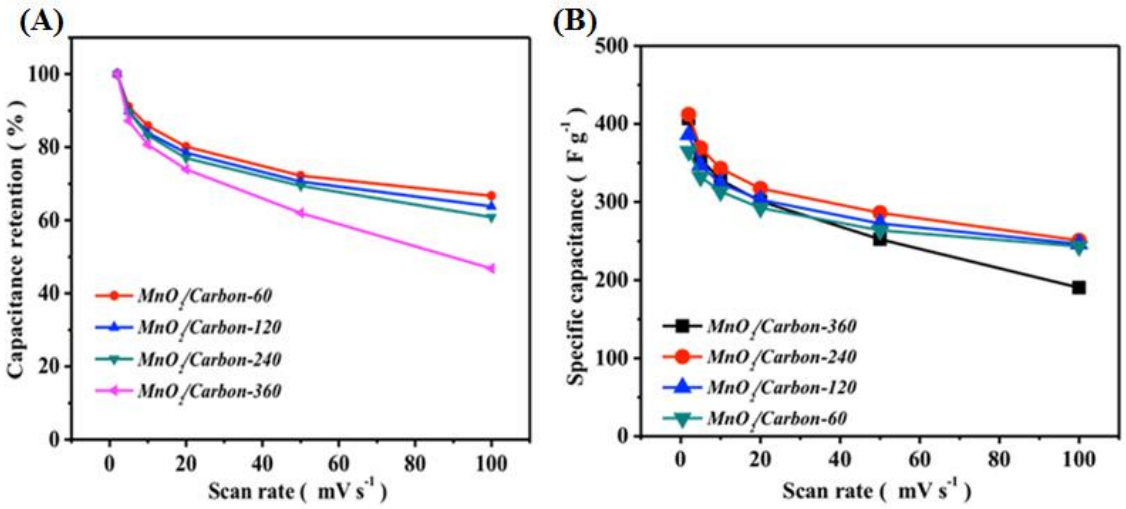

Figure 36: Comparison of rate capability of MnO_2/C composites with different MnO_2 contents (A). Dependence of specific capacitance of MnO_2/C composites on different MnO_2 contents

The rate capability of MnO_2/Carbon composites (MnO_2/C-240) were further compared with that of a series of MnO_2/porous carbon composites including MnO_2/hierarchically porous carbon,[160] MnO_2/graphitic disordered mesoporous carbon,[161] MnO_2/CMK-3,[162] and mesoporous MnO_2/carbon aerogel.[146] As shown in **Figure 37**, the MnO_2/Carbon from this work outperforms most of the others. Although mesoporous MnO_2/carbon aerogel shows a little higher capacitance at low scan rate, its deteriorative capacitance retention at higher scan rates is unsatisfactory.

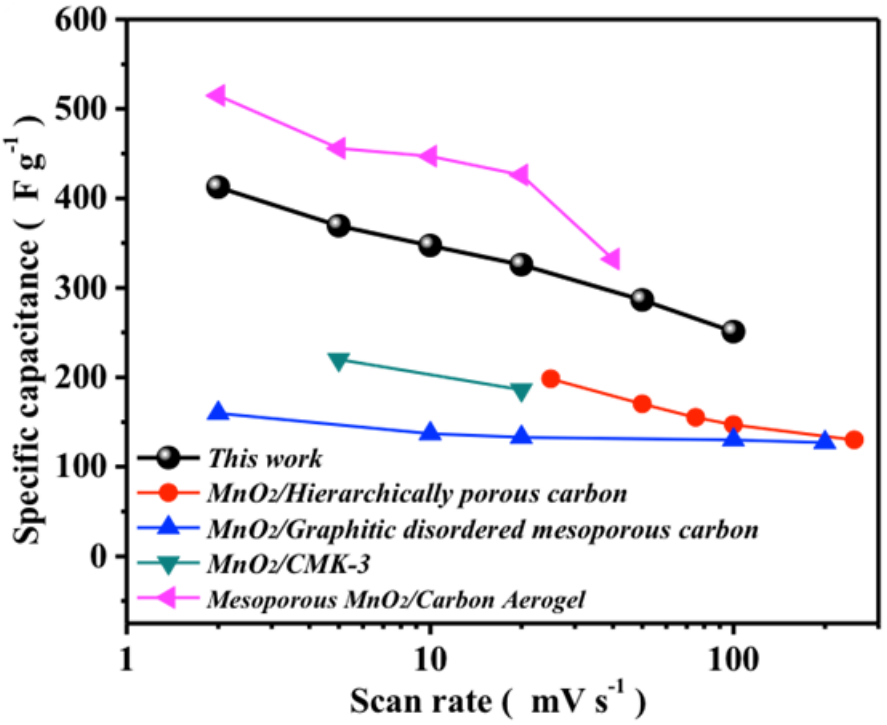

Figure 37: Comparison of specific capacitance of MnO_2/C-240 dependence on scan rates with a series of MnO_2/porous carbon composites.

In order to further evaluate the capacitive behavior of MnO_2/C composites, galvanostatic charge-discharge measurements were applied at various current densities. **Figure 38** shows the galvanostatic charge-discharge profiles of MnO_2/C-240 electrode at current densities from 0.5 to 5.0 A g^{-1} between 1.0 and 0.0 V (*vs.* SCE). Symmetrical charge and discharge profiles can be obtained, suggesting typical and excellent capacitive property of the composites, which is consistent with CV observations. The specific capacitance derived from the discharge curve is calculated to be 328 F g^{-1} at a current density of 0.5 A g^{-1} (discharging time: 656 s); while at 5.0 A g^{-1}, the MnO_2/C-240 electrode still possesses a discharge capacitance of 266 F g^{-1} (discharging time: 52 s).

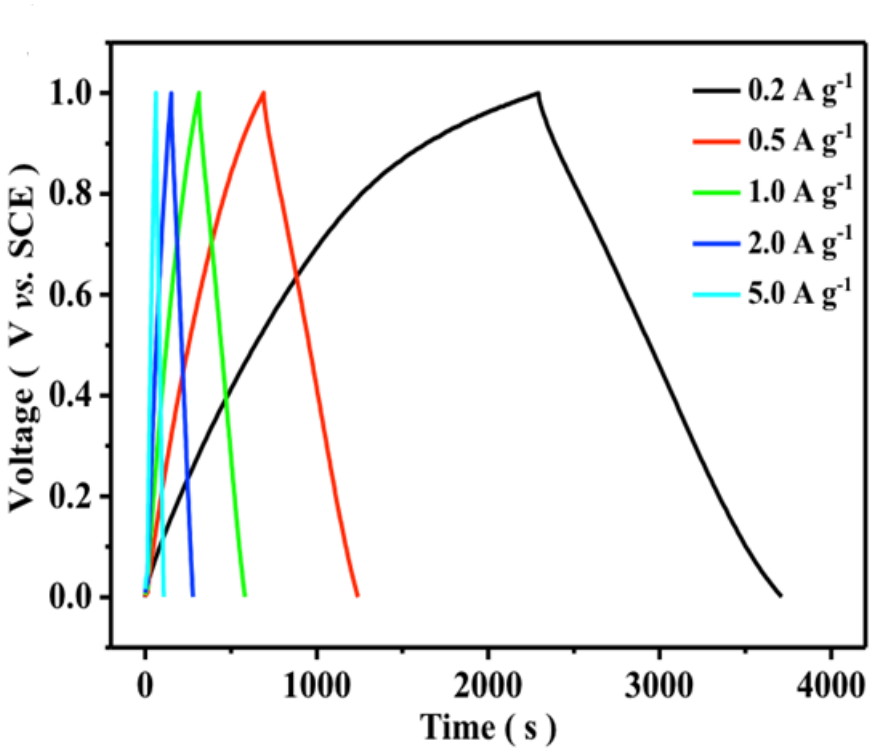

Figure 38: Galvanostatic charge-discharge profiles of MnO_2/C-240 with the cur-off voltage of 1.0 and 0.0 *vs.* SCE at various current densities ranging from 0.2 to 5.0 A g^{-1}.

The corresponding rate performance is clearly observed from **Figure 39**. At the current density of 5.0 A g^{-1}, the MnO_2/C-240 electrode still possesses ~81 % of its specific capacitance at 0.5 A g^{-1}. This performance is much better than that of MnO_2/graphitic carbon spheres[163] and hierarchically MnO_2/carbon nanocomposites.[164] As we mentioned above, this excellent rate capability is mainly attributed to the highly conductive graphitic pore walls. As shown in Raman spectrum, two peaks can be easily found at 1327 (D band) and 1588 (G band) cm^{-1} with a relative intensity ratio (I_D/I_G) of 1.48, which confirms that a large amount of graphitized carbon exists (**Figure 40**). Even after the MnO_2 deposition, the two peaks can still be observed with an I_D/I_G of 1.50, suggesting that $KMnO_4$ preferably reacts with amorphous carbon, leaving highly conductive graphitized carbon which facilitates the electron transfer.

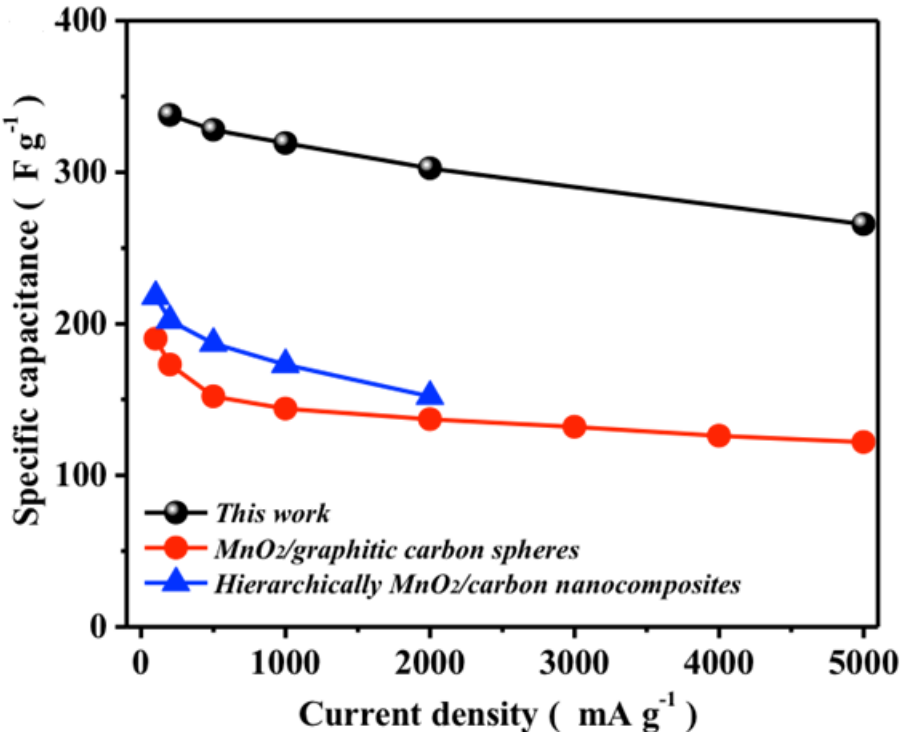

Figure 39: Specific capacitance derived from galvanostatic charge-discharge dependence on current density.

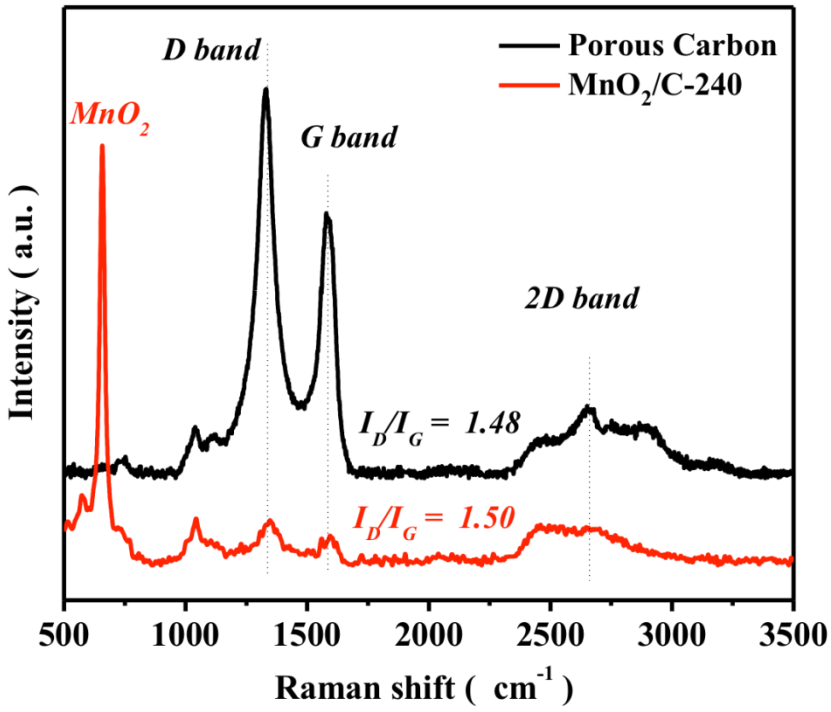

Figure 40: Raman spectra of MnO_2/C composites and pure MnO_2.

Such a good performance can be further confirmed by electrochemical impedance spectroscopy (EIS) result. As shown in **Figure 41**, each Nyquist plot is composed of a semicircle at high frequency region representing the resistance of electrolyte and charge-transfer, and a Warburg tail at low-frequency region representing the diffusion-resistance from the electrode materials. Obviously, as-synthesized hierarchically porous carbon spheres exhibit a high conductivity according to the small semicircle and low slope of the Warburg tail. Remarkably, the MnO_2/C-240 shows a comparable conductivity, which is mainly due to the in-situ growth of MnO_2 on highly conductive networks formed within the carbon spheres

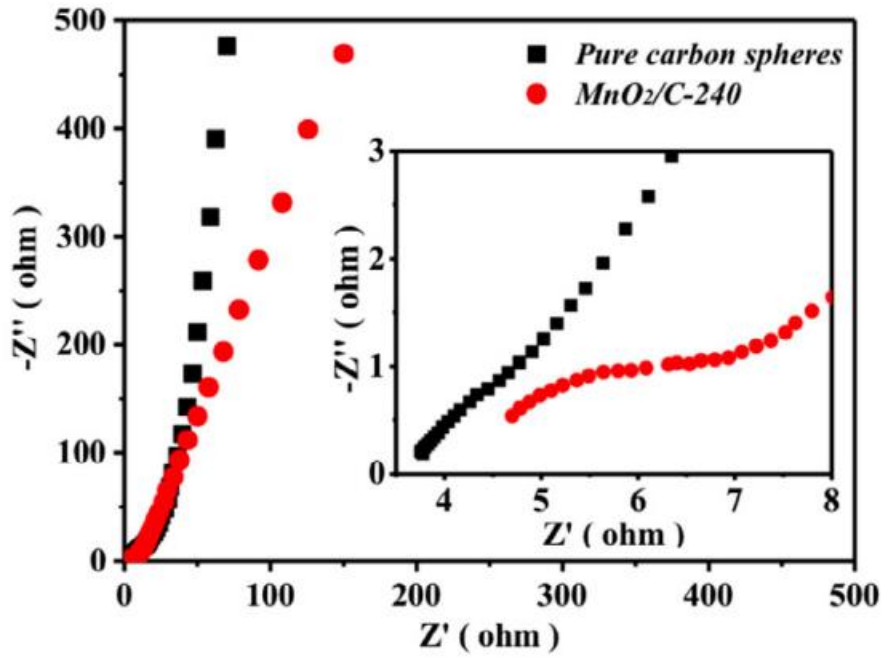

Figure 41: Comparison of Nyquist plots of as-synthesized hierarchically porous carbon spheres and MnO_2/C-240.

In addition to the excellent rate capability, a long cycling stability of the MnO_2/C composites can be also achieved. Cycling life test over 4000 cycles for MnO_2/C-240 electrode was carried out at 1.0 A g^{-1}, and the corresponding normalized capacitance retention is shown in **Figure 42**. After 4300 cycles, the MnO_2/C-240 electrode still possesses ~88% of its initial specific capacitance after 4300 cycles with very symmetric and stable charge-discharge profiles. Such a cycling stability is mainly attributed to the robust composite structure. On one hand, the unique graphitic pore walls server as a robust scaffold preventing the porous structure from collapse. On the other hand, the growth of MnO_2 from *in-situ* reaction of $KMnO_4$ with carbon materials ensures an intimate contact, where MnO_2 and carbon are firmly connected. Moreover, the hierarchically porous framework can effectively suppress the MnO_2 from aggregation.

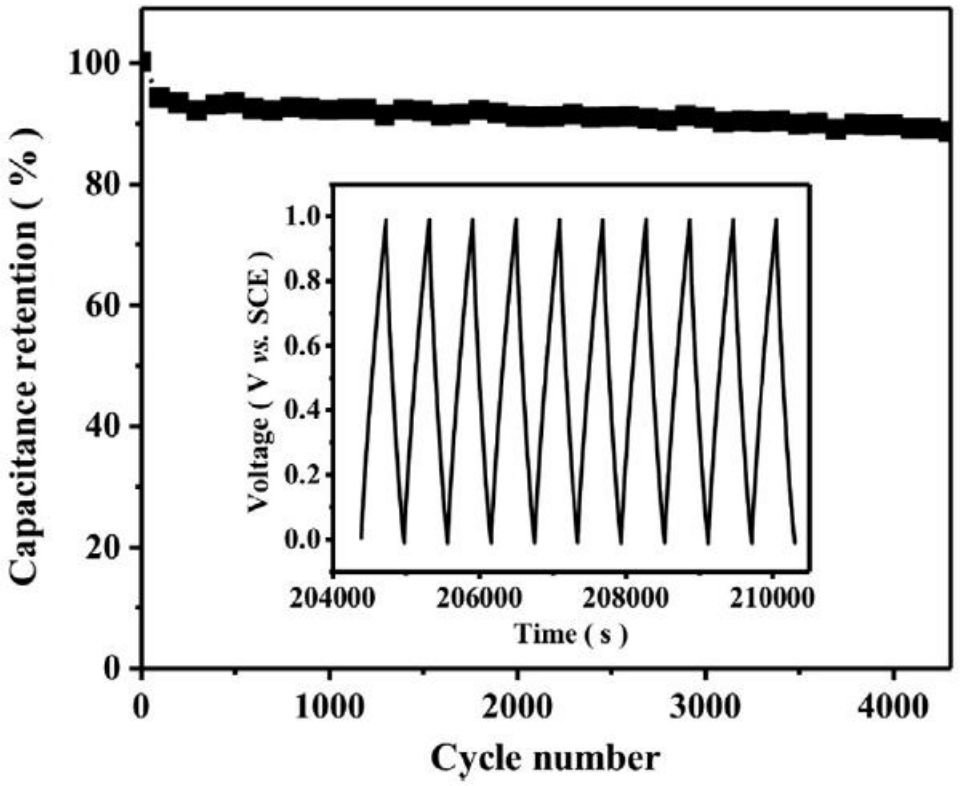

Figure 42: Long-term cycling stability of MnO_2/C-240 composite electrode at a current density of 1.0 A g^{-1} for over 4000 cycles.

4.4 Summary

The MnO_2/C composites have been successfully synthesized by react the as-synthesized hierarchical porous carbon with $KMnO_4$ solution. The spherical morphology of the as-synthesized MnO_2/C composites has been revealed by SEM and TEM. Compared to pure hierarchical porous carbon spheres, the darker color of the SEM and TEM of MnO_2/C composites can suggest the successful growth of MnO_2 on carbon sphere scaffold. To further confirm the presence of MnO_2 in the composites, XPS is utilized to analyze the MnO_2/C composites. High-resolution TEM can help to reveal the graphitic carbon that exists on the pore walls of MnO_2/C composites, suggesting that amorphous carbon has the priority to react with $KMnO_4$ solution.

MnO_2/C composites with different contents of MnO_2 are synthesized by control the reaction times. The ratio of MnO_2 in MnO_2/C composites is analyzed by TGA, which indicates that the highest MnO_2 ratio is 84 %. The pore structure is analyzed by Nitrogen adsorption/ desorption technique. Compared to the

pure hierarchical porous carbon, MnO_2/C composites have much lower surface area and pore volume, which is ascribed of the growth of MnO_2. However, both Nitrogen adsorption/ desorption isotherms and pore size distribution can suggest that the hierarchical structure still exist although there is a shrinkage of the mesopores.

The electrochemical analysis is conducted in an open cell system. A high specific capacitance of 412 F g^{-1} and excellent rate capability of these composites can be achieved owing to the interconnected meso- and micro- porous structure and the graphitic pore walls facilitating the ion diffusion and electron transportation, respectively. Even at a high scan rate of 100 mV s^{-1}, a specific capacitance of 251 F g^{-1} can be obtained, corresponding to 61 % capacitance retention. Galvanostatic charge-discharge is also conducted to further confirm the capacitance of the MnO_2/C composites. Dependence on the content of MnO_2, an optimum MnO_2 content is obtained at reaction time of 240 min to achieve both high specific capacitance and good rate capability. A long cycling stability with initial capacitance retention of 88 % is obtained after over 4000 cycles at a current density of 1.0 A g^{-1}. Thus, this work presents an efficient electrode materials design and a novel composite which holds great promise in high-performance supercapacitor applications.

Chapter 5
Prospective of Future Work

In summary, we have designed and synthesized a type of templated carbon with unique pore structure and high electrical conductivity as carbon materials for the next generation supercapacitor devices. On one hand, the special hierarchical porous structure with meso- and micro- pores enables the fast ion diffusion in the electrode. On the other hand, the partially graphitized pore walls can facilitate the electron transportation in the electrode. Thus, this carbon material is designed with both fast ion and electron channels, which can effectively solve the inferior rate capability problem that occurs in most of the supercapaitors. In addition, this carbon material is synthesized with one-step aerosol assisted spray drier method, which is much faster than the traditional two-step templated carbon synthesis method. Briefly, aerosol assisted spray direr technique can synthesize template and carbon material at the same time with self-assembly process instead of synthesizing the template separately. [131, 165-168]

In the first study, the hierarchical porous carbon spheres were synthesized. Due to the presence of colloidal silica and TEOs, there are two types of pores exist in the carbon material. The pore structure has been revealed by SEM, TEM, and Nitrogen adsorption/ desorption technique. According to the BET theory, the hierarchical porous carbon has large surface area, which is ideal electrode for electric double capacitors. Besides, High conductivity offered by the graphitic carbon pore walls that can be determined by high-resolution TEM is also crucial for high-performance supercapacitors. In summary, structural characterization has indicated the successful synthesis of the expected templated carbon, suggesting the feasibility of synthesizing the carbon materials with high rate capability.

In the second study, to enhance energy density, hierarchical porous and graphitized carbon has been combined with high pseudocapacitive manganese dioxide to use as supercapacitor electrodes. In the new system, the electron and ion channels still retain. The good ion diffusion can be determined by the high loading of MnO_2, indicating that the hierarchical structure is benefit for the ion transportation. The conductivity of MnO_2/C is analyzed by EIS, which shows reasonable performance even after growing low conductive MnO_2. Thus, with the unique structure, the MnO_2/C composites shows high capacitance and good capability in electrochemical analysis such as CV, GCD, and cycling life test.

Based on the results of these studies, some future work for high-performance supercapacitors can be considered by using hierarchical porous and graphitized carbon materials.

1. Investigation of the effect of pore size on the ion diffusion in the hierarchical porous carbon material.
2. Synthesize of other types of transition metal oxide/hierarchical porous carbon material to further study the effect of this unique carbon scaffold.
3. Synthesize the same hierarchical porous and graphitized carbon with sol-gel method to determine the difference between the materials synthesized with aerosol assisted spray direr method.
4. Investigation of the ideal pore size of the hierarchical porous carbon to achieve high electrolyte diffusion, if the aqueous electrolyte is replaced by organic electrolyte.
5. Utilization of the hierarchical porous carbon spheres to wrap active materials which are easy to lose during charging and discharging to obtain long cycling life.

References

1. *a brief history of supercapacitors* batteries and energy storage technology, (AUTUMN 2007).
2. Maruyama, T., Y. Ikeda, and N. Kuroki, *Aluminum electrolytic capacitor*, 2001, Google Patents.
3. Booe, J.M., *Tantalum electrolytic capacitor with iron chloride depolarizer*, 1958, Google Patents.
4. Yoshida, K. and N. Kuge, *Solid electrolytic capacitor and manufacturing method thereof*, 2001, Google Patents.
5. Fishler, M.G., *Electrolytic capacitor with multiple independent anodes*, 1999, Google Patents.
6. Boos, D.L., *Electrolytic capacitor having carbon paste electrodes*, 1970, Google Patents.
7. Pandolfo, A. and A. Hollenkamp, *Carbon properties and their role in supercapacitors.* Journal of power sources, 2006. **157**(1): p. 11-27.
8. Conway, B.E., *Electrochemical supercapacitors: scientific fundamentals and technological applications*2013: Springer Science & Business Media.
9. Conway, B.E., *Transition from "Supercapacitor" to "Battery" Behavior in Electrochemical Energy Storage.* Journal of The Electrochemical Society, 1991. **138**(6): p. 1539-1548.
10. Zhao, X., C. Johnston, and P.S. Grant, *A novel hybrid supercapacitor with a carbon nanotube cathode and an iron oxide/carbon nanotube composite anode.* Journal of Materials Chemistry, 2009. **19**(46): p. 8755-8760.
11. Singh, S., et al. *Electrochemical Performance of Lithium-Ion Hybrid Supercapacitors based on Activated Carbon and Nanoplatelet Li 4 Ti 5 O 12 Insertion Electrode Synthesized by Nanoscission Technique*. in *MRS Proceedings*. 2015. Cambridge Univ Press.
12. Luo, J.-Y., et al., *A novel LiTi 2 (PO 4) 3/MnO 2 hybrid supercapacitor in lithium sulfate aqueous electrolyte.* Electrochimica Acta, 2008. **53**(28): p. 8128-8133.
13. Belhachemi, F., S. Rael, and B. Davat. *A physical based model of power electric double-layer supercapacitors*. in *Industry Applications Conference, 2000. Conference Record of the 2000 IEEE*. 2000. IEEE.
14. Conway, B., *Electrochemical supercapacitors: scientific fundamentals and technological applications, 1999*, Kluwer Academic/Plenum Publishers, New York.
15. Ohshima, H. and K. Furusawa, *Electrical Phenomena at Interfaces: Fundamentals: Measurements, and Applications*. Vol. 76. 1998: CRC Press.
16. Halper, M.S. and J.C. Ellenbogen, *Supercapacitors: A brief overview.* The MITRE Corporation, McLean, Virginia, USA, 2006: p. 1-34.
17. Okamura, M., *A basic study on power storage capacitor systems.* Electrical engineering in Japan, 1996. **116**(3): p. 40-51.
18. Tarascon, J.-M. and M. Armand, *Issues and challenges facing rechargeable lithium batteries.* Nature, 2001. **414**(6861): p. 359-367.
19. Kim, W.-S. and W.-Y. Yoon, *Observation of dendritic growth on Li powder anode using optical cell.* Electrochimica acta, 2004. **50**(2): p. 541-545.
20. Morcrette, M., et al., *A reversible copper extrusion–insertion electrode for rechargeable Li batteries.* Nature materials, 2003. **2**(11): p. 755-761.
21. Rosso, M., et al., *Dendrite short-circuit and fuse effect on Li/polymer/Li cells.* Electrochimica Acta, 2006. **51**(25): p. 5334-5340.

22. Ng, S.H., et al., *Highly Reversible Lithium Storage in Spheroidal Carbon‐Coated Silicon Nanocomposites as Anodes for Lithium‐Ion Batteries.* Angewandte Chemie International Edition, 2006. **45**(41): p. 6896-6899.
23. Lee, J.K., et al., *Silicon nanoparticles–graphene paper composites for Li ion battery anodes.* Chemical Communications, 2010. **46**(12): p. 2025-2027.
24. Hwang, T.H., et al., *Electrospun core–shell fibers for robust silicon nanoparticle-based lithium ion battery anodes.* Nano letters, 2012. **12**(2): p. 802-807.
25. Koo, B., et al., *A Highly Cross‐Linked Polymeric Binder for High‐Performance Silicon Negative Electrodes in Lithium Ion Batteries.* Angewandte Chemie International Edition, 2012. **51**(35): p. 8762-8767.
26. Chan, C.K., et al., *High-performance lithium battery anodes using silicon nanowires.* Nature nanotechnology, 2008. **3**(1): p. 31-35.
27. Wang, H., et al., *Graphene-wrapped sulfur particles as a rechargeable lithium–sulfur battery cathode material with high capacity and cycling stability.* Nano letters, 2011. **11**(7): p. 2644-2647.
28. Zheng, G., et al., *Hollow carbon nanofiber-encapsulated sulfur cathodes for high specific capacity rechargeable lithium batteries.* Nano letters, 2011. **11**(10): p. 4462-4467.
29. Su, Y.-S. and A. Manthiram, *A new approach to improve cycle performance of rechargeable lithium–sulfur batteries by inserting a free-standing MWCNT interlayer.* Chemical Communications, 2012. **48**(70): p. 8817-8819.
30. Seh, Z.W., et al., *Sulphur–TiO2 yolk–shell nanoarchitecture with internal void space for long-cycle lithium–sulphur batteries.* Nature communications, 2013. **4**: p. 1331.
31. Holmberg, S., et al., *3-D Micro and Nano Technologies for Improvements in Electrochemical Power Devices.* Micromachines, 2014. **5**(2): p. 171-203.
32. Yuan, L., et al., *Flexible solid-state supercapacitors based on carbon nanoparticles/MnO2 nanorods hybrid structure.* ACS Nano, 2011. **6**(1): p. 656-661.
33. Lu, X., et al., *WO3‐x@ Au@ MnO2 Core‐Shell Nanowires on Carbon Fabric for High‐Performance Flexible Supercapacitors.* Advanced materials, 2012. **24**(7): p. 938-944.
34. Lang, X., et al., *Nanoporous metal/oxide hybrid electrodes for electrochemical supercapacitors.* Nature Nanotechnology, 2011. **6**(4): p. 232-236.
35. Peng, L., et al., *Ultrathin two-dimensional MnO2/graphene hybrid nanostructures for high-performance, flexible planar supercapacitors.* Nano letters, 2013. **13**(5): p. 2151-2157.
36. Chen, P., et al., *Inkjet printing of single-walled carbon nanotube/RuO2 nanowire supercapacitors on cloth fabrics and flexible substrates.* Nano Research, 2010. **3**(8): p. 594-603.
37. Hu, C.-C., et al., *Design and tailoring of the nanotubular arrayed architecture of hydrous RuO2 for next generation supercapacitors.* Nano Letters, 2006. **6**(12): p. 2690-2695.
38. Zhang, X., et al., *Synthesis of porous NiO nanocrystals with controllable surface area and their application as supercapacitor electrodes.* Nano Research, 2010. **3**(9): p. 643-652.
39. Lu, Q., et al., *Supercapacitor Electrodes with High‐Energy and Power Densities Prepared from Monolithic NiO/Ni Nanocomposites.* Angewandte Chemie, 2011. **123**(30): p. 6979-6982.
40. Wang, B., et al., *Green synthesis of NiO nanobelts with exceptional pseudo‐capacitive properties.* Advanced Energy Materials, 2012. **2**(10): p. 1188-1192.
41. Lu, Z., et al., *Stable ultrahigh specific capacitance of NiO nanorod arrays.* Nano research, 2011. **4**(7): p. 658-665.

42. Liao, Q., et al., *All-Solid-State Symmetric Supercapacitor Based on Co3O4 Nanoparticles on Vertically Aligned Graphene.* ACS nano, 2015.
43. Wang, Y., et al., *Reduced Mesoporous Co3O4 Nanowires as Efficient Water Oxidation Electrocatalysts and Supercapacitor Electrodes.* Advanced Energy Materials, 2014. **4**(16).
44. Feng, C., et al., *Sub-3 nm Co3O4 Nanofilms with Enhanced Supercapacitor Properties.* ACS nano, 2015. **9**(2): p. 1730-1739.
45. Foo, C.Y., et al., *Flexible and Highly Scalable V2O5‐rGO Electrodes in an Organic Electrolyte for Supercapacitor Devices.* Advanced Energy Materials, 2014. **4**(12).
46. Chu, Q., et al., *Hierarchical NiCo 2 O 4@ nickel-sulfide nanoplate arrays for high-performance supercapacitors.* Journal of Power Sources, 2015. **276**: p. 19-25.
47. Liu, B., et al., *New Energy Storage Option: Toward ZnCo2O4 Nanorods/Nickel Foam Architectures for High-Performance Supercapacitors.* ACS applied materials & interfaces, 2013. **5**(20): p. 10011-10017.
48. Huang, Y., et al., *Hierarchical ZnCo2O4@ NiCo2O4 Core‐Sheath Nanowires: Bifunctionality towards High‐Performance Supercapacitors and the Oxygen Reduction Reaction.* Chemistry-A European Journal, 2015.
49. Cheng, J., et al., *Mesoporous ZnCo2O4 nanoflakes grown on nickel foam as electrodes for high performance supercapacitors.* Physical Chemistry Chemical Physics, 2015.
50. Tang, Z., C.h. Tang, and H. Gong, *A High Energy Density Asymmetric Supercapacitor from Nano‐architectured Ni (OH) 2/Carbon Nanotube Electrodes.* Advanced Functional Materials, 2012. **22**(6): p. 1272-1278.
51. Zhou, W., et al., *One-step synthesis of Ni 3 S 2 nanorod@ Ni (OH) 2 nanosheet core–shell nanostructures on a three-dimensional graphene network for high-performance supercapacitors.* Energy & Environmental Science, 2013. **6**(7): p. 2216-2221.
52. Jiang, H., et al., *High-performance supercapacitor material based on Ni (OH) 2 nanowire-MnO 2 nanoflakes core–shell nanostructures.* Chemical Communications, 2012. **48**(20): p. 2606-2608.
53. Yang, S., et al., *Spherical α-Ni (OH) 2 nanoarchitecture grown on graphene as advanced electrochemical pseudocapacitor materials.* Chemical Communications, 2012. **48**(22): p. 2773-2775.
54. Jagadale, A., et al., *Performance evaluation of symmetric supercapacitor based on cobalt hydroxide [Co (OH) 2] thin film electrodes.* Electrochimica Acta, 2013. **98**: p. 32-38.
55. Mondal, C., et al., *Fabrication of porous β-Co (OH) 2 architecture at room temperature: a high performance supercapacitor.* Langmuir, 2013. **29**(29): p. 9179-9187.
56. Snook, G.A., P. Kao, and A.S. Best, *Conducting-polymer-based supercapacitor devices and electrodes.* Journal of Power Sources, 2011. **196**(1): p. 1-12.
57. Zhao, Y., et al., *3D nanostructured conductive polymer hydrogels for high-performance electrochemical devices.* Energy & Environmental Science, 2013. **6**(10): p. 2856-2870.
58. Hu, Y.-S., et al., *Porous carbon electrode with conductive polymer coating*, 2012, Google Patents.
59. Hou, Y., et al., *Ultrahigh capacitance of nanoporous metal enhanced conductive polymer pseudocapacitors.* Journal of Power Sources, 2013. **225**: p. 304-310.
60. Duay, J., et al., *Highly flexible pseudocapacitor based on freestanding heterogeneous MnO 2/conductive polymer nanowire arrays.* Physical Chemistry Chemical Physics, 2012. **14**(10): p. 3329-3337.

61. Cao, L., et al., *Preparation of the Novel Nanocomposite Co (OH) 2/Ultra‐Stable Y Zeolite and Its Application as a Supercapacitor with High Energy Density.* Advanced materials, 2004. **16**(20): p. 1853-1857.
62. Chen, Z., et al., *High‐Performance Supercapacitors Based on Intertwined CNT/V2O5 Nanowire Nanocomposites.* Advanced materials, 2011. **23**(6): p. 791-795.
63. Maiti, S., A. Pramanik, and S. Mahanty, *Extraordinarily high pseudocapacitance of metal organic framework derived nanostructured cerium oxide.* Chemical Communications, 2014. **50**(79): p. 11717-11720.
64. Zhu, Y., et al., *Carbon-based supercapacitors produced by activation of graphene.* Science, 2011. **332**(6037): p. 1537-1541.
65. Wang, G., L. Zhang, and J. Zhang, *A review of electrode materials for electrochemical supercapacitors.* Chemical Society Reviews, 2012. **41**(2): p. 797-828.
66. Fan, Z., et al., *Asymmetric supercapacitors based on graphene/MnO2 and activated carbon nanofiber electrodes with high power and energy density.* Advanced Functional Materials, 2011. **21**(12): p. 2366-2375.
67. Hulicova‐Jurcakova, D., et al., *Combined Effect of Nitrogen‐and Oxygen‐Containing Functional Groups of Microporous Activated Carbon on its Electrochemical Performance in Supercapacitors.* Advanced functional materials, 2009. **19**(3): p. 438-447.
68. Mastragostino, M., et al., *Electronically conducting polymers and activated carbon: electrode materials in supercapacitor technology.* Advanced materials, 1996. **8**(4): p. 331-334.
69. Ruiz, V., et al., *An activated carbon monolith as an electrode material for supercapacitors.* Carbon, 2009. **47**(1): p. 195-200.
70. Liu, H., et al., *A novel nickel-based mixed rare-earth oxide/activated carbon supercapacitor using room temperature ionic liquid electrolyte.* Electrochimica Acta, 2006. **51**(10): p. 1925-1931.
71. Chen, L.-F., et al., *Synthesis of nitrogen-doped porous carbon nanofibers as an efficient electrode material for supercapacitors.* ACS nano, 2012. **6**(8): p. 7092-7102.
72. Fan, L.Z., et al., *High electroactivity of polyaniline in supercapacitors by using a hierarchically porous carbon monolith as a support.* Advanced Functional Materials, 2007. **17**(16): p. 3083-3087.
73. Kim, C., et al., *Self‐Sustained Thin Webs Consisting of Porous Carbon Nanofibers for Supercapacitors via the Electrospinning of Polyacrylonitrile Solutions Containing Zinc Chloride.* Advanced materials, 2007. **19**(17): p. 2341-2346.
74. Yang, K.-L., et al., *Electrosorption of ions from aqueous solutions by carbon aerogel: an electrical double-layer model.* Langmuir, 2001. **17**(6): p. 1961-1969.
75. An, K.H., et al., *Electrochemical properties of high-power supercapacitors using single-walled carbon nanotube electrodes.* Advanced functional materials, 2001. **11**(5): p. 387-392.
76. Fan, Z., et al., *A Three‐Dimensional Carbon Nanotube/Graphene Sandwich and Its Application as Electrode in Supercapacitors.* Advanced materials, 2010. **22**(33): p. 3723-3728.
77. Futaba, D.N., et al., *Shape-engineerable and highly densely packed single-walled carbon nanotubes and their application as super-capacitor electrodes.* Nature materials, 2006. **5**(12): p. 987-994.
78. Liu, C., et al., *Graphene-based supercapacitor with an ultrahigh energy density.* Nano letters, 2010. **10**(12): p. 4863-4868.
79. Zhao, Y., et al., *Highly Compression‐Tolerant Supercapacitor Based on Polypyrrole‐mediated Graphene Foam Electrodes.* Advanced materials, 2013. **25**(4): p. 591-595.

80. Wen, Z., et al., *Crumpled Nitrogen‐Doped Graphene Nanosheets with Ultrahigh Pore Volume for High‐Performance Supercapacitor.* Advanced materials, 2012. **24**(41): p. 5610-5616.
81. Qu, D. and H. Shi, *Studies of activated carbons used in double-layer capacitors.* Journal of Power Sources, 1998. **74**(1): p. 99-107.
82. Shi, H., *Activated carbons and double layer capacitance.* Electrochimica Acta, 1996. **41**(10): p. 1633-1639.
83. Yang, H., et al., *Improvement of commercial activated carbon and its application in electric double layer capacitors.* Electrochemical and solid-state letters, 2002. **5**(6): p. A141-A144.
84. Kim, Y.J., et al., *Easy preparation of nitrogen-enriched carbon materials from peptides of silk fibroins and their use to produce a high volumetric energy density in supercapacitors.* Carbon, 2007. **45**(10): p. 2116-2125.
85. Nakagawa, H., A. Shudo, and K. Miura, *High‐Capacity Electric Double‐Layer Capacitor with High‐Density‐Activated Carbon Fiber Electrodes.* Journal of the Electrochemical Society, 2000. **147**(1): p. 38-42.
86. Kyotani, T., et al., *Formation of new type of porous carbon by carbonization in zeolite nanochannels.* Chemistry of materials, 1997. **9**(2): p. 609-615.
87. Matsuoka, K., et al., *Extremely high microporosity and sharp pore size distribution of a large surface area carbon prepared in the nanochannels of zeolite Y.* Carbon, 2005. **43**(4): p. 876-879.
88. Hou, P.-X., et al., *Synthesis of nitrogen-containing microporous carbon with a highly ordered structure and effect of nitrogen doping on H2O adsorption.* Chemistry of materials, 2005. **17**(20): p. 5187-5193.
89. Nishihara, H., et al., *Investigation of the Ion Storage/Transfer Behavior in an Electrical Double‐Layer Capacitor by Using Ordered Microporous Carbons as Model Materials.* Chemistry-A European Journal, 2009. **15**(21): p. 5355-5363.
90. Huang, J., B.G. Sumpter, and V. Meunier, *Theoretical model for nanoporous carbon supercapacitors.* Angewandte Chemie International Edition, 2008. **47**(3): p. 520-524.
91. Wigmans, T., *Industrial aspects of production and use of activated carbons.* Carbon, 1989. **27**(1): p. 13-22.
92. Kierzek, K., et al., *Electrochemical capacitors based on highly porous carbons prepared by KOH activation.* Electrochimica Acta, 2004. **49**(4): p. 515-523.
93. Zhi, M., et al., *Effects of Pore Structure on Performance of An Activated-Carbon Supercapacitor Electrode Recycled from Scrap Waste Tires.* ACS Sustainable Chemistry & Engineering, 2014. **2**(7): p. 1592-1598.
94. Gualous, H., et al., *Calendar and cycling ageing of activated carbon supercapacitor for automotive application.* Microelectronics Reliability, 2012. **52**(9): p. 2477-2481.
95. Redondo, E., et al., *Effect of pore texture on performance of activated carbon supercapacitor electrodes derived from olive pits.* Electrochimica Acta, 2015. **160**: p. 178-184.
96. Won, J.H., et al., *Preparation of Solid Polymer Electrolytes by Ultraviolet Radiation and the Electrochemical Properties of Activated Carbon Supercapacitor Adopting Them.* Journal of the Korean Electrochemical Society, 2013. **16**(2): p. 91-97.
97. Zhang, L.L. and X. Zhao, *Carbon-based materials as supercapacitor electrodes.* Chemical Society Reviews, 2009. **38**(9): p. 2520-2531.
98. Wang, Q., Z. Wen, and J. Li, *A hybrid supercapacitor fabricated with a carbon nanotube cathode and a TiO2–B nanowire anode.* Advanced Functional Materials, 2006. **16**(16): p. 2141-2146.

99. Li, L., et al., *Facile synthesis of MnO2/CNTs composite for supercapacitor electrodes with long cycle stability*. The Journal of Physical Chemistry C, 2014. **118**(40): p. 22865-22872.
100. Salunkhe, R.R., et al., *Rational design of coaxial structured carbon nanotube–manganese oxide (CNT–MnO2) for energy storage application.* Nanotechnology, 2015. **26**(20): p. 204004.
101. Wang, J., et al. *Synthesis of Nano-MnO2/CNTs Composite and Electrochemical Properties as Electrode Material for Supercapacitor*. in *Advanced Materials Research*. 2012. Trans Tech Publ.
102. Wang, H., et al., *Design, synthesis and the electrochemical performance of MnO 2/C@ CNT as supercapacitor material*. Materials Research Bulletin, 2013. **48**(9): p. 3389-3393.
103. Tan, D.Z.W., et al., *Controlled synthesis of MnO2/CNT nanocomposites for supercapacitor applications.* Materials Technology: Advanced Functional Materials, 2014. **29**(A2): p. A107-A113.
104. Zhao, X., et al., *Templating methods for preparation of porous structures.* Journal of Materials Chemistry, 2006. **16**(7): p. 637-648.
105. Li, W., et al., *Nitrogen-containing carbon spheres with very large uniform mesopores: the superior electrode materials for EDLC in organic electrolyte*. Carbon, 2007. **45**(9): p. 1757-1763.
106. Wang, D.-w., et al., *Improved capacitance of SBA-15 templated mesoporous carbons after modification with nitric acid oxidation.* New Carbon Materials, 2007. **22**(4): p. 307-314.
107. Feng, X., et al., *Synthesis of a graphene/polyaniline/MCM-41 nanocomposite and its application as a supercapacitor*. New Journal of Chemistry, 2013. **37**(7): p. 2203-2209.
108. Ania, C.O., et al., *The large electrochemical capacitance of microporous doped carbon obtained by using a zeolite template.* Advanced Functional Materials, 2007. **17**(11): p. 1828-1836.
109. Roberts, A.D., X. Li, and H. Zhang, *Porous carbon spheres and monoliths: morphology control, pore size tuning and their applications as Li-ion battery anode materials*. Chemical Society Reviews, 2014. **43**(13): p. 4341-4356.
110. Liang, J., et al., *N‐Doped Graphene Natively Grown on Hierarchical Ordered Porous Carbon for Enhanced Oxygen Reduction.* Advanced materials, 2013. **25**(43): p. 6226-6231.
111. Novoselov, K.S., et al., *Electric field effect in atomically thin carbon films.* science, 2004. **306**(5696): p. 666-669.
112. Le, L.T., et al., *Graphene supercapacitor electrodes fabricated by inkjet printing and thermal reduction of graphene oxide*. Electrochemistry Communications, 2011. **13**(4): p. 355-358.
113. Zhao, X., et al., *Incorporation of manganese dioxide within ultraporous activated graphene for high-performance electrochemical capacitors*. ACS nano, 2012. **6**(6): p. 5404-5412.
114. Zhong, M., et al., *Effect of reduced graphene oxide on the properties of an activated carbon cloth/polyaniline flexible electrode for supercapacitor application.* Journal of Power Sources, 2012. **217**: p. 6-12.
115. Long, J.W., et al., *Voltammetric characterization of ruthenium oxide-based aerogels and other RuO2 solids: the nature of capacitance in nanostructured materials*. Langmuir, 1999. **15**(3): p. 780-785.
116. Juan, L., L. Qingwen, and X. Xi, *Synthesis of Nanosize MnO2 by Solid State Reaction and Its Electrochemical Property. Synthesis and Performance of MnO2 [J]*. Chinese Journal of Applied Chemistry, 1999. **3**.
117. Lee, H.Y. and J. Goodenough, *Ideal supercapacitor behavior of amorphous V 2 O 5 ·nH 2 O in potassium chloride (KCl) aqueous solution.* Journal of Solid State Chemistry, 1999. **148**(1): p. 81-84.

118. Nam, K.-W. and K.-B. Kim, *A study of the preparation of NiO x electrode via electrochemical route for supercapacitor applications and their charge storage mechanism.* Journal of the Electrochemical Society, 2002. **149**(3): p. A346-A354.
119. Wang, Y., et al., *Synthesis of 3D-nanonet hollow structured Co3O4 for high capacity supercapacitor.* ACS applied materials & interfaces, 2014. **6**(9): p. 6739-6747.
120. Zheng, J., P. Cygan, and T. Jow, *Hydrous ruthenium oxide as an electrode material for electrochemical capacitors.* Journal of the Electrochemical Society, 1995. **142**(8): p. 2699-2703.
121. Bi, R.-R., et al., *Highly dispersed RuO2 nanoparticles on carbon nanotubes: facile synthesis and enhanced supercapacitance performance.* The Journal of Physical Chemistry C, 2010. **114**(6): p. 2448-2451.
122. Song, M.-K., et al., *Anomalous pseudocapacitive behavior of a nanostructured, mixed-valent manganese oxide film for electrical energy storage.* Nano letters, 2012. **12**(7): p. 3483-3490.
123. Tao, J., et al., *Solid-state high performance flexible supercapacitors based on polypyrrole-MnO2-carbon fiber hybrid structure.* Scientific reports, 2013. **3**.
124. Hu, L., et al., *Symmetrical MnO2–Carbon Nanotube–Textile Nanostructures for Wearable Pseudocapacitors with High Mass Loading.* ACS Nano, 2011. **5**(11): p. 8904-8913.
125. Sawangphruk, M., et al., *High-performance supercapacitor of manganese oxide/reduced graphene oxide nanocomposite coated on flexible carbon fiber paper.* Carbon, 2013. **60**: p. 109-116.
126. Zhang, Z., F. Xiao, and S. Wang, *Hierarchically structured MnO 2/graphene/carbon fiber and porous graphene hydrogel wrapped copper wire for fiber-based flexible all-solid-state asymmetric supercapacitors.* Journal of Materials Chemistry A, 2015.
127. Zhou, W. and Z.L. Wang, *Scanning microscopy for nanotechnology: techniques and applications*2007: Springer science & business media.
128. Chen, X.Y., et al., *A rational template carbonization method for producing highly porous carbon for supercapacitor application.* Electrochimica Acta, 2014. **117**: p. 55-61.
129. Gao, Y., et al., *Simple synthesis of hierarchical porous carbon from Enteromorpha prolifera by a self-template method for supercapacitor electrodes.* Journal of Power Sources, 2014. **270**: p. 403-410.
130. Chen, Z., et al., *High‐performance supercapacitors based on hierarchically porous graphite particles.* Advanced Energy Materials, 2011. **1**(4): p. 551-556.
131. Lu, Y., et al., *Aerosol-assisted self-assembly of mesostructured spherical nanoparticles.* Nature, 1999. **398**(6724): p. 223-226.
132. Winter, M. and R.J. Brodd, *What Are Batteries, Fuel Cells, and Supercapacitors?* Chemical Reviews, 2004. **104**(10): p. 4245-4270.
133. Simon, P. and Y. Gogotsi, *Materials for electrochemical capacitors.* Nature Material, 2008. **7**(11): p. 845-854.
134. Conway, B.E., *Electrochemical Supercapacitors: Scientific Fundamentals and Technological Applications*, 1999, Kluwer Academic/Plenum Pblishers: New York. p. 29.
135. Simon, P., Y. Gogotsi, and B. Dunn, *Where Do Batteries End and Supercapacitors Begin?* . Science Magazine, 2014. **343**: p. 1201-1211.
136. Zheng, J.P., *The Limitations of Energy Density of Battery/Double-Layer Capacitor Asymmetric Cells.* Journal of The Electrochemical Society, 2003. **150**(4): p. A484-A492.
137. Zhang, L.L. and X.S. Zhao, *Carbon-based materials as supercapacitor electrodes.* Chemical Society Reviews, 2009. **38**(9): p. 2520-2531.
138. Augustyn, V., et al., *High-rate electrochemical energy storage through Li+ intercalation pseudocapacitance.* Nature Material, 2013. **12**(6): p. 518-522.

139. Augustyn, V., P. Simon, and B. Dunn, *Pseudocapacitive oxide materials for high-rate electrochemical energy storage.* Energy & Environmental Science, 2014. **7**(5): p. 1597-1614.
140. Whittingham, M.S., *Materials Challenges Facing Electrical Energy Storage.* MRS Bulletin, 2008. **33**(04): p. 411-419.
141. Wu, Z.-S., et al., *High-energy MnO2 nanowire/graphene and graphene asymmetric electrochemical capacitors.* ACS nano, 2010. **4**(10): p. 5835-5842.
142. Qu, Q., et al., *Electrochemical Performance of MnO2 Nanorods in Neutral Aqueous Electrolytes as a Cathode for Asymmetric Supercapacitors.* The Journal of Physical Chemistry C, 2009. **113**(31): p. 14020-14027.
143. Xu, C., et al., *Recent progress on manganese dioxide based supercapacitors.* Journal of Materials Research, 2010. **25**(08): p. 1421-1432.
144. Wei, W., et al., *Manganese oxide-based materials as electrochemical supercapacitor electrodes.* Chemical Society Reviews, 2011. **40**(3): p. 1697-1721.
145. Liu, C., et al., *Advanced Materials for Energy Storage.* Advanced Materials, 2010. **22**(8): p. E28-E62.
146. Li, G.-R., et al., *Mesoporous MnO2/Carbon Aerogel Composites as Promising Electrode Materials for High-Performance Supercapacitors.* Langmuir, 2010. **26**(4): p. 2209-2213.
147. Yuan, L., et al., *Flexible Solid-State Supercapacitors Based on Carbon Nanoparticles/MnO2 Nanorods Hybrid Structure.* ACS Nano, 2011. **6**(1): p. 656-661.
148. Chen, S., et al., *Graphene Oxide−MnO2 Nanocomposites for Supercapacitors.* ACS Nano, 2010. **4**(5): p. 2822-2830.
149. Jiang, H., et al., *A green and high energy density asymmetric supercapacitor based on ultrathin MnO2 nanostructures and functional mesoporous carbon nanotube electrodes.* Nanoscale, 2012. **4**(3): p. 807-812.
150. Chou, S.-L., et al., *Electrodeposition of MnO2 nanowires on carbon nanotube paper as free-standing, flexible electrode for supercapacitors.* Electrochemistry Communications, 2008. **10**(11): p. 1724-1727.
151. Li, Z., et al., *Flexible graphene/MnO2 composite papers for supercapacitor electrodes.* Journal of Materials Chemistry, 2011. **21**(38): p. 14706-14711.
152. Prasad, K.R. and N. Miura, *Polyaniline- MnO2 Composite Electrode for High Energy Density Electrochemical Capacitor.* Electrochemical and Solid-State Letters, 2004. **7**(11): p. A425-A428.
153. Sharma, R.K., A.C. Rastogi, and S.B. Desu, *Manganese oxide embedded polypyrrole nanocomposites for electrochemical supercapacitor.* Electrochimica Acta, 2008. **53**(26): p. 7690-7695.
154. Yu, G., et al., *Enhancing the Supercapacitor Performance of Graphene/MnO2 Nanostructured Electrodes by Conductive Wrapping.* Nano Letters, 2011. **11**(10): p. 4438-4442.
155. Long, J.W., et al., *Three-Dimensional Battery Architectures.* Chemical Reviews, 2004. **104**(10): p. 4463-4492.
156. Fischer, A.E., et al., *Incorporation of Homogeneous, Nanoscale MnO2 within Ultraporous Carbon Structures via Self-Limiting Electroless Deposition: Implications for Electrochemical Capacitors.* Nano Letters, 2007. **7**(2): p. 281-286.
157. Wang, J.-G., et al., *Rational synthesis of MnO2/conducting polypyrrole@carbon nanofiber triaxial nano-cables for high-performance supercapacitors.* Journal of Materials Chemistry, 2012. **22**(33): p. 16943-16949.

158. Chen, H., et al., *Templated synthesis of hierarchically porous manganese oxide with a crystalline nanorod framework and its high electrochemical performance.* Journal of Materials Chemistry, 2007. **17**(9): p. 855-860.
159. Shen, B. and Qinlei, *Study on MSW catalytic combustion by TGA.* Energy Conversion and Management, 2006. **47**(11–12): p. 1429-1437.
160. Chou, T.-c., et al., *Hierarchically Porous Carbon with Manganese Oxides as Highly Efficient Electrode for Asymmetric Supercapacitors.* ChemSusChem, 2014. **7**(3): p. 841-847.
161. Patel, M.N., et al., *High pseudocapacitance of MnO2 nanoparticles in graphitic disordered mesoporous carbon at high scan rates.* Journal of Materials Chemistry, 2012. **22**(7): p. 3160-3169.
162. Dong, X., et al., *MnO2-Embedded-in-Mesoporous-Carbon-Wall Structure for Use as Electrochemical Capacitors.* The Journal of Physical Chemistry B, 2006. **110**(12): p. 6015-6019.
163. Lei, Z., J. Zhang, and X.S. Zhao, *Ultrathin MnO2 nanofibers grown on graphitic carbon spheres as high-performance asymmetric supercapacitor electrodes.* Journal of Materials Chemistry, 2012. **22**(1): p. 153-160.
164. Peng, Y., et al., *Hierarchical manganese oxide/carbon nanocomposites for supercapacitor electrodes.* Nano Research, 2011. **4**(2): p. 216-225.
165. Ji, X., et al., *Synthesis and characterization of functionalized mesoporous silica by aerosol-assisted self-assembly.* Chemistry of materials, 2006. **18**(9): p. 2265-2274.
166. âEric Hampsey, J., *A general approach towards hierarchical porous carbon particles.* Chemical communications, 2005(28): p. 3606-3608.
167. Hampsey, J.E., et al., *Templating synthesis of ordered mesoporous carbon particles.* Carbon, 2005. **43**(14): p. 2977-2982.
168. Yan, Y., et al., *One-step synthesis of ordered mesoporous carbonaceous spheres by an aerosol-assisted self-assembly.* Chem. Commun., 2007(27): p. 2867-2869.